Numerical Modelling of Atmospheric Interactions with Wildland Fire

---

A thesis submitted in partial fulfillment
of the requirements of the
Degree of Doctoral of Philosophy in Environmental Science
at the
University of Canterbury
by
Colin Campbell Simpson

May 2013

Abstract

Wildland fires are a type of vegetation fire that burn in a rural or wild landscape and affect many countries worldwide. They are an important mechanism in ecosystem maintenance, although in certain cases wildland fires can adversely affect both people and the environment. A wildland fire can interact with the surrounding topography, vegetation and weather in a complex manner, which makes microscale prediction of wildland fire behaviour difficult in many situations. This thesis focused on the application of the Weather Research and Forecast (WRF) numerical weather prediction (NWP) and WRF-Fire coupled atmosphere-fire models to investigating aspects of atmospheric interactions with wildland fire. The research covered a wide range of atmospheric scales, from a seasonal mesoscale analysis of fire weather conditions across New Zealand to a microscale analysis of complex atmosphere-fire interactions over idealised terrain.

The first study investigated the suitability of WRF modelling of fire weather conditions for the 2009/10 wildland fire season in New Zealand. The WRF model horizontal grid spacing was 8 km and the model output was directly compared with near-surface fire weather conditions meaured and derived at 23 weather stations located throughout New Zealand. The analysis considered the air temperature, relative humidity, wind conditions, rainfall and the New Zealand Fire Weather Index (FWI) and Continuous Haines Index (CHI) on observed high-end fire weather days. WRF typically underpredicted the air temperatures and relative humidities, whereas it typically overpredicted the wind speeds, CHI and the number of high-end fire weather days. WRF was assessed to be unsuitable for accurately modelling particular aspects of fire weather, such as the wind speed and direction, in mountainous terrain and near complex coastlines. Further research is needed to investigate how varying the horizontal resolution in WRF affects the assessed accuracy of modelled fire weather conditions.

The second study investigated the behaviour of the Haines Index (HI), CHI and FWI, and their associated atmospheric properties for the 2009/10 wildland fire season in New Zealand. The analysis demonstrated that there was a large degree of spatial variability in fire weather conditions throughout New Zealand, particularly in or near mountainous terrain. The fire weather severity was highest in the eastern South Island and appeared to be closely associated with mesoscale atmospheric processes over mountainous terrain,

although the relationship between these atmospheric processes and fire weather conditions requires further investigation. The HI and CHI were both limited in their utility at measuring aloft fire weather conditions in high altitude regions. Finally, the fire weather conditions associated with the 36 largest wildland fires of the fire season were evaluated, although no statistical relationships were found between the wildland fire size and either the CHI or FWI.

The third study investigated the fire weather conditions across the South Island associated with an extreme foehn event on 6 February 2011. Mountain waves developed in the northwesterly synoptic flow over the Southern Alps and were found to directly influence the fire weather conditions near the surface and aloft in the lee of the mountains. A hydraulic jump along the foothills of the Canterbury Plains resulted in a downslope windstorm with wind speeds exceeding 80 km h^{-1}. Further south, large amplitude mountain lee waves directly influenced the near-surface wind speeds and atmospheric stability aloft. The foehn winds were associated with peak air temperatures over 35°C in the eastern South Island, which are significantly higher than the climatological average. The FWI indicated widespread extreme near-surface fire weather conditions in the lee of the mountains. The subsequent passge of a cold front on 7 February brought a marked reduction in fire weather severity across the South Island.

The fourth study investigated atypical wildland fire behaviour on steep leeward slopes through a series of idealised WRF-Fire simulations. The analysis considered both the leeward flow characteristics over a triangular ridge line and the fire spread from an ignition point at the base of the leeward slope. The fire spread was modelled for two different fuel types and with two-way atmosphere-fire coupling both enabled and disabled. The modelled fire spread in the heavy fuel type with coupling enabled closely resembled the fire channelling wildland fire behaviour phenomenon. The initial fire spread was initially dominated by upslope fire spread to the mountain ridge line at an average rate of ∼2.0 km h^{-1}. This was followed by a phase of intermittent rapid lateral fire spread close to the ridge line at a maximum rate of 3.6 km h^{-1}. The intermittent rapid lateral fire spread was driven by strongly circulating horizontal near-surface winds that were associated with updraft-downdraft interfaces. These updraft-downdraft interfaces formed due to an interaction between the strong pyro-convection and terrain-modified winds.

The presented research collectively demonstrated the versatility and effectiveness of NWP and coupled atmosphere-fire modelling for studying various aspects of atmospheric interactions with wildland fire. The research further highlighted the effects of atmospheric processes over complex terrain on fire weather conditions and wildland fire behaviour. Although three of the studies in the thesis had a regional focus on New Zealand, the research outcomes should benefit end users in fire management worldwide.

Contents

Chapter 1

Introduction

1.1 Opening Statement

Wildland fires are a natural phenomenon that occur in many countries throughout the world and play an important role in maintaining ecosystems such as forests and grasslands (Mutch, 1970). However, wildland fires can present a risk to people and the environment, and there have been a number of fatal wildland fires in recent decades. For example, the Black Saturday bushfires in February 2009 claimed 173 lives and burned over 450,000 hectares in southern Australia (Cruz et al., 2012). Wildland fire management is therefore an important issue in many countries worldwide and will become increasingly important in the coming decades due to projected changes in fire climate (Stocks et al., 1998; Brown et al., 2004; Pearce et al., 2005; Flannigan et al., 2009) and population density in the urban-wildland interface (Radeloff et al., 2005; Mell et al., 2010).

Wildland fire behaviour is widely understood to be affected by the local terrain, vegetation and weather (Countryman, 1972). These environmental components are closely associated to each other and interactions between them can result in complex and unpredictable fire behaviour. Atmospheric properties such as the air temperature, humidity, wind conditions and stability can have a direct or indirect influence on fire behaviour through their effects on vegetation, flames and combustion products such as heat (Potter, 2012a,b). Despite the importance of atmosphere-fire interactions for fire behaviour and therefore also fire management, many aspects of these interactions, particularly in complex terrain (Sharples, 2009), are not currently well understood.

The primary objective of this thesis is to investigate atmospheric interactions with wildland fire through the application of numerical modelling. This broad objective is addressed through a series of four interrelated studies that investigate specific aspects of fire weather and atmosphere-fire interaction processes. Three of the studies focus regionally on New Zealand, which is located in the southern mid-latitudes of the Pacific

Ocean and experiences highly variable weather and climate due to its complex and high relief terrain, and extensive coastline (Sturman et al., 1999). Although New Zealand has a moderate fire climate compared to countries such as Australia and the United States, it still typically experiences several thousand wildland fires annually (Pearce et al., 2011b). In addition, the complex terrain and highly variable weather of New Zealand make it an ideal location for investigating atmosphere-fire interactions in complex terrain. The research outcomes of this thesis are intended to directly benefit end users in the fire management community both in New Zealand and internationally.

The remainder of this chapter provides background information on aspects of wildland fire behaviour, fire management and numerical modelling that are relevant to this thesis, followed by an introduction to the specific topics addressed in this thesis. Chapters 2 – 5 present the results of scientific research into the specific topics outlined at the end of Chapter 1. Finally, Chapter 6 summarises the key research outcomes and presents a number of conclusions.

1.2 Wildland Fire Behaviour

Wildland fires burn vegetation in a rural or wild landscape (Pyne et al., 1996) and are therefore distinct from structural and laboratory fires. Prescribed and experimental fires are ignited intentionally for either land management or research purposes, although they can develop into wildland fires if they become uncontrollable. Wildland fires are also commonly referred to as wildfires in the United States and bushfires in Australia. They can also be referred to as forest fires, grass fires, savannah fires, and so on depending on the local ecosystem or dominant vegetation type. Throughout this thesis the term wildland fire will be used where possible to describe vegetation fires in a rural or wild landscape.

Wildland fires can be ignited through a number of mechanisms that can be broadly categorised as either natural ignition or anthropogenic ignition. Natural ignition mechanisms include lightning strikes, volcanic eruptions, rockfall-induced sparking and spotting by existing fires. In the United States, lightning strikes are a leading natural ignition mechanism (Rorig and Ferguson, 1999). Anthropogenic ignition mechanisms can be further categorised into deliberate ignition, such as land clearing burns or arson, and accidental ignition, such as camp fires or sparks from machinery. In many countries worldwide anthropogenic ignition mechanisms are an important factor in wildland fire regimes (Guyette et al., 2002).

Wildland fires most commonly burn organic woody materials, which are primarily composed of hydrocarbons (Byram, 1959; Potter, 2005). The major products of combustion of woody materials include energy, carbon dioxide, water vapour and particulate

matter. For example, the combustion of 1 kg of woody material can release up to 20 MJ of energy (Johnson and Miyanishi, 2001). The transfer of energy as heat from the combustion region to the surrounding vegetation occurs via convective and radiative processes and allows a wildland fire to spread through unburned vegetation (Rothermel, 1972). As the heat transfer increases the vegetation temperature, the vegetation can release volatile gases that, when mixed with oxygen in the air supplied by the local winds, form a combustible mixture. This combustible mixure of volatile gases and oxygen can be ignited once it reaches its ignition temperature through additional heat exchange.

A wildland fire is a complex chemical and physical system and its behaviour can be highly variable, both spatially and temporally. It is therefore useful to characterise various aspects of fire behaviour through a set of physically based variables. Fire behaviour variables that are commonly used include the fire front location, forward rate and direction of fire spread, fire intensity in terms of heat release per unit length, flame height, plume height and so on. A large number of fire behaviour variables exist due to the differing interests of various groups within the fire management and research communities. These fire behaviour variables can be used in a variety of ways, including prediction of future fire behaviour, fire suppression strategy planning and evaluation of the effects on the local environment.

The complexity of wildland fire behaviour is associated both with the complexity of combustion as a chemical process and the physical interactions of a wildland fire with its surrounding environment. Wildland fire behaviour is widely acknowledged to be affected by the local topography, vegetation and weather, which are collectively known as the "fire environment" (Countryman, 1972). Two-way coupled interactions between a wildland fire and the vegetation and weather add to the complexity of wildland fire behaviour, as does the interdependency of the three components of the fire environment over a range of physical scales.

Topography is the only effectively constant component of the fire environment and can directly influence wildland fire behaviour. For example, the forward rate of fire spread is typically higher along an upward slope than along flat terrain or a downward slope (Rothermel, 1972; Weise and Biging, 1997; Whiteman, 2000; Viegas, 2004; Sharples, 2008). Two physical mechanisms are believed to be responsible for slope effects on fire behaviour. First, there is increased radiative heating of the unburned vegetation uphill of the fire front due to the reduced angle between the flames and vegetation. Second, there is increased convective heating of the unburned vegetation uphill of the fire front due to tendency for convectively heated air to rise. Topography also indirectly influences fire behaviour through its effects on spatial and temporal variations in vegetation characteristics and weather. For example, topographical layouts such as canyons and valleys are associated with mountain wind systems that can result in extreme fire behaviour

(Sharples, 2009; Viegas and Pita, 2004).

A number of vegetation, also commonly referred to as fuel, properties can directly influence wildland fire behaviour, including the fuel moisture content, surface area to volume ratio, vertical extent, chemical composition and so on. The dominant fuel type and its associated properties can vary in response to topography and weather over a wide range of timescales, from hourly changes in the fuel moisture content of fine fuels to annual changes in the fuel density of forested regions. The dominant fuel type and its associated properties can directly influence various aspects of wildland fire behaviour, such as the fire intensity and rate of forward fire spread. For example, grass fires are typically characterised by low intensity and rapid fire spread (Cheney et al., 1998; Clements et al., 2006, 2007), whereas forest canopy fires are characterised by high intensity and rapid fire spread (Rothermel, 1991; Butler et al., 2004). In addition, vegetation can directly affect the local weather through the release of moisture by evapotranspiration and its influence on surface friction (Raupach, 1995).

There is currently a lack of informative observational data on wildland fire behaviour and its interaction with the surrounding fire environment. This is an important issue as observational data are needed to develop a better understanding of these interaction processes and to validate wildland fire behaviour models (Sullivan, 2009a). Observational techniques include visual estimates of fire behaviour and quantitative measurements of flame temperatures and heat fluxes using infrared imaging (Clark et al., 1999; Coen et al., 2004; Clements et al., 2007). However, directly observing wildland fire behaviour can be difficult due to personnel safety and equipment survivability issues. Remote sensing techniques are therefore commonly used to overcome these safety and equipment issues (Lentile et al., 2006).

Observational data on fire behaviour is instead often collected for prescribed and experimental fires. Controlled fires typically offer a less complex fire environment and are safer and logistically simpler to observe. Observational instruments can be set up and tested prior to ignition of a controlled fire, which allows for observation of fire behaviour in greater detail. However, this approach is limited in that observations of fire behaviour during controlled fires may not accurately represent the complexity of fire behaviour and atmosphere-fire interactions during wildland fires. Despite these limitations, observations of controlled fires are commonly used to derive empirical relationships between wildland fire behaviour and the fire environment (Albini, 1976).

1.3 Atmospheric Interactions with Wildland Fire

The weather is commonly the most variable and least predictable component of the fire environment and can affect fuel properties and wildland fire behaviour (Whiteman,

2000; Potter, 2012a,b). In addition, the release of combustion products such as energy, water vapour and particulate matter by a wildland fire affects the surrounding atmospheric conditions (Clark et al., 1996b,a; Potter, 2002). The resulting two-way coupled atmosphere-fire interaction processes can modify fire behaviour in a complex manner across a range of physical scales. Throughout this thesis the term "fire weather" is used to refer to atmospheric conditions that can directly or indirectly influence fire behaviour, whereas the term "atmosphere-fire interaction processes" is used to refer to the two-way coupled interactions between a wildland fire and the surrounding atmosphere.

Fire weather indices are widely used in wildland fire management and research to assess the fire weather conditions and are derived from weather variables that are known to directly or indirectly influence fire behaviour (Chandler et al., 1983). There exists a large number of fire weather indices worldwide and they differ from each other in their choice of weather variables and mathematical equations used to assess fire weather. For example, the New Zealand Fire Weather Index (FWI) (Anderson, 2005) is derived from the air temperature, relative humidity, wind speed and rainfall at or below 10 m above ground level, whereas the Haines Index (Haines, 1988) is derived from the air temperature lapse rate and dew point depression aloft. Fire weather indices can exist either as a stand-alone index or as part of a wider fire danger rating system that also accounts for the fuel conditions and topography to allow assessment of wildland fire risk and behaviour. For example, the FWI is an important component of the New Zealand Fire Danger Rating System (NZFDRS) (Anderson, 2005) and is combined with information on fuel properties and topography to determine fire danger classifications across New Zealand.

A number of recent studies have reviewed the scientific literature on various aspects of research into atmospheric interactions with wildland fire (Potter, 2012a,b; Sharples, 2009; Forthofer and Goodrick, 2011). Sharples (2009) focused specifically on the effects of atmospheric processes over complex terrain on wildland fire behaviour and risk, whereas Forthofer and Goodrick (2011) focused on the interaction of atmospheric vortices and wildland fire behaviour. The following discussion of atmospheric interactions with wildland fire is broadly based on these review papers, but does not go into the same level of detail. The review papers and references therein can be consulted for additional information.

1.3.1 Atmospheric Properties

The air temperature, which is closely associated with the incident solar radiation, can indirectly affect fire behaviour through its influence on fuel properties such as the fuel temperature and moisture content (Van Wagner, 1979). Increased fuel temperatures can contribute towards the evaporation of internal moisture and therefore increase the fuel

flammability. Studies have shown that major wildland fires are more likely to occur under high air temperatures (Robin and Wilson, 1958; Potter, 1996). Major fires that have occurred during high air temperatures include the Black Saturday bushfires in southern Australia in 2009 (Cruz et al., 2012).

The atmospheric moisture content and precipitation can also indirectly affect fire behaviour primarily through their influence on the fuel moisture content. Studies have identified statistical relationships between the atmospheric moisture content and fire behaviour (Van Wagner, 1979; Robin and Wilson, 1958; Potter, 1996). Many different variables can be used to measure the atmospheric moisture content, including the absolute humidity, specific humidity, relative humidity, dew point temperature, dew point depression and so on. It remains unclear which measure of atmospheric moisture content is most suitable for assessment of wildland fire risk and behaviour (Potter, 2012a), although relative humidity is most commonly used in wildland fire management and research.

The horizontal winds can both directly and indirectly affect various aspects of fire behaviour, such as the forward direction and rate of fire spread (McArthur, 1966; Rothermel, 1972; Beer, 1991, 1993), through a number of mechanisms. First, the winds can influence the exchange of moisture between the atmosphere and vegetation, and therefore affect the fuel moisture content. Second, the winds supply oxygen to the combustion region and can therefore influence the rate of release of combustion products, such as heat and moisture, into the surrounding atmosphere. Third, the horizontal winds at the flame height can change the relative angle between the flames and the unburned fuel ahead of them, which subsequently affects the radiative and convective heating rates of the unburned fuel. Under uniform fuel conditions and flat terrain, the forward direction of fire spread is typically approximately parallel to the ambient wind direction and the forward rate of fire spread typically increases with increasing wind speed. However, the forward rate and direction of fire spread are widely understood to also be closely associated with local fuel conditions and topography. A number of empirical models of fire spread have been developed for varying wind speeds, fuel types and terrain slopes, based on experimental and laboratory fires (Sullivan, 2009a,b,c).

The vertical temperature, moisture and wind profiles can directly and indirectly affect fire behaviour through their influence on the pyro-convective plume and vortex dynamics. The vertical wind profile plays a role in the lofting and transportation of firebrands, which can result in the ignition of spot fires outside of the combustion zone of the wildland fire from which they were emitted (Albini, 1983a,b). The distance and direction travelled by the lofted firebrands is closely associated with the three-dimensional winds and the likelihood of spot fire ignition due to the deposition of firebrands is associated with the firebrand properties, such as the material temperature, and vegetation characteristics.

1.3.2 Pyro-Convective Plume and Vortex Dynamics

A pyro-convective plume is formed above a wildland fire due to the release of combustion products such as heat and moisture into the surrounding atmosphere. This release of heat and moisture influences the local buoyancy gradient over the combustion region, which often forms a visible updraft containing smoke (Whiteman, 2000; Clements et al., 2007; Kiefer et al., 2009; Luderer et al., 2009). The pyro-convective plume dynamics include the updraft associated with the combustion region, the vertical and horizontal circulations into and around the base of the plume, and the generation of vortices by the plume (Potter, 2012b). The pyro-convective plume dynamics and its interaction with the surrounding atmosphere can be very complex and can directly influence wildland fire behaviour.

The vertical development of a pyro-convective plume is closely associated with atmospheric stability, heat and moisture fluxes from the combustion region, and the entrainment rate of ambient winds into the plume. A pyro-convective plume can extend vertically into the stratosphere or until it encounters a stable atmospheric layer that suppresses further vertical development (Potter, 2002; Fromm and Servranckx, 2003; Luderer et al., 2006; Trentmann et al., 2006). The heat and moisture fluxes associated with combustion influence the local buoyancy gradient, the magnitude of which affects the vertical development of the plume (Taylor et al., 1973). The ambient winds act to advect heat and moisture away from the combustion region before the plume can strengthen and therefore influence its vertical development. The entrainment rate of ambient air into the plume is associated with atmospheric turbulence and ambient wind shear, and a high entrainment rate can limit the vertical development of the plume (Taylor et al., 1973). There are contrasting opinions on whether unstable atmospheric conditions result in a higher or lower entrainment rate of ambient air into the plume (Potter, 2012b).

A pyro-convective plume that contains moisture can form pyrocumulus or pyrocumulonimbus clouds if it reaches the lifting condensation level (Fromm et al., 2010; Gatebe et al., 2012). Pyrocumulonimbus clouds share a number of characteristics in common with regular cumulonimbus clouds and can ignite further wildland fires through lightning strikes (Rosenfeld et al., 2007). Particulate matter released through combustion and carried in a pyro-convective plume can act as cloud condensation nuclei (CCN) in a pyrocumulus or pyrocumulonimbus cloud, which influences the potential of these clouds to form precipitation (Luderer et al., 2009; Hennigan et al., 2012). However, precipitation is not commonly observed at the surface below a pyrocumulus or pyrocumulonimbus cloud for two possible reasons. First, the fast updrafts within the plume could limit the time that water droplets are able to grow on the CCN. Second, the presence of large quantities of CCN could promote the growth of many small water droplets instead of

larger water droplets that are capable of surviving the descent to the surface through the heated air. The release of latent heat at the lifting condensation level warms up the surrounding air and therefore leads to a second stage of vertical development of the pyro-convective plume (Taylor et al., 1973). Pyro-convective plumes are capable of extending in height to the lower stratosphere, where they can inject aerosols and particulate matter (Siddaway and Petelina, 2011).

A pyro-convective plume is anchored to the combustion region and it can be tilted by the ambient winds, which subsequently affects the vertical return circulations and can therefore influence fire behaviour (Banta et al., 1992; Potter, 2002, 2005). It is possible for multiple updraft cores to develop above a wildland fire, depending on the wildland fire geometry. The turbulent vertical circulations in the atmosphere surrounding a pyro-convective plume include updrafts within the plume and downdrafts outside of the plume. Vertical circulations outside of the plume can vertically transport atmospheric quantities, such as moisture and momentum, down to lower levels and can result in downdrafts or downbursts at the surface (Goens and Andrews, 1998). Subsequent changes in near-surface atmospheric moisture and momentum can subsequently influence fire behaviour. A number of atmospheric variables have been used in previous studies to assess the nature of pyro-convective plume dynamics, including the convective Froude number, CAPE and Descent CAPE (DCAPE) (Clark et al., 1996b,a; Potter, 2002, 2005).

In addition to these vertical circulations in and around the pyro-convective plume, there are also horizontal and vertical inflows towards the base of the plume. There is observational evidence of a downward inflow jet at the base of the plume in some cases, rather than just horizontal inflow (Palmer, 1981). These horizontal and vertical inflows can modify the wind conditions near a wildland fire and therefore influence the fire behaviour in a complex manner. The relative locations of the inflow convergence zone and the combustion region, which are associated with the ambient wind conditions, can affect the influence of the inflow on the fire behaviour. For example, under light ambient winds the convergence zone is often located close to the fire front, which results in stronger inflow at its centre than at the outer edges. This can result in the development of a parabolic fire geometry over time (Clark et al., 1996b,a). Alternatively, under strong ambient winds the convergence zone can move downwind of the fire front, which limits the influence of the inflow on the fire behaviour.

The three sources of atmospheric moisture during a wildland fire are the background atmospheric moisture, the combustion released moisture and the moisture released from vegetation by evapotranspiration (Potter, 2005). Energy is required to evaporate liquid water contained within the vegetation and up to 0.56 kg of water vapour can be released through complete combustion of 1 kg of totally dry woody material (Johnson and Miyanishi, 2001). The fuel moisture content prior to combustion therefore affects both the heat

and moisture fluxes associated with combustion. The total atmospheric moisture content can influence the vertical development of pyro-convective plumes, the formation of pyrocumulus and pyrocumulonimbus clouds and the likelihood of downbursts at the surface (Potter, 2005; Luderer et al., 2009). The precise role of atmospheric moisture on pyro-convective plume dynamics is under debate and remains an active area of research (Potter, 2012b).

Turbulent air motions, such as eddies and vortices, can affect fire behaviour through their influence on local winds, turbulent mixing of atmospheric properties and entrainment of ambient air into pyro-convective plumes (Clark et al., 1999; Coen et al., 2004). Vortices are typically present in turbulent planetary boundary layers and can also be generated by the thermal effects of wildland fires or through interaction of pyro-convective plumes with the surrounding atmosphere (Countryman, 1964, 1969). These vortices have a wide range of physical diameters, from several metres to hundreds of metres, and their axis of rotation can vary from horizontal to vertical. Vortices generated directly by a wildland fire are commonly referred to as "fire whirls" and their characteristics are associated with the rate of energy released through combustion, the atmospheric stability and the ambient wind conditions. Vortices embedded in the ambient flow can be modified as they pass over a wildland fire. For example, horizontal vortices can be modified to vertical vortices as they pass over a wildland fire due to the injection of energy, which lifts the axis of rotation (Clark et al., 1996b,a). Observed forward rates of fire spread are often highly variable and could be associated with the effects of turbulent air motions such as vortices.

Fire whirls share a number of characteristics in common with dust devils and tornadoes, and fire whirls have previously been observed to cause extensive wind damage to trees and man-made structures (Byram and Nelson, 1951; McRae et al., 2013). Pyro-convective plumes can interact with the ambient winds to form counter-rotating vortices downwind of the plume, which have previously been observed to confine the horizontal spread of smoke along the length of the plume (Cunningham et al., 2005). Vortices also play an important role in lofting and transporting firebrands outside of the combustion region. Counter-rotating vertical near-surface vortex pairs have previously been proposed as a mechanism for driving rapid wildland fire spread between them in a process known as "dynamic fingering" (Clark et al., 1996b,a, 1999; Coen et al., 2004).

1.3.3 Effects of Complex Terrain

Foehn winds are a common meteorological phenomenon worldwide that occur in the lee of mountainous terrain. The classic foehn mechanism involves orographic lifting of horizontal motion of air over mountainous terrain (Barry, 1992). If the rising air reaches the lifting condensation level, the latent heat release warms up the surrounding

atmosphere and results in orographic rainfall along the windward mountain slopes. As the drier air descends the leeward mountain slopes, the difference in saturated and dry adiabatic lapse rates results in increased air temperatures in the lee of the mountainous terrain relative to the windward side. Foehn winds can occur without accompanying precipitation if a regional pressure gradient drives horizontal motion of dry air above a mountain plateau downslope, or if orographic blocking of lower-level air allows drier upper-level air to flow across the mountains and downslope on the leeward side. Foehn winds are associated with increased air temperatures, with an increase of up to ∼15–20°C (Brinkmann, 1974), decreased relative humidities and increased wind speeds, often in excess of 100 km h^{-1}, in the lee of the mountains. Foehn winds have been observed to result in extreme wildland fire behaviour (Gorski and Farnsworth, 2000; Westerling et al., 2004) and contribute to loss of life and property (Miller and Schlegel, 2006).

Mountain waves are atmospheric internal gravity waves that can develop in horizontal motion of air over mountainous terrain under stable atmospheric conditions. Mountain wave characteristics are controlled by the vertical wind profile, atmospheric stability and terrain profile (Barry, 1992; Whiteman, 2000). The Froude number is commonly used to assess the likelihood of orographic blocking on the windward side of the mountains (Smolarkiewicz and Rotunno, 1989) and Scorer's parameter is commonly used to assess the likelihood of trapped lee waves developing (Scorer, 1949). Rotors can develop under mountain lee waves and are associated with localised high vertical and horizontal wind speeds (Doyle and Durran, 2002). Internal gravity wave breaking results in intense atmospheric turbulence and can result in severe downslope windstorms (Klemp and Lilly, 1975; Lilly, 1978; Whiteman, 2000).

Diurnal variations in insolation and air temperatures can drive diurnal anabatic upslope and katabatic downslope mountain winds. There are four wind systems that can occur in combination on mountainous terrain and are known as along-slope, along-valley, cross-valley and mountain-plain winds (Whiteman, 2000). The mechanical mechanisms that are involved in valley winds include the downward transport of momentum, forced channelling and pressure-driven channelling (Whiteman and Doran, 1993). Horizontal momentum can be transported vertically downwards through turbulent mixing and mountain waves, and the resulting winds are often in a similar direction to the winds aloft due to conservation of momentum. Forced-channelling occurs due to the greater surface friction along a valley than across it, and results in the realignment of partially cross-valley winds along the valley. Pressure-driven channelling occurs due to the along-valley component of the geostrophic pressure gradient, resulting in along-valley flow that can be in an opposite direction to the upper-level winds. The intense atmospheric turbulence associated with channelled flow and flow separation in the lee of a mountain ridge can transport large quantities of firebrands downwind (Sharples, 2009). Dynamic

channelling of winds in mountainous terrain was observed to be important in the 1994 South Canyon Fire in Colorado (Butler et al., 2001). The complexity of wind-terrain interactions, particularly in valleys and canyons, can lead to unpredictable and extreme wildland fire behaviour (Viegas and Pita, 2004).

Incident solar radiation can be highly variable across complex terrain and is controlled by the slope, aspect and relief of the terrain. The interaction of topography and solar insolation can influence atmospheric properties, such as the air temperature and humidity (McCutchan and Fox, 1986), and fuel properties, such as its moisture content. The ambient winds can influence the interaction of topography and insolation. In a well-mixed planetary boundary layer the altitude can directly affect the air temperature and relative humidity, with decreasing air temperatures and increasing relative humidities with increasing altitude (Whiteman, 2000). However, the relationship between altitude and the air temperature and relative humidity can be reversed during nighttime inversions, cold air drainage and subsidence inversions associated with synoptic high pressure systems (Sharples, 2009).

1.4 Wildland Fire Management

Wildland fire management is an important issue in many countries due to positive and negative impacts that wildland fires can have on people and the environment. Effective wildland fire management is therefore concerned with maximising the positive aspects of wildland fire, such as ecosystem maintenance of fire-prone vegetation types, and minimising the negative aspects, such as damage to property and loss of life. Fire management therefore encompasses a wide and complex range of issues and can be categorised into four broad objectives: reduction, readiness, response and recovery.

Reduction involves the minimisation of risk associated with wildland fire through the management of vegetation and people. It is widely accepted that forests and other ecosystems can benefit from a specific fire regime, in which wildland fires periodically burn off understory and dead vegetation, and promote growth of new vegetation. Fuel reduction burns are a common method of maintaining ecosystems and preventing the build-up of potentially dangerous heavy fuel loadings. However, there is still significant debate over the extent of fuel reduction burning (Penman et al., 2011). The communities at greatest risk from wildland fires are those in wild landscapes and the urban-wildland interface. A number of methods are used to reduce the risk of these vulnerable communities, including educating them about how to prepare for and respond to wildland fires and updating building codes to improve the wildland fire resistance of man-made structures. As the number of people living in the urban-wildland interface is projected to continue rising over the coming decades in many countries, reduction will become

increasingly important in fire management (Gibbons et al., 2012).

Readiness involves the preparation of fire suppression resources and vulnerable communities for wildland fires based on assessment of wildland fire risk. Although reduction can mitigate some of the risks associated with wildland fire, many countries still experience wildland fires that are destructive for people and the environment. Fire weather indices and fire danger rating systems are widely used by fire management to assess the state of the fire environment and wildland fire risk. This allows fire management agencies to prepare and allocate fire suppression resources, issue national and local fire danger warnings and prepare vulnerable communities.

Response involves suppression of wildland fires, particularly when they pose an appreciable risk to people, properties or the environment. This involves the deployment of fire fighting personnel and fire suppression equipment, such as wildland fire engines, bulldozers and helicopters, to suppress and bring under control a wildland fire. Incident management controllers and teams are used in many countries to manage the fire suppression resources and the level of incident management often varies with fire size or behaviour. Wildland fire suppression can involve both direct and indirect attack tactics, although indirect attack allows more effective planning. The techniques used in indirect attack include the construction of fire lines, using either hand tools or machinery, back burning using drip torches and dropping flame retardant chemicals on unburnt fuel ahead of the fire. Effective wildland fire suppression requires accurate information on the state of the fire environment and predictions of future wildland fire behaviour.

Recovery involves dealing with the post-fire impacts on affected communities and the surrounding environment. For example, wildland fires and associated fire suppression activities can result in soil erosion due to the loss of vegetation and affect local water quality. They can also affect local flora and fauna through changes to the local habitat and vegetation, which influences the population dynamics of many species. Smouldering of dense fuels can continue for many weeks after a wildland fire and result in further wildland fire ignitions. The emission of particulate matter and aerosols by a wildland fire can affect air quality and visibility in the surrounding area (Achtemeier, 2008). This can directly harm human health through aggravating respiratory problems, and reduced visibility can result in traffic and other accidents (Whiteman, 2000).

Scientific research has an important role to play in supporting all aspects of wildland fire management. Further research is needed to better understand how wildland fire behaviour responds to the surrounding fire environment through interactions across a wide variety of physical scales. Further research is also required into quantifying fire weather and fire danger using fire weather indices and fire danger rating systems, and effectively communicating fire danger warnings to communities. There is also a need for further research into the impact of wildland fires on ecosystems and communities.

1.5 Numerical Weather Prediction and Wildland Fire Behaviour Modelling

A broad range of numerical modelling tools are used to conduct scientific research into wildland fires and support wildland fire management in the assessment and prediction of wildland fire risk and behaviour. The numerical models utilised throughout this thesis fall into three categories: numerical weather prediction (NWP) modelling, wildland fire behaviour modelling and coupled atmosphere-fire modelling. A brief background of these categories is provided below.

NWP models use mathematical models of the atmosphere to predict the weather based on a set of initial conditions. Depending on the specific NWP model, they can be applied across a range of atmospheric scales, from planetary scale atmospheric Rossby waves to microscale atmospheric turbulence in the planetary boundary layer. NWP models are used operationally to predict fire weather conditions and are therefore utilised in wildland fire risk assessment and wildland fire behaviour modelling. NWP models can also be used to study long-term projected changes in fire weather and climate, which affects long-term planning in fire management. NWP models can also be used to study the influence of synoptic and mesoscale atmospheric processes on fire weather conditions. The wide range of applications of NWP modelling demonstrates their importance in wildland fire management and research.

Wildland fire behaviour models use mathematical models to predict fire behaviour based on a set of initial conditions. A number of different wildland fire behaviour models have been developed over the past few decades and they vary considerably in the complexity with which they represent wildland fire interactions with the surrounding fire environment, ranging from empirical to physical models (Sullivan, 2009a,b,c). These models have applications in supporting a range of fire management activities, including fire suppression, preparedness planning and incident response team training. At present, fire response teams predominantly use empirically based models due to their simplicity and ease of use. However, these empirical models are limited by their overly simplistic representation of the complex interactions between the fire environment and wildland fire behaviour. Although physical models can more realistically represent these complex interactions, they are often more difficult to use and require greater computational resources, which is not pratical during fire suppression operations. Validation of wildland fire behaviour models is currently an issue due to a lack of high quality observational data on wildland fire behaviour and its interaction with the fire environment.

Coupled atmosphere-fire models combine a wildland fire behaviour model with either an NWP or computational fluid dynamics (CFD) model. Unlike NWP models that are heated using a steady state heat source (Heilman, 1992; Heilman and Fast, 1992; Kiefer et al., 2008, 2009), the atmospheric model in a coupled atmosphere-fire model

is heated by a simulated wildland fire whose geometry and properties are modelled to change with time. This allows coupled atmosphere-fire models to directly simulate two-way coupled atmosphere-fire interaction processes like those described earlier. This is achieved through quasi-simultaneous modelling of wildland fire behaviour, which is influenced by the local atmospheric conditions, and the weather, which is influenced by the release of heat and moisture from the modelled fire. Only a few coupled atmosphere-fire models currently exist, including WRF-Fire (Mandel et al., 2011; Coen et al., 2013), FIRETEC (Linn et al., 2002) and WFDS (Mell et al., 2007, 2009). These coupled models have been shown to be capable of simulating physically realistic wildland fire behaviour in a number of different fire environments (Clark et al., 1996b,a; Cunningham et al., 2005; Cunningham and Linn, 2007; Mell et al., 2007; Sun et al., 2009). However, the complexity of operating these coupled models currently prevents their use in fire management.

1.6 Outline of Thesis

The main objective of this thesis is to investigate atmospheric interactions with wildland fire in a manner that will directly benefit end users in the fire management community both in New Zealand and internationally. This is achieved through the application of the WRF NWP and WRF-Fire coupled atmosphere-fire models across a broad range of physical scales. Chapters 2 – 5 present a series of interrelated studies that fit into the main objective of this thesis. Chapter 2 examines the suitability of WRF to simulate fire weather across New Zealand for the 2009/10 wildland fire season. Chapter 3 follows directly on from Chapter 2 and investigates the behaviour of modelled fire weather indices across New Zealand for the same wildland fire season. Chapter 4 then examines the fire weather conditions associated with an extreme foehn event across the South Island of New Zealand on 6 February 2011. Chapter 5 investigates the atmosphere-fire interaction processes associated with an atypical wildland fire spread phenomenon in high relief terrain known as fire channelling.

The NWP model used in Chapters 2 – 4 is version 3 of the Weather Research and Forecasting (WRF) model (Skamarock et al., 2008). The WRF model is being actively developed by the scientific community and is widely used in synoptic and mesoscale atmospheric modelling. The coupled atmosphere-fire model used in Chapter 5 is the WRF-Fire model, which combines a large eddy simulation variant of WRF with the SFIRE wildland fire behaviour model. WRF and WRF-Fire were chosen for use in this thesis as together they are capable of studying numerous aspects of atmospheric interactions with wildland fire behaviour over a range of physical scales.

At the time of writing, Chapters 2 – 5 are included in this thesis largely unchanged

from a series of research articles submitted for publication in peer reviewed scientific journals. Chapters 2 (Simpson et al., 2013b) and 3 (Simpson et al., 2013a) have been accepted pending minor and major revisions, respectively, by the International Journal of Wildland Fire. Chapter 4 has been submitted for peer review at Monthly Weather Review (Simpson et al., 2013d). Chapter 5 has been published online early by the International Journal of Wildland Fire (Simpson et al., 2013c). Some editorial changes, such as replacing grayscale figures with equivalent colour figures, have been made to the papers for their inclusion in this thesis. There is inevitably some overlap in the background material covered in these chapters due to their existence as independent self-contained research articles.

Chapter 2

Verification of WRF Modelled Fire Weather for the 2009/10 New Zealand Wildland Fire Season

C. C. Simpson[A], H. G. Pearce[B], A. P. Sturman[A], P. Zawar-Reza[A]

[A] Department of Geography, University of Canterbury, Christchurch, New Zealand
[B] Scion, Rural Fire Research Group, Christchurch, New Zealand

Abstract

The Weather Research and Forecasting (WRF) mesoscale model was used to simulate the fire weather conditions for the 2009/10 wildland fire season in New Zealand. The suitability of WRF to simulate the high-end fire weather conditions for this period was assessed through direct comparison with observational data taken from 23 surface and two upper-air stations located across New Zealand. The weather variables and fire weather indices considered in the verification were the 1200 NZST air temperature, relative humidity, wind speed and direction, 24-hr rainfall, New Zealand Fire Weather Index (FWI) and Continuous Haines Index (CHI). On observed high-end fire weather days, WRF underpredicted the air temperatures and relative humidities, and overpredicted the wind speeds and 24-hr rainfall at most weather stations. The results demonstrated that although WRF is suitable for modelling the air temperatures, there are issues with modelling the wind speeds and rainfall quantities. The model error in the wind speeds and 24-hr rainfall contributed significantly towards the model underprediction of the FWI on observed high-end fire weather days. In addition, the modelled was not suitable for predicting the number of high-end fire weather days at most weather stations, which represents a serious operational limitation of the WRF model for fire management applications. Finally, the modelled CHI values were only in moderate agreement with the observed values, principally

due to the model error in the dew point depression at 850 hPa.

2.1 Introduction

It is widely acknowledged that the weather is an important component of the wildland fire environment, alongside the fuel characteristics and topography (Countryman, 1972). The close association between wildland fires and the weather has led to worldwide development of fire weather indices to support fire management activities. Fire weather indices summarise specific aspects of the local atmospheric conditions and typically rate the severity of fire weather conditions using a numerical scale. These indices commonly incorporate weather variables such as the air temperature, relative humidity, wind conditions, precipitation and atmospheric stability. A number of fire weather indices form part of a more complete fire danger rating system. Examples include the Canadian Forest Fire Danger Rating System (CFFDRS) used in Canada (Van Wagner and Pickett, 1985; Van Wagner, 1987; Stocks et al., 1989), the National Fire Danger Rating System used in the United States (Deeming et al., 1977) and the McArthur Forest Fire Danger Index used in Australia (McArthur, 1966, 1967).

The New Zealand Fire Danger Rating System (NZFDRS) is used operationally in New Zealand to support a wide variety of fire management activities, including allocation of firefighting equipment and development of fire suppression strategies (Anderson, 2005). The NZFDRS is based on the CFFDRS and has been specifically modified for use in New Zealand (Alexander, 1992, 1994, 2008; Fogarty et al., 1998). The New Zealand Fire Weather Index (FWI) is an important component of the NZFDRS and is the primary tool used for fire weather assessment in New Zealand. The FWI is calculated at individual weather stations located across New Zealand using near-surface weather station measurements taken at 1200 New Zealand Standard Time (NZST). The Haines Index (Haines, 1988) is also used in a limited context operationally, although there is little understanding of how the index relates to fire danger and behaviour specifically in New Zealand. National gridded forecasts of the FWI and Haines Index are issued by the New Zealand MetService (NZMS) and are derived from numerical weather prediction (NWP) model output.

Previous studies on fire weather and climate in New Zealand have typically focused specifically on the FWI and observational data collected at weather stations (Pearce, 1996, 2003; Pearce et al., 2011b). There are two main limitations to this approach. First, the weather station data are only available at relatively coarse spatial resolution across New Zealand, particularly in mountainous regions such as the Southern Alps. This is an important issue given the highly variable nature of weather throughout the complex terrain of New Zealand. Second, there has been limited consideration of fire weather

conditions aloft and there are few upper-air stations in New Zealand. NWP modelling of the three-dimensional fire weather conditions at high spatial resolution could partially resolve these two issues. However, there have been no dedicated studies on the suitability of NWP modelling of fire weather in New Zealand. Oreskes et al. (1994) have previously highlighted the importance of building trust in numerical modelling through careful evaluation of its output.

There have been few studies worldwide on the suitability of NWP modelling of fire weather conditions. Mölders (2008) investigated the accuracy with which the Weather Research and Forecasting (WRF) model predicted the fire weather in a boreal forest environment in interior Alaska. Hoadley et al. (2004) investigated the accuracy with which the Pennsylvania State University – National Center for Atmospheric Research Mesoscale Model predicted the fire weather for western Montana and northern Idaho at three different horizontal resolutions. The results presented in these studies suggest that there may be significant model errors for important fire weather variables, including the relative humidity and wind speed. This has implications for NWP modelling of the FWI, which is partially derived from these weather variables.

New Zealand has extensive areas of rural land, which are primarily covered by natural forests, scrubland and agricultural grasslands. According to National Rural Fire Authority data, in the 2009/10 fire season there were a total of 3,858 recorded wildland fires, which burned a total area of 5,253 ha. The number of wildland fires and total area burned was highest in the eastern South Island and northern North Island. The majority of these fires were ignited anthropogenically, through ignition mechanisms such as land clearing, camp fires and machinery. The 2009/10 fire season was chosen as it is the most recent season for which a high-quality fire weather climatology is available for comparison with NWP model output. It was not an especially severe fire season and could be considered relatively average compared to previous fire seasons.

The principal aim of this study is therefore to investigate the suitability of NWP modelling of fire weather conditions for the 2009/10 wildland fire season in New Zealand. This is achieved through a direct comparison of the NWP model output with observational data taken from weather stations across New Zealand. The next section describes the methods used throughout this paper, and includes a description of the NWP model configuration, the fire weather indices and the model verification techniques. The model verification results and a discussion of these results are provided in the subsequent two sections. This is followed by the summary and conclusions in the closing section.

2.2 Methods

2.2.1 Numerical Weather Prediction Model

Version 3.2 of the WRF mesoscale NWP model (Skamarock et al., 2008) is used to simulate the fire weather conditions of the 2009/10 wildland fire season. The WRF model was chosen as it is widely used by the scientific community to model synoptic and mesoscale atmospheric processes.

A two-way nested two domain configuration is used to model synoptic and mesoscale atmospheric processes across New Zealand. The parent and nested domains have a horizontal grid spacing of 24 and 8 km, respectively, and a computational domain of 100×100 and 142×196 grid points, respectively. The parent domain extends far out into the Tasman Sea and Pacific Ocean, and the nested domain covers all of mainland New Zealand. The two domains share an identical configuration of 50 vertical levels, which extend from a height of around 16 m above ground level to a fixed model pressure top of 50 hPa. The parent domain is nudged at six-hourly intervals using the National Centers for Environmental Prediction (NCEP) Final Analyses (FNL).

WRF utilises fully compressible non-hydrostatic equations and has a mass-based terrain-following coordinate system. The microphysics are represented by a single-moment six-class scheme with mixed-phase processes (Hong and Lim, 2006). The sub-grid scale effects of convective or shallow clouds are modelled in the parent domain using the modified Kain-Fritsch scheme (Kain, 2004). The surface layer and planetary boundary layer are represented by the Eta schemes (Janjic, 1990, 1996, 2002). The heat and moisture fluxes over land are provided by the Noah Land Surface Model (Chen and Dudhia, 2001), which has soil temperature and moisture in four layers, fractional snow cover and frozen soil physics. The short-wave and long-wave radiation are represented by a simple short-wave radiation scheme (Dudhia, 1989) and the Rapid Radiative Transfer Model (Mlawer et al., 1997), respectively. A gravity wave damping layer (Klemp et al., 2008) is used to prevent gravity wave reflection off the upper boundary. Due to the long duration of the simulation, the deep soil and sea surface temperature are regularly updated (Zeng and Beljaars, 2005), and the albedo and vegetation fractions are re-evaluated monthly. The main model time steps are 60 and 20 s for the parent and nested domains, respectively, with time integration performed using a third-order Runge-Kutta scheme (Wicker and Skamarock, 2002). This setup for the physics and dynamics options represents a relatively standard WRF model configuration.

The WRF model simulation covers the period from 0000 NZST on 1 July 2009 to 0000 NZST on 1 April 2010. The first month of the simulation is regarded as the spin-up period and is not considered in the results. The remaining eight month period covers the 2009/10 New Zealand fire season. The model output is taken at hourly intervals

and matches the timing of the weather station measurements. The air temperature and relative humidity are taken at a height of 2 m above ground level, whereas the wind speed and direction are taken at a height of 10 m above ground level.

2.2.2 Fire Weather Indices

Fire weather conditions are commonly assessed through consideration of weather variables associated with wildland fire behaviour, such as the relative humidity and wind speed, and fire weather indices derived from such weather variables. The fire weather indices specifically considered in this study are the New Zealand Fire Weather Index (FWI) and Continuous Haines Index (CHI) (Mills and McCaw, 2010). Although the FWI is used operationally in New Zealand, the CHI is currently under consideration for operational implementation in New Zealand.

The FWI is a fire behaviour index that represents the wildland fire intensity for a reference fuel type, although it is also commonly used as an indicator of fire danger (Lawson and Armitage, 2008). The FWI is derived from two intermediate fire behaviour indices, known as the Initial Spread Index (ISI) and Build Up Index (BUI). The ISI represents the expected rate of spread and the BUI represents the fuel available for combustion. The ISI is derived from the wind speed and Fine Fuel Moisture Code (FFMC), whereas the BUI is derived from the Duff Moisture Code (DMC) and Drought Code (DC). The FFMC, DMC and DC are fuel moisture indices that are calculated once daily based on the near-surface air temperature, relative humidity, wind speed and 24-hr rainfall at 1200 NZST. They are calculated iteratively, such that their value on a given day is directly dependent on the previous day's value. The FFMC represents the ease of ignition and flammability of fine fuels, the DMC represents the expected fuel consumption in duff layers and moderately sized fuels, and the DC represents the seasonal drought effect on deep organic layers and large sized fuels.

This system of indices collectively accounts for the impact of near-surface weather conditions on the fuel moisture and potential fire behaviour. The FWI is typically around 5 to 15 across most of New Zealand, although it can exceed 80 under extreme fire weather conditions (Pearce et al., 2011b). Four fire danger classes, which are determined directly from the FWI, have been developed for use in forested regions in New Zealand (Alexander, 1994, 2008). These fire danger classes are: "Low" (0 – 7), "Moderate" (8 – 16), "High" (17 – 31) and "Extreme" (32+).

The CHI is a stand-alone fire weather index that is based on the widely used Haines Index (Haines, 1988). The CHI provides a combined measure of the instantaneous atmospheric stability and humidity aloft. The stability index is calculated from the air temperature difference between 850 and 700 hPa, and the humidity index is calculated from the dew point depression at 850 hPa. More unstable atmospheric conditions, which

result in a higher air temperature lapse rate, and drier atmospheric conditions, which result in a higher dew point depression, both result in higher CHI values. The CHI is mathematically limited to a minimum value of zero and does not typically exceed values of 12 to 14 in southern Australia.

2.2.3 Model Verification

Figure 2.1 shows the geographical location of the 25 weather stations used in the model verification. This includes 23 stations with near-surface observations suitable for deriving the FWI, and two stations, Whenupai and Paraparaumu, with upper-air observations suitable for deriving the CHI. The 23 surface stations collectively represent most of the main fire climate regions of New Zealand (NZMS, 1983) and are located at a mix of coastal and inland locations. The near-surface data include 1200 NZST observations of the air temperature, relative humidity, wind speed and direction, and 24-hr rainfall. The air temperature and relative humidity are measured at 1.2 m above ground level, whereas the wind conditions are measured at 10 m above ground level. The two upper-air stations are the only sites with regularly available 1200 NZST observations of the air and dew point temperatures at 850 and 700 hPa. Most of the weather stations are operated by either the NZMS or the National Institute of Water and Atmospheric Research (NIWA).

Weather station data were obtained from the National Climate Database (NCD), which is maintained by NIWA, and the fire weather climatology (FWC) developed by Pearce (1996, 2003) and Pearce et al. (2011b). The NCD data are available hourly with one decimal point precision, whereas the FWC data are available once daily at 1200 NZST with integer precision. The NCD data are primarily used in the model verification, although there are some missing observations, which typically occur in groupings of a few hours and are likely due to equipment faults. The FWC data are used to initialise the FFMC, DMC and DC values on 31 July 2009, and are used in place of missing NCD data. Across the 23 surface weather stations, the FWC data are used in place of the missing NCD data on 27, 29, 29 and 33 instances for the air temperature, relative humidity, wind speed and wind direction, respectively.

In order to assess the model accuracy, a nearest neighbour algorithm is used to match each weather station to its nearest WRF model grid cell over land. No interpolation of the WRF model output is required as each model grid cell represents the average atmospheric conditions across it (Pielke Sr., 2002). However, there are limitations to this approach that can result in large apparent model errors at specific locations (White et al., 1999; Davis and Carr, 2000; Mass et al., 2002). For example, small errors in the timing and spacing of otherwise accurately modelled weather features can result in large apparent model errors if the fire weather conditions vary considerably over short distances.

The weather variables and fire weather indices specifically considered in the model

verification are the air temperature, relative humidity, wind speed and direction, 24-hr rainfall, FWI and CHI. These variables are all assessed at 1200 NZST, as this represents the time of greatest relevance to fire management operations in New Zealand. The first step in the model verification involves determining the observed and modelled daily FWI values and fire danger classes (Low, Moderate, High and Extreme) at the 23 surface weather stations. For the wind direction on observed high-end fire weather days, the model output and weather station data are compared visually using wind roses. A set of verification statistics is calculated for the air temperature, relative humidity, wind speed, 24-hr rainfall and FWI at the 15 weather stations that have ten or more observed high-end fire weather days (High or Extreme fire danger class). The verification statistics are calculated only for those observed high-end fire weather days and include the number of days (N), mean of observed values ($\bar{O}$), mean of modelled values ($\bar{M}$), standard deviation of observed values (S_O), standard deviation of modelled values (S_M), mean bias error (MBE), mean absolute error (MAE) and index of agreement (IOA) (Willmott, 1981; Jolliffe and Stephenson, 2003).

The IOA is a desciptive statistic that reflects the degree to which the observed variate is accurately estimated by the simulated variate (Willmott, 1981). Unlike the Pearson product-moment correlation coefficient, the IOA is not a measure of correlation, but instead measures the degree to which model predictions are free of error. It varies between 0.0 and 1.0, where a value of 1.0 indicates perfect agreement and a value 0.0 indicates complete disagreement. It is calculated as:

$$\mathrm{IOA} = 1 - \frac{\sum_{i=1}^{N} \left(M_i - O_i\right)^2}{\sum_{i=1}^{N} \left[\left|M_i - \bar{O}\right| + \left|O_i - \bar{O}\right|\right]^2} \tag{2.1}$$

where M_i and O_i are the modelled and observed values of data point i, respectively.

An additional set of five verification statistics are calculated for the 24-hr rainfall. The 24-hr rainfall is given a binary value based on a rainfall threshold of 0.5 mm, which is the minimum quantity required to directly influence the FWI. The binary values are used to assign one of four classifications to each day: "hit", "false alarm", "miss" or "correct rejection". These four binary classifications are used to determine the following statistics: observed rate (OR), modelled rate (MR), hit rate (HR), false alarm rate (FR) and percentage correct (PC) (Jolliffe and Stephenson, 2003).

An additional set of four IOA values are calculated for the FWI, based on independent substitution of the observed 1200 NZST air temperature (IOA_T), relative humidity (IOA_H), wind speed (IOA_W) and 24-hr rainfall (IOA_R). Direct comparison of these IOA values indicates the relative importance of the model error in each individual weather variable for the model error in the FWI.

As the FWI is derived from the FFMC, DMC and DC, which are calculated iteratively

each day, it is possible for the model error in the FWI to accumulate over monthly to seasonal timescales. The importance of this model error accumulation is investigated through resetting the modelled FFMC, DMC and DC values with corresponding observed values at specific intervals. The reset period is varied from 5 to 50 days, inclusive, in steps of five days and the IOA statistic is calculated at the 15 weather stations for each reset period considered. If the IOA values decrease significantly with increasing reset period, this would indicate that model error accumulation over monthly to seasonal timescales is important for the FWI.

A similar methodology to that used to assess the modelled FWI is used to evaluate the modelled CHI at the Whenupai and Paraparaumu upper-air stations. The verification statistics are calculated for days where the observed CHI is greater than or equal to five, which represents the upper end of the index scale. The IOA is then re-calculated at both stations for independent substitution of the observed air temperature difference between 850 and 700 hPa, and the dew point depression at 850 hPa.

2.3 Results

Table 2.1 presents the number of observed and modelled days in each fire danger class at the 23 surface weather stations. At all stations the observed and modelled Low class occurs most frequently, although the number of days within this class varies significantly across the stations. There are observed High or Extreme days at 19 stations, although there are only 15 stations at which the number of high-end fire weather days is greater than or equal to ten. These are the same 15 stations at which the verification statistics are calculated for the weather variables and FWI. The Wellington and Tara Hills stations have the highest number of observed Extreme days with 17 days each. The number of modelled Extreme days is higher than that observed at 16 stations, with the highest overprediction at stations in the eastern South Island, including Kaikoura, Christchurch and Dunedin.

Figure 2.2 shows the frequency distributions of the observed and modelled fire danger classes at Wellington and Tara Hills. At Wellington the number of modelled Extreme days is zero, compared with 17 observed days. Wellington is the only station at which the model underpredicts the number of observed Extreme days by more than one day. This represents a significant shift of the modelled frequency distribution towards lower values relative to the observed distribution. At Tara Hills the model underpredicts the number of observed Low days by 22 days and overpredicts the number of High and Extreme days by 10 days each. This represents a significant shift of the modelled frequency distribution towards higher values relative to the observed distribution. The results presented in Table 2.1 indicate that at most stations the modelled probability

distribution is shifted rightwards towards higher values.

Table 2.2 presents the verification statistics calculated for the air temperature on observed high-end fire weather days. The mean observed air temperature ranges from a minimum of 18.1°C at Queenstown to a maximum of 24.1°C at Gisborne. In contrast, the mean modelled air temperatures vary more widely, from a minimum of 14.2°C at Queenstown to a maximum of 23.4°C at Gisborne. The MBE is negative at each station aside from Rotorua, where it is zero. The MBE is most negative at Wellington, Queenstown and Tara Hills, and the MAE is also highest at these same stations. The MAE is considerably lower at the other 12 stations, varying from 1.1 to 2.4°C. The IOA is greater than 0.80 at nine stations, indicating a good level of agreement, and has a minimum of 0.63 and 0.65 at Wellington and Kaitaia, respectively.

Table 2.3 presents the verification statistics calculated for the relative humidity on the observed high-end fire weather days. The mean observed relative humidities range from a minimum of 31.2 % at Tara Hills to a maximum of 62.4 % at Wellington. In comparison, the mean modelled relative humidity ranges from a minimum of 41.3 % at Rotorua to 65.1 % at Wellington. The standard deviations of the modelled relative humidities are higher than those observed at 12 stations, often by a significant margin at stations located in the North Island. The MBE is negative at ten stations and is lowest at Rotorua, where it is −17.0 %. In comparison, the MBE is highest at Queenstown and Tara Hills, where it is 9.2 and 13.8 %, respectively. The MAE ranges from a minimum of 4.2 % at Gore to a maximum of 19.7 % at Rotorua. In contrast to the air temperature, the IOA is only greater than 0.80 at Kaikoura and Dunedin, and is lower than 0.60 at seven stations, indicating only moderate level of agreement.

Table 2.4 presents the verification statistics calculated for the 24-hr rainfall on observed high-end fire weather days. The mean observed 24-hr rainfall is low at each station, ranging from a minimum of 0.01 mm at Christchurch to a maximum of 0.22 and 0.24 mm at Dunedin and Kaikoura, respectively. In contrast, the mean modelled 24-hr rainfall is typically significantly higher than that observed, and ranges from a minimum of 0.11 mm at Rotorua and Tauranga, to a maximum of 1.03 and 1.07 mm at Kaikoura and Dunedin, respectively. The MBE is positive at each station and is greater than or equal to 0.20 mm at ten stations. Similarly, the MR is greater than the OR at each station, and the OR is zero at Hamilton, Palmerston North and Christchurch, resulting in an undefined HR. Unlike the HR and FR, which vary significantly across the 15 stations, the PC is relatively consistent and ranges from a minimum of 69 % at Kaikoura to a maximum of 94 % at Rotorua.

Table 2.5 presents the verification statistics calculated for the wind speed on observed high-end fire weather days. The mean observed and modelled wind speeds are both highly variable, ranging from a minimum of 21.3 and 22.9 km h^{-1} at Hamilton and Kaitaia,

respectively, to a maximum of 45.5 and 50.0 km h^{-1} at Gore, respectively. The standard deviations of the observed and modelled wind speeds are typically higher at the stations located in the South Island, including at Kaikoura, Timaru and Tara Hills. The MBE is positive at 12 stations and is greater than or equal to 8.5 km h^{-1} at five stations located in the southern and eastern South Island. In contrast, at Wellington the mean observed wind speed is high, with a value of 38.7 km h^{-1}, and the MBE is most negative, with a value of -5.0 km h^{-1}. The IOA ranges from a minimum of 0.50 at Christchurch to a maximum of 0.79 at Kaitaia, Rotorua and Taupo, and is higher than 0.70 at eight stations.

Figure 2.3 shows the observed and modelled wind roses for observed high-end fire weather days. The most frequently observed and modelled wind directions are south-westerly, westerly and northwesterly. The exceptions are Wellington, where the most frequent observed and modelled wind direction is northerly, and Christchurch, where the most frequent observed wind direction is northeasterly. The most frequently observed and modelled wind directions match at seven of the eight North Island stations, and only at Gore in the South Island.

Table 2.6 presents the verification statistics calculated for the FWI on observed high-end fire weather days. The mean observed FWI varies from a minimum of 19.2 at Rotorua, where there are 17 and zero observed High and Extreme days, respectively, to a maximum of 31.7 at Tara Hills, where there are 22 and 17 observed High and Extreme days, respectively. The MBE is negative at 12 stations and is lower than -7.0 at eight stations, six of which are located in the North Island. The MAE is high at all stations, ranging from a minimum of 8.3 and 8.6 at Palmerston North and Gore, respectively, to a maximum of 17.2 and 18.4 at Rotorua and Timaru, respectively. The standard deviations of the modelled FWI are typically significantly higher than the standard deviations of the observed FWI, and is only lower at Wellington. The IOA varies significantly and ranges from a minimum of 0.16 and 0.19 at Gisborne and Hamilton, respectively, to a maximum of 0.55 and 0.63 at Wellington and Christchurch, respectively.

Substitution of the observed air temperatures typically results in limited improvement in the IOA and even results in a decreased IOA at eight stations. Substitution of the observed relative humidities, wind speeds and 24-hr rainfall results in the greatest improvement in the IOA at three, seven and six weather stations, respectively. At Tara Hills, substitution of the observed relative humidities and 24-hr rainfall both independently result in an improvement in the IOA from 0.51 to 0.66. At Rotorua there is no improvement in the IOA from its original value of 0.26 through substitution of observed weather variables.

Figure 2.4 shows the variation of the IOA, calculated for the FWI on observed high-end fire weather days, with reset period for the FFMC, DMC and DC at the 15 weather

stations. At most stations there is a slight downward trend in the IOA with increasing reset period. However, the absolute change in the IOA between a reset period of 5 and 50 days is typically relatively small. For three stations the IOA is higher for a reset period of 50 days than for 5 days. At a number of stations there is considerable variability in the IOA with varying reset period.

Table 2.7 presents the verification statistics calculated for the CHI on days with an observed CHI greater than five. The number of days that fall within this high-end range represent around 21 % of all fire season days at both stations. On those days, the model typically underpredicts the observed CHI, as demonstrated by the negative MBE values of -0.9 and -1.5 at Whenupai and Paraparaumu, respectively. The IOA values of 0.61 and 0.62 at Whenupai and Paraparaumu, respectively, indicate only a moderate level of agreement between the observed and modelled CHI. Substitution of the observed air temperature difference between 850 and 700 hPa results in only a moderate improvement in the IOA, whereas substitution of the observed dew point depression at 850 hPa results in a significantly greater improvement in the IOA to 0.92 at Whenupai and 0.91 at Paraparaumu.

Figure 2.5 shows the frequency distributions of the observed and modelled CHI at Whenupai and Paraparaumu. The frequency distributions of the observed CHI are broadly similar at both stations and there are 28 and 31 days with a CHI value of zero at Whenupai and Paraparaumu, respectively. The model significantly underpredicts the number of days with a zero CHI value at both stations. At both stations the modelled and observed CHI values do not exceed a value of 12 and are relatively infrequently greater than 5. At both stations the model slightly overpredicts the number of days with a CHI value exceeding 5. This represents a rightward shift of the modelled frequency distributions towards higher CHI values than those derived from observations.

2.4 Discussion

On average, the model underpredicted the air temperatures on the observed high-end fire weather days. However, this cold bias had only a limited impact on the assessed accuracy of the modelled FWI. The air temperature was arguably the most accurately modelled of the four weather variables considered across New Zealand. In addition, the model also underpredicted the relative humidities at most weather stations located in the North Island on the observed high-end fire weather days. In comparison with the air temperatures, the model error in the relative humidities had a more notable impact on the accuracy of the modelled FWI. Although not specifically tested, the model bias in the air temperatures and relative humidities could be related to errors in the NCEP FNL, which are used to nudge the model outer domain.

The model error characteristics are somewhat unique at Queenstown and Tara Hills compared to the other stations. The MBE is at its lowest and highest for the air temperature and relative humidity, respectively, at these two stations. The Queenstown and Tara Hills stations are located inland in relatively complex terrain, where the weather station surface elevation is considerably lower than the corresponding WRF model grid cell surface elevation. The height difference is 260 and 196 m at Queenstown and Tara Hills, respectively, compared with a height difference of less than 80 m at the other stations. If the air temperature lapse rate was a constant 6.5°C km^{-1}, then the MBE at Queenstown and Tara Hills due to the height difference alone would be −1.7 and −1.3°C, respectively. The height difference therefore likely accounts for a significant fraction of the model error in the air temperatures and relative humidities at Queenstown and Tara Hills.

The wind conditions on observed high-end fire weather days were arguably least accurately modelled at Kaikoura, Christchurch, Timaru, Queenstown and Dunedin. Queenstown is located inland in relatively complex terrain, whereas the other stations are located in comparatively flat terrain near complex coastlines. It is unclear if the model error at these stations is mainly associated with the relatively coarse model representation of the terrain and coastline, or the modelled atmospheric processes that affect local wind conditions on high-end fire weather days in the southern and eastern South Island. For example, the Kaikoura station is located on a peninsula that extends approximately 5 km into the Pacific Ocean and is therefore too small to be represented in the relatively coarse model terrain.

The most frequent modelled wind direction at Christchurch was northwesterly, which can be associated with a local northwesterly foehn wind known as the "Canterbury Northwester". In contrast, the most frequent observed wind direction was northeasterly, which is not commonly associated with foehn winds. It is possible that the model overpredicted the occurrence of northwesterly foehn winds at Christchurch, and possibly also Kaikoura. This could also explain the notable model overprediction of the number of modelled Extreme fire danger class days in the eastern South Island, particularly at Christchurch, Kaikoura, Timaru and Dunedin.

On average the model overpredicted the number High and Extreme fire danger class days at most weather stations, particularly in the eastern South Island as described above. The main exception to this model overprediction was at Wellington, where there were 17 and zero observed and modelled Extreme days, respectively. The observed weather variables imply that the high wind speeds are mainly responsible for the large number of observed high-end fire weather variables at Wellington. However, the model underpredicted the wind speeds at Wellington by 5.0 km h^{-1} on average, suggesting that the model underprediction of the wind speeds at 1200 NZST was mainly responsible for

the model's inability to accurately capture the number of Extreme days at Wellington.

Somewhat counter-intuitively, the model underpredicted the FWI on the observed high-end fire weather days at most weather stations, in addition to overpredicting the number of high-end fire weather days. This result indicates that the model must overpredict the FWI on observed Low or Moderate fire danger class days at most weather stations. The model underprediction of the FWI on observed high-end fire weather days seems to be mainly associated with the often significant model overprediction of the 24-hr rainfall at each weather station. In contrast, the model underprediction of the relative humidities and overprediction of the wind speeds would act to overpredict the FWI. The lack of a downward trend of the IOA calculated for the FWI with varying reset period at most weather station suggests that there is only limited model error accumulation in the fuel moisture and fire behaviour indices.

Similarly to the FWI, on average the model underpredicted the CHI on days with a high observed CHI value, but overpredicted the number of days with a high observed CHI value. For the limited sample of two stations considered, the modelled CHI was only in moderate agreement with the observed values, and the model error was mainly associated with the model error in the dew point depression at 850 hPa. The CHI is likely to exhibit considerable spatial variability across New Zealand, particularly near the mountainous terrain of the Southern Alps, and it is unclear if these model errors will apply throughout New Zealand.

2.5 Summary and Conclusions

This paper has investigated the suitability of the WRF NWP model to simulate the fire weather conditions during the 2009/10 New Zealand wildland fire season. The weather variables and fire weather indices considered in the model verification were the air temperature, relative humidity, wind speed and direction, 24-hr rainfall, FWI and CHI taken at 1200 NZST. The model verification was primarily performed through the calculation of a set of verification statistics for each weather variable and fire weather index at a total of 25 weather stations located across New Zealand. The analysis concentrated on the observed high-end fire weather days, which were determined using the derived FWI and CHI values at each weather station.

The model underpredicted the air temperatures and relative humidities at most weather stations across New Zealand. Further research is required to identify the cause of this model bias, although it could be related to errors in the NCEP FNL used to periodically nudge the outer model domain. Further research is needed to identify the suitability of bias correction of the modelled air temperatures and relative humidities, particularly at those weather stations where there is a known difference in surface elevation between

the WRF model grid cell and the station. In addition, the model overpredicted the rainfall quantity and number of rainfall events at each weather station, which contributed significantly towards the model underprediction of the FWI at most weather stations. It is widely accepted that accurate prediction of rainfall events and the rainfall quantity is difficult to achieve with NWP modelling. Finally, the model overpredicted the wind speeds at most weather stations, particularly in the eastern South Island. The modelled wind conditions were typically least accurate for weather stations located in complex terrain or near complex coastlines, which is alo a widely acknowledged issue with NWP modelling.

The model typically underpredicted the FWI on the observed high-end fire weather days, whereas it also overpredicted the number of High and Extreme fire danger class days at most weather stations. In particular, the model overpredicted the number of Extreme days by ten or more days at seven of the 23 surface weather stations, icluding several stations located along the eastern North Island and South Island. The most notable exception to this was at Wellington, where there were 17 and zero observed and modelled Extreme days, respectively. These large errors in the number of modelled High and Extreme days represent a serious limitation of the operational utility of the WRF model for fire management activities. The model errors in the FWI had a high degree of spatial variability across New Zealand, which implies that local terrain effects and atmospheric processes play an important role in modifying these errors. Further research is required to identify the spatial weather patterns associated with the FWI model errors across New Zealand.

Similarly to the FWI, the model underpredicted the CHI on days with an observed value greater than or equal to five, but overpredicted the number of these days, at both the Whenupai and Paraparaumu stations. The model error in the CHI was principally due to the model error in the dew point depression at 850 hPa, and not the air temperature difference between 850 and 700 hPa. There is a lack of additional upper-air stations at which to assess the suitability of WRF to model the CHI. It is therefore unclear how accurately the model can predict the CHI across most of New Zealand.

The results presented in this study have clearly demonstrated that, as has been found in other geographical regions (Hoadley et al., 2004; Mölders, 2008), there are several issues with NWP modelling of fire weather conditions in New Zealand. It remains unclear what benefits NWP modelling of fire weather and climate in New Zealand offers over other methods, such as interpolation of weather station data (Pearce, 2003; Pearce et al., 2011b). This could be more comprehensively tested through a direct comparison of NWP model output with the NIWA "virtual climate station network", which offers 5×5 km gridded interpolated observational data across New Zealand daily at 0900 NZST.

Further research is required to examine in detail the effects of varying the NWP model

setup on the assessed accuracy of modelled fire weather conditions in New Zealand. First, a variety of different model horizontal resolutions could be tested to examine the associated changes in the modelled fire weather conditions, particularly the wind conditions over complex terrain on extreme fire weather days. This could be done over a shorter case study period of, for example, one month. Second, a series of different combinations of model parameterisatons could be tested to determine which setup is most appropriate for modelling fire weather conditions in New Zealand. Particular attention will be paid to the microphysics and cumulus parameterisations, because of the close association between the 24-hr rainfall and the FWI. Third, the ECMWF re-analysis will be used instead of the NCEP FNL to nudge the model. Fourth, the NWP model used operationally by the NZMS to provide FWI forecasts across New Zealand will be tested and compared with the WRF model.

Table 2.1: Number of observed (AWS) and modelled (WRF) days in each fire danger class at the 23 surface weather stations. The fire danger classes are determined based on the FWI value: Low (0–7), Moderate (8–16), High (17–31), Extreme (32+).

Weather Station	Low		Moderate		High		Extreme	
	AWS	WRF	AWS	WRF	AWS	WRF	AWS	WRF
Kaitaia	130	153	59	53	53	37	1	0
Auckland	167	150	67	62	8	31	1	0
Tauranga	143	157	58	51	36	29	6	6
Hamilton	180	164	43	50	19	25	1	4
Rotorua	180	166	46	39	17	32	0	6
Gisborne	157	119	61	64	24	48	1	12
Taupo	165	163	61	45	16	31	1	4
New Plymouth	218	190	21	36	4	14	0	3
Waiouru	217	162	26	44	0	32	0	5
Palmerston North	179	151	54	49	10	40	0	3
Wellington	103	127	79	77	44	39	17	0
Westport	220	223	20	16	3	4	0	0
Kaikoura	154	109	73	58	14	54	2	22
Hokitika	242	238	1	5	0	0	0	0
Christchurch	130	113	69	53	35	51	9	26
Timaru	123	121	81	53	26	44	13	25
Tara Hills	167	145	37	39	22	32	17	27
Milford Sound	238	229	5	13	0	1	0	0
Queenstown	123	131	71	47	44	48	5	17
Manapouri	218	117	17	62	7	54	1	10
Dunedin	140	89	61	65	38	59	4	30
Gore	216	165	17	49	8	25	2	4
Invercargill	236	141	7	73	0	23	0	6

Table 2.2: Verification statistics calculated for the air temperature (°C) at 1200 NZST on observed high-end fire weather days.

Weather Station	N	$\bar{O}$	$\bar{M}$	S_O	S_M	MBE	MAE	IOA
Kaitaia	54	22.1	20.2	1.6	2.2	−1.9	2.1	0.65
Tauranga	42	22.3	20.7	2.1	2.4	−1.6	2.0	0.72
Hamilton	20	20.7	19.5	2.0	2.5	−1.2	1.5	0.81
Rotorua	17	20.2	20.2	1.8	2.2	0.0	1.9	0.89
Gisborne	25	24.1	23.4	3.0	3.2	−0.7	2.1	0.78
Taupo	17	19.4	18.0	2.1	2.9	−1.4	1.6	0.84
Palmerston North	10	19.0	16.7	3.2	3.3	−2.3	2.4	0.84
Wellington	61	18.8	15.5	2.8	2.3	−3.3	3.4	0.63
Kaikoura	16	19.2	18.5	4.3	5.1	−0.7	2.0	0.88
Christchurch	44	20.1	19.1	4.5	4.3	−1.0	2.3	0.88
Timaru	39	20.2	18.8	5.6	5.2	−1.4	2.3	0.93
Tara Hills	39	19.0	14.6	4.0	4.1	−4.4	4.4	0.74
Queenstown	49	18.1	14.2	4.4	4.3	−3.9	4.0	0.79
Dunedin	42	19.3	18.6	5.1	4.8	−0.7	1.7	0.94
Gore	10	20.0	19.5	3.2	3.2	−0.5	1.1	0.95

Table 2.3: Verification statistics calculated for the relative humidity (%) at 1200 NZST on observed high-end fire weather days.

Weather Station	N	$\bar{O}$	$\bar{M}$	S_O	S_M	MBE	MAE	IOA
Kaitaia	54	56.2	55.5	9.6	11.3	−0.7	8.4	0.69
Tauranga	42	50.3	50.0	6.6	10.3	−0.3	7.8	0.63
Hamilton	20	56.1	53.1	6.5	11.3	−3.0	9.7	0.57
Rotorua	17	58.3	41.3	10.5	15.9	−17.0	19.7	0.48
Gisborne	25	48.1	41.8	8.9	11.1	−6.3	10.8	0.56
Taupo	17	59.8	52.0	8.3	13.3	−7.8	11.6	0.56
Palmerston North	10	57.2	50.9	8.1	15.1	−6.3	12.1	0.47
Wellington	61	62.4	65.1	13.0	14.2	2.7	9.8	0.75
Kaikoura	16	52.0	47.5	24.9	20.5	−4.5	13.5	0.85
Christchurch	44	46.0	44.0	13.6	12.0	−2.0	10.9	0.66
Timaru	39	36.9	42.0	13.0	14.5	5.1	11.3	0.70
Tara Hills	39	31.2	45.0	7.2	13.4	13.8	16.7	0.23
Queenstown	49	41.5	50.7	10.0	10.1	9.2	12.4	0.51
Dunedin	42	47.0	46.2	13.1	11.2	−0.8	7.7	0.82
Gore	10	50.0	52.3	4.8	5.0	2.3	4.2	0.70

Table 2.4: Verification statistics calculated for the 24-hr rainfall (mm) at 1200 NZST on observed high-end fire weather days.

Weather Station	N	$\bar{O}$	$\bar{M}$	S_O	S_M	MBE	OR	MR	HR	FR	PC
Kaitaia	54	0.10	0.30	0.26	0.83	0.20	0.07	0.09	0.00	0.10	83
Tauranga	42	0.07	0.11	0.22	0.27	0.04	0.05	0.10	0.00	0.10	86
Hamilton	20	0.02	0.49	0.09	1.11	0.47	0.00	0.20	-	0.20	80
Rotorua	17	0.04	0.11	0.14	0.28	0.07	0.06	0.12	1.00	0.60	94
Gisborne	25	0.06	0.13	0.20	0.44	0.07	0.04	0.08	0.00	0.08	88
Taupo	17	0.09	0.48	0.35	1.02	0.39	0.06	0.24	1.00	0.19	82
Palmerston North	10	0.02	0.52	0.06	1.15	0.50	0.00	0.30	-	0.30	70
Wellington	61	0.11	0.33	0.37	0.74	0.22	0.08	0.18	0.40	0.16	80
Kaikoura	16	0.24	1.03	0.69	2.28	0.79	0.13	0.31	0.50	0.29	69
Christchurch	44	0.01	0.26	0.05	0.76	0.25	0.00	0.11	-	0.11	89
Timaru	39	0.07	0.32	0.31	0.97	0.25	0.05	0.10	0.50	0.08	90
Tara Hills	39	0.03	0.55	0.13	1.34	0.52	0.05	0.21	0.00	0.22	74
Queenstown	49	0.05	0.33	0.16	0.66	0.28	0.02	0.22	1.00	0.21	80
Dunedin	42	0.22	1.07	0.59	4.24	0.85	0.12	0.14	0.40	0.11	83
Gore	10	0.08	0.37	0.18	0.69	0.29	0.10	0.20	1.00	0.11	90

Table 2.5: Verification statistics calculated for the wind speed (km h^{-1}) at 1200 NZST on observed high-end fire weather days.

Weather Station	N	$\bar{O}$	$\bar{M}$	S_O	S_M	MBE	MAE	IOA
Kaitaia	54	22.5	22.9	5.8	7.0	0.4	4.3	0.79
Tauranga	42	23.5	24.6	7.2	7.7	1.1	5.5	0.74
Hamilton	20	21.3	25.2	6.0	4.6	3.9	5.5	0.64
Rotorua	17	22.8	27.2	7.1	8.5	4.4	5.9	0.79
Gisborne	25	21.4	25.9	7.0	8.0	4.5	6.8	0.68
Taupo	17	26.2	26.8	7.2	9.2	0.6	5.9	0.79
Palmerston North	10	32.7	31.4	6.9	7.3	−1.3	5.6	0.78
Wellington	61	38.7	33.7	8.5	8.1	−5.0	7.5	0.71
Kaikoura	16	29.4	27.0	14.2	17.1	−2.4	16.2	0.53
Christchurch	44	25.2	33.7	8.2	14.5	8.5	13.7	0.50
Timaru	39	24.2	35.7	10.5	14.9	11.5	13.8	0.64
Tara Hills	39	22.0	30.6	12.9	13.7	8.6	10.8	0.74
Queenstown	49	21.5	30.9	7.0	10.7	9.4	11.5	0.51
Dunedin	42	26.7	40.0	10.2	11.9	13.3	13.4	0.59
Gore	10	45.5	50.0	14.4	6.3	4.5	8.9	0.74

Table 2.6: Verification statistics calculated for the FWI at 1200 NZST on observed high-end fire weather days. The highest IOA value at each weather station is shown in bold font.

Weather Station	N	$\bar{O}$	$\bar{M}$	S_O	S_M	MBE	MAE	IOA	IOA_T	IOA_H	IOA_W	IOA_R
Kaitaia	54	22.9	14.0	4.1	10.9	-8.9	11.2	0.30	0.28	0.33	0.30	**0.58**
Tauranga	42	24.9	14.9	6.6	14.3	-10.0	14.1	0.40	0.34	0.40	0.44	**0.72**
Hamilton	20	21.9	12.4	4.3	13.3	-9.5	15.8	0.19	0.21	0.21	0.21	**0.47**
Rotorua	17	19.2	10.2	1.9	16.7	-9.0	17.2	**0.26**	0.25	0.20	**0.26**	0.18
Gisborne	25	23.2	23.4	5.5	12.3	0.2	12.6	0.16	0.17	**0.63**	0.24	0.51
Taupo	17	21.6	14.2	4.2	12.7	-7.4	11.6	0.40	0.39	0.35	**0.47**	0.24
Palmerston North	10	20.9	20.8	2.5	9.5	-0.1	8.3	0.22	0.12	0.30	0.23	**0.34**
Wellington	61	26.5	17.0	7.7	6.4	-9.5	10.0	0.55	0.59	0.55	**0.72**	0.58
Kaikoura	16	23.4	26.2	6.5	20.4	2.8	13.6	0.49	0.50	0.54	**0.56**	0.41
Christchurch	44	27.9	27.7	12.3	19.9	-0.2	14.4	0.63	0.69	0.67	**0.74**	0.58
Timaru	39	29.4	24.4	9.8	20.8	-5.0	18.4	0.41	0.39	**0.45**	0.42	0.39
Tara Hills	39	31.7	19.7	13.4	13.5	-12.0	16.1	0.51	0.50	**0.66**	0.52	**0.66**
Queenstown	49	23.7	16.2	6.6	14.0	-7.5	13.5	0.38	0.40	0.51	0.38	**0.54**
Dunedin	42	23.0	31.7	5.7	13.3	8.7	11.7	0.47	0.45	0.52	**0.67**	0.44
Gore	10	25.9	25.8	5.3	7.5	-0.1	8.6	0.35	0.35	0.36	**0.66**	0.50

Table 2.7: Verification statistics calculated for the CHI at 1200 NZST on days with an observed CHI value greater than or equal to five. The highest IOA value at both weather stations is shown in bold font. IOA_T is calculated based on substitution of the observed air temperature difference between 850 and 700 hPa, whereas IOA_D is calculated based on substitution of the observed dew point depression at 850 hPa.

Weather Station	N	$\bar{O}$	$\bar{M}$	S_O	S_M	MBE	MAE	IOA	IOA_T	IOA_D
Whenupai	51	7.5	6.6	1.6	2.2	−0.9	1.8	0.61	0.69	**0.92**
Paraparaumu	50	7.4	5.9	1.5	2.5	−1.5	2.0	0.62	0.75	**0.91**

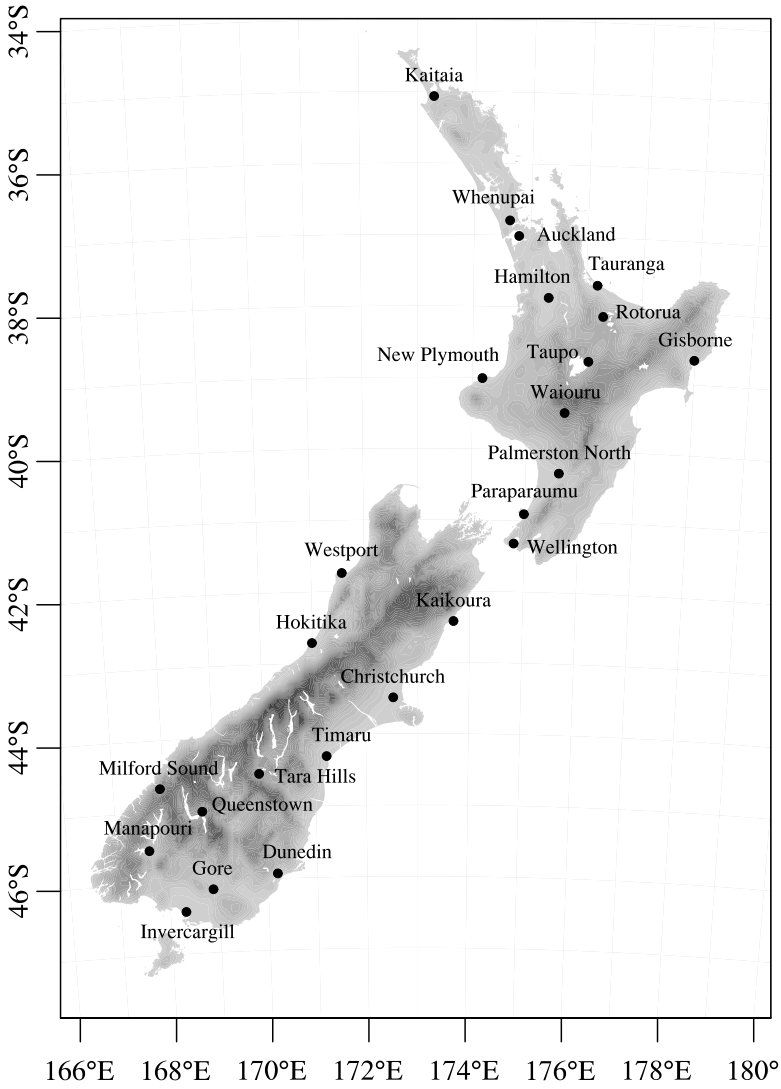

Figure 2.1: Location and name of the 23 surface weather stations and two upper-air stations used in the model verification. The grey shading represents the model surface elevation, with darker shading indicating higher surface elevation. The plot window shows the region covered by the model nested domain.

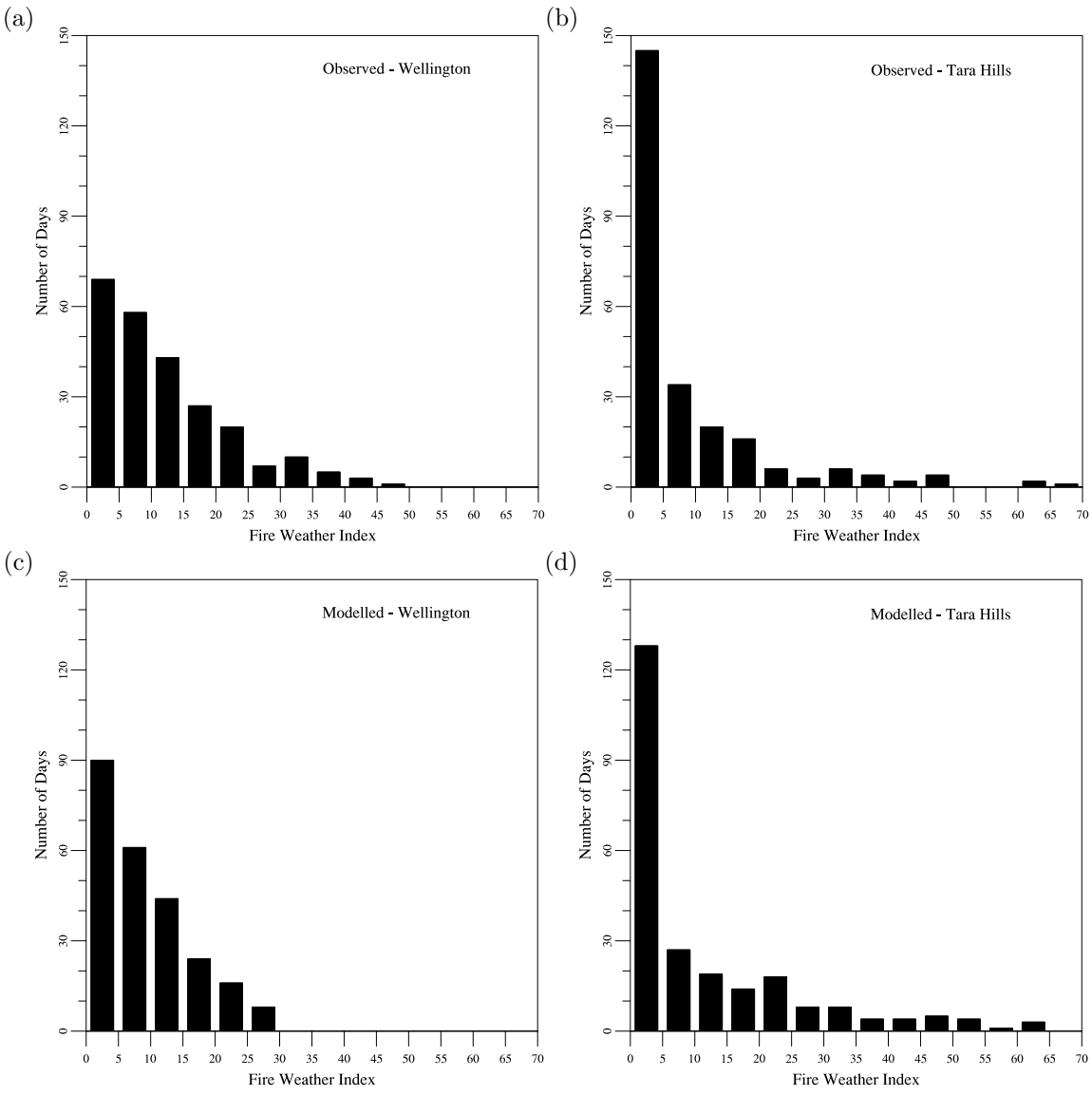

Figure 2.2: Histogram plots showing the frequency distribution of the (a,b) observed and (c,d) modelled FWI at the (a,c) Wellington and (b,d) Tara Hills stations.

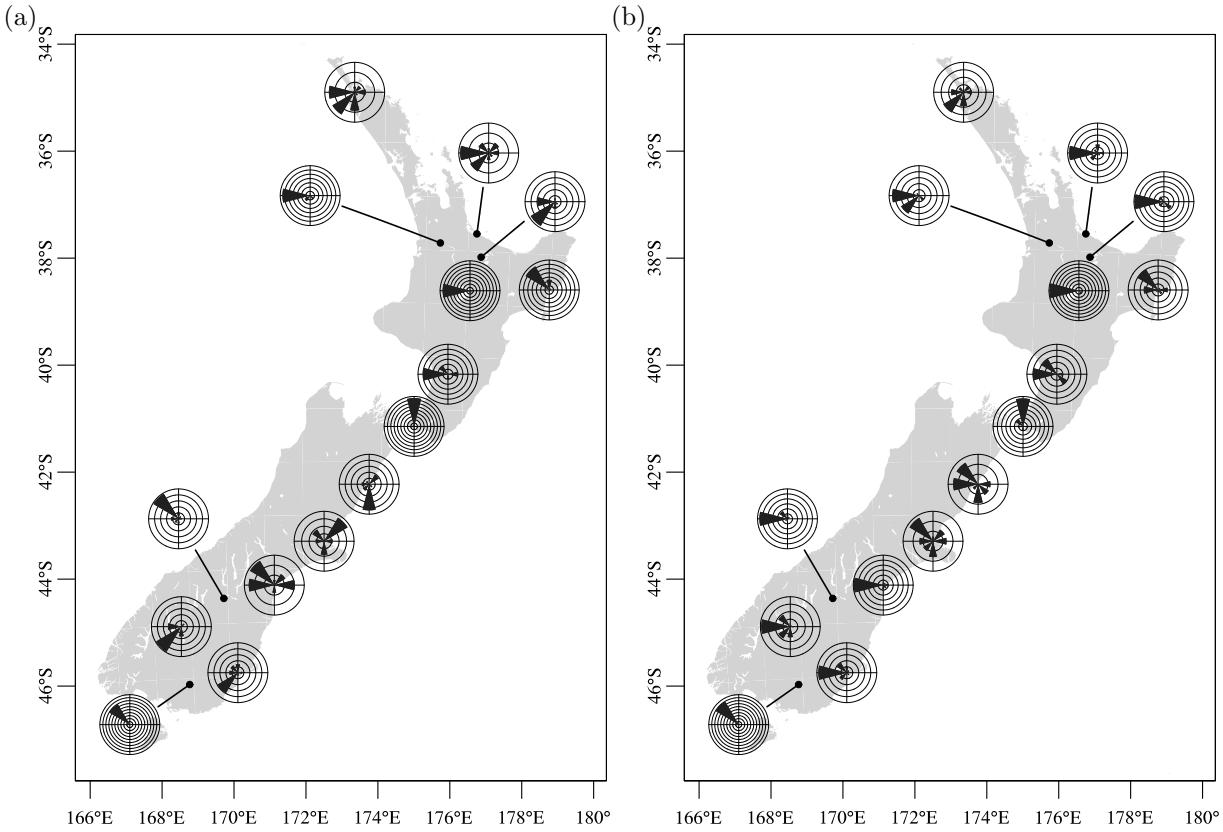

Figure 2.3: Wind roses overlaid on a map of New Zealand showing the distribution of the (a) observed and (b) modelled wind direction at 1200 NZST on observed high-end fire weather days. The length of each wind rose petal represents the wind direction frequency and each concentric circle represents a frequency of 10 %. The number of concentric circles varies between individual wind roses.

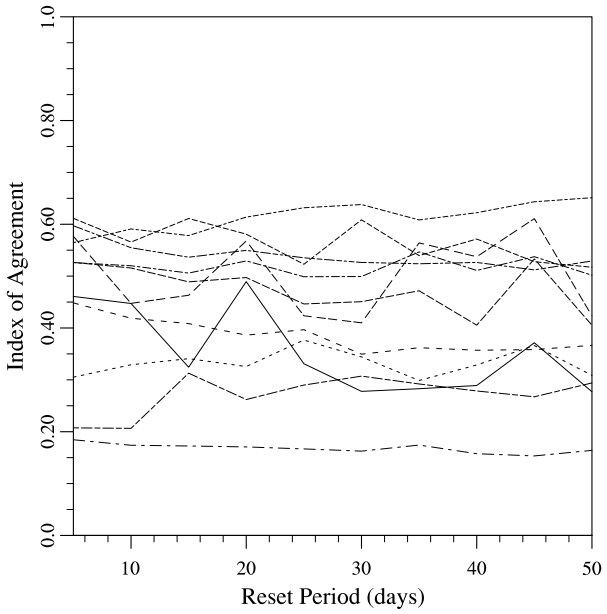

Figure 2.4: Variation of the IOA value with varying reset period for the FFMC, DMC and DC at the 15 weather stations with ten or more observed high-end fire weather days. A different line dash pattern is used to represent each station.

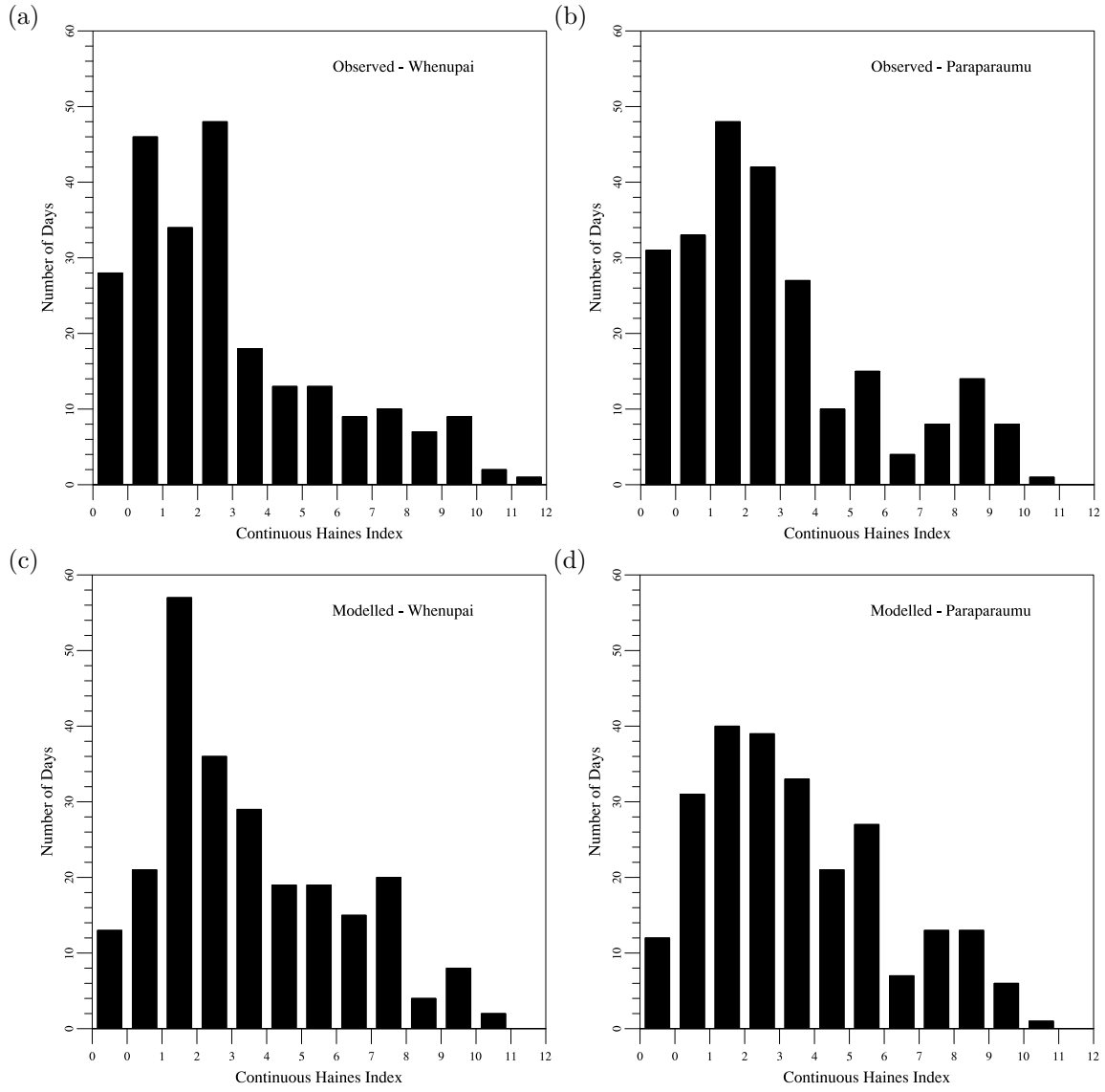

Figure 2.5: Histogram plots showing the frequency distribution of the (a,b) observed and (c,d) modelled CHI at the (a,c) Whenupai and (b,d) Paraparaumu stations. The leftmost bar is for CHI values precisely equal to zero.

Chapter 3

Behaviour of WRF Modelled Fire Weather Indices for the 2009/10 New Zealand Wildland Fire Season

C. C. Simpson[A], H. G. Pearce[B], A. P. Sturman[A], P. Zawar-Reza[A]

[A] Department of Geography, University of Canterbury, Christchurch, New Zealand
[B] Scion, Rural Fire Research Group, Christchurch, New Zealand

Abstract

The Weather Research and Forecasting (WRF) model was used to investigate the behaviour of the Haines Index (HI), Continuous Haines Index (CHI) and New Zealand Fire Weather Index (FWI) and their associated atmospheric properties for the 2009/10 New Zealand wildland fire season. Their behaviour was analysed using the season-averaged means and standard deviations, and the time series of daily values for three locations with distinct fire climates. The analysis demonstrated that there was significant spatial and temporal variability in the fire weather indices and their associated atmospheric properties, particularly in or near mountainous terrain. The season-averaged near-surface and aloft fire weather severity was highest on the eastern side of the Southern Alps and the North Island's dividing mountain ranges. The high degree of spatial variability could be associated with mesoscale atmospheric processes over complex terrain, although this requires further investigation. The time series demonstrated that there was no significant seasonality in the HI or CHI, although there was limited seasonality in the FWI. Most of the considered fire weather indices and atmospheric properties were highly variable on a daily and weekly timescale, particularly at Christchurch. Further research is required to determine the precise cause of intermittent extreme FWI values at Christchurch, which were believed to be associated with northwesterly foehn winds. The HI and CHI were

both found to be limited in their utility at measuring aloft fire weather conditions for high altitude regions, although this is not a significant issue due to the mild fire climate of mountainous terrain in New Zealand. The fire weather conditions associated with the 36 largest recorded wildland fires of the 2009/10 fire season were evaluated. The wildland fires occurred under a broad range of near-surface and aloft fire weather conditions, and no statistical relationship between the wildland fire size and either the CHI or FWI was found.

3.1 Introduction

Wildland fire behaviour is widely understood to be closely associated with the local weather, fuel characteristics and topography, which are collectively known as the fire environment (Countryman, 1972). Although the highly variable nature of weather makes deterministic prediction of microscale atmosphere-fire interactions difficult, fire weather indices can be used to predict the likelihood and impact of such atmosphere-fire interactions. Fire danger rating systems, which typically combine a fire weather index with information on the fuel characteristics and topography, are widely used in assessment of wildland fire risk and behaviour. Examples include the Canadian Forest Fire Danger Rating System (CFFDRS) used in Canada (Stocks et al., 1989; Van Wagner and Pickett, 1985; Van Wagner, 1987), the National Fire Danger Rating System used in the United States (Deeming et al., 1977) and the McArthur Forest Fire Danger Index used in Australia (McArthur, 1966, 1967). Fire weather indices and fire danger rating systems are used operationally to support a variety of fire management activities, including preparedness planning and wildland fire suppression.

The New Zealand Fire Danger Rating System (NZFDRS) is based on the CFFDRS and has been specifically modified for the unique fire environment of New Zealand (Fogarty et al., 1998; Anderson, 2005). The Fire Weather Index (FWI) is a fire behaviour index that represents the fire intensity for a reference fuel type (Lawson and Armitage, 2008), and is the primary tool used in fire weather assessment in New Zealand. The FWI is combined with information on fuel characteristics and terrain slopes to provide fire danger classifications across New Zealand. The FWI is calculated daily at individual weather stations distributed throughout New Zealand using near-surface weather station measurements made at 1200 New Zealand Standard Time (NZST). National gridded forecasts of the FWI are issued by the New Zealand Meteorological Service and are derived from numerical weather prediction (NWP) model output.

Many of the fire weather indices that are currently used worldwide were originally developed based on observed relationships between regional atmospheric conditions and wildland fire behaviour (Potter, 2002). It is necessary to carefully evaluate the suitability of applying a fire weather index to a region that is distinct from the one in which the index

was originally developed. For example, the Haines Index (Haines, 1988) was originally developed for use in the United States and was found to be unsuitable for use in southern Australia, due to a saturation of the index at its maximum value (Mills and McCaw, 2010). Potter et al. (2003) have highlighted some of the difficulties in developing a framework for statistical validation of fire weather indices. Further validation of the FWI and NZFDRS are still required in New Zealand (Anderson, 2005).

A number of studies have investigated various aspects of fire weather and climate in New Zealand. Pearce (2003) and Pearce et al. (2011a) have developed a fire weather climatology, based on weather station data throughout New Zealand, that has a particular focus on the FWI. Pearce (1996), Heydenrych and Salinger (2002), and Pearce and Clifford (2008) have attempted to characterise and describe the fire climate regions of New Zealand. Heydenrych et al. (2001), Gosai et al. (2003), Gosai et al. (2004) and Griffiths (2004) have investigated the relationship between synoptic weather types and severe fire weather conditions throughout New Zealand. Pearce and Moore (2004) have investigated different methods for measuring and predicting fire season severity in New Zealand. Gosai and Griffiths (2004) and Renwick and Salinger (2004) have investigated methods for improving fire season forecasting, and Simmers (2005), Hamilton (2007) and Renwick et al. (2007) have discussed operational fire weather forecasting tools. Pearce et al. (2005, 2007, 2011b) have studied the influence of climatic variability, such as global warming and the El Niño-Southern Oscillation, on fire season severity. Pearce and Whitmore (2009) have studied seasonal trends in the Drought Code, which is a fuel moisture index used in deriving the FWI. Finally, Clifford and Pearce (2009) have studied the fire behaviour of the Mount Cook Station Fire in 2008.

These studies on fire weather and climate in New Zealand have mostly been limited to consideration of the FWI and the weather variables used to derive it. A limitation of this approach is that the FWI does not directly account for fire weather conditions aloft or atmospheric stability, which can influence wildland fire behaviour (Potter, 2012a,b). Therefore, vertical atmosphere-fire interactions have largely been ignored, and could be better represented through the use of other fire weather indices, such as the Haines Index (Haines, 1988). In addition, many of these studies have focused on weather station data, which provides only limited spatial coverage across New Zealand. A limitation of this approach is that the relatively sparsely distributed weather station measurements could fail to adequately measure the highly spatially variable fire weather and climate of New Zealand. Numerical weather prediction (NWP) modelling can provide high spatial resolution data and could be more suitable for investigating spatial variability in fire weather and climate in New Zealand.

The primary aim of this study is to use NWP modelling to investigate the spatial and temporal variability of a number of fire weather indices and their associated atmospheric

properties for the 2009/10 New Zealand wildland fire season. The analysis considers the FWI, Haines Index (Haines, 1988) and Continuous Haines Index (CHI) (Mills and McCaw, 2010). The analysis covers the 2009/10 fire season and therefore represents a seasonal and not a climatological analysis. The length of the analysis is short due to the high spatial resolution required in the NWP model to suitability simulate the highly variable weather of New Zealand (Sturman et al., 1999). This fire season was chosen as Simpson et al. (2013b) have previously investigated the suitability of NWP modelling of near-surface fire weather conditions throughout New Zealand for the 2009/10 fire season.

The next section discusses the NWP model configuration and is followed by background information on each of the fire weather indices considered in the anaysis. The behaviour of a number of atmospheric properties that are associated with the fire weather indices is discussed in the subsequent section and is followed by a similar discussion on the behaviour of the fire weather indices themselves. The subsequent section presents the fire weather conditions associated with the major wildland fires of the 2009/10 fire season. Finally, a summary of the study is provided alongside a number of conclusions.

3.2 Numerical Weather Prediction Model

The NWP model used to simulate the weather for the 2009/10 fire season is version 3.2 of the Weather Research and Forecasting (WRF) model (Skamarock et al., 2008). The WRF model was chosen as it is widely used in the scientific community to model mesoscale atmospheric processes. WRF has previously been assessed for its suitability in modelling fire weather in New Zealand (Simpson et al., 2013b) and an identical model configuration is used in this study.

A two-way nested two domain configuration is used to model synoptic and mesoscale weather processes across New Zealand. The parent and nested domains have a horizontal grid spacing of 24 and 8 km, respectively, and a computational domain of 100×100 and 142×196 grid points, respectively. Both domains cover mainland New Zealand and the parent domain extends far out into the Tasman Sea and Pacific Ocean. The two domains share an identical configuration of 50 vertical levels, which extend from a height of ∼16 m above ground level to a fixed model pressure top of 50 hPa. Four-dimensional data assimilation is used to nudge the parent domain at six-hourly intervals using the National Centers for Environmental Prediction (NCEP) Final Analyses (FNL).

WRF utilises fully compressible non-hydrostatic equations and has a mass-based terrain-following coordinate system. The microphysics is represented by a single-moment six-class scheme with mixed-phase processes (Hong and Lim, 2006). The sub-grid scale effects of convective or shallow clouds are modelled in the parent domain using a modified Kain-Fritsch scheme (Kain, 2004). The surface layer and planetary boundary layer are

represented by the Eta schemes (Janjic, 1990, 1996, 2002). The heat and moisture fluxes over land are provided by the Noah Land Surface Model (Chen and Dudhia, 2001), which has soil temperature and moisture in four layers, fractional snow cover and frozen soil physics. The short-wave and long-wave radiation are represented by a simple short-wave radiation scheme (Dudhia, 1989) and the Rapid Radiative Transfer Model (Mlawer et al., 1997), respectively. A gravity wave damping layer (Klemp et al., 2008) is used in the top 1 km to prevent unphysical wave reflection off the upper boundary. Due to the long duration of the simulation, the deep soil and sea surface temperatures are regularly updated (Zeng and Beljaars, 2005), and the albedo and vegetation fractions are re-evaluated monthly. The main model time steps are 60 and 20 s for the parent and nested domains, respectively, with time integration performed using a third-order Runge-Kutta scheme (Wicker and Skamarock, 2002).

The WRF model simulation covers the period from 0000 NZST on 1 July to 0000 NZST on 1 April 2010. The first month of the simulation is regarded as the spin-up period and is not considered in the results. The remaining eight month period is chosen to represent the 2009/10 New Zealand fire season, as all major wildland fires greater than 5 ha occurred within this period. The model output is provided at hourly intervals and matches the standard timing of hourly weather station measurements.

3.3 Fire Weather Indices

International studies have shown that the HI is influenced by the time of day at which it is measured, although there is no apparent consensus on what time is most suitable for fire weather assessment (Winkler et al., 2007). In this study, the daily maximum HI and CHI, and daily FWI are considered in the analysis.

The HI is calculated through the summation of an atmospheric stability index, HA, and a humidity index, HB. HA is calculated based on the air temperature lapse rate between two fixed pressure levels, whereas HB is calculated based on the dew point depression at one of these fixed levels. HA and HB can take on integer values of one, two or three, and the HI can therefore take on integer values between two and six, inclusive. As a consequence of using fixed pressure levels, the height above ground level at which the temperature lapse rate and dew point depression are evaluated varies with surface elevation. To accomodate for varying surface elevation across a landscape, there are three variants of the HI, known as the Low Haines Index (LHI), Mid Haines Index (MHI) and High Haines Index (HHI). Winkler et al. (2007) has previously adopted elevation thresholds of 300 and 1000 m to determine which variant of the HI should be used at each location and this study has adopted the same elevation thresholds. Further details on the equations used to calculate the LHI, MHI and HHI are provided in Table 3.1.

Although the HI was originally developed for use in the United States it is currently used operationally in countries worldwide. However, Mills and McCaw (2010) discovered that the HI had a high frequency of maximum HI values in the severe fire climate of southern Australia, which limited the utility of the index. Mills and McCaw (2010) therefore proposed the CHI, which extends the MHI to a continuous number scale that provides greater determination of fire weather severity, particularly at the upper end of the scale. The CHI is calculated through the summation of an atmospheric stability index, CA, and a humidity index, CB. The CA and CB are evaluated at the same fixed pressure levels as the MHI i.e. 850 and 700 hPa. The CHI is therefore not suitable for use in regions with a surface elevation over 1000 m. The CA and CB are calculated as:

$$\mathrm{CA} = \frac{\mathrm{T}_{850} - \mathrm{T}_{700}}{2} - 2 \tag{3.1}$$

$$\mathrm{CB} = \frac{\mathrm{T}_{850} - \mathrm{D}_{850}}{3} - 1 \tag{3.2}$$

where T_{850} is the air temperature at 850 hPa, T_{700} is the air temperature at 700 hPa and D_{850} is the dew point temperature at 850 hPa. There are an additional three constraints that are applied to the CHI. First, negative values of the CHI are set equal to zero. Second, the dew point depression used to calculate the CB is limited to a maximum value of 30°C. Third, if the CB is greater than five, then it is re-calculated as:

$$\mathrm{CB} = \frac{\mathrm{CB} - 5}{2} + 5 \tag{3.3}$$

Figure 3.1a shows the variation in WRF model surface elevation across New Zealand and the corresponding Haines elevation categories, based on elevation thresholds of 300 and 1000 m, respectively. The Southern Alps mountain range, which can significantly modify the local weather and climate, stretches from the southwest to the northeast of the South Island. In the North Island there are a series of dividing mountain ranges that stretch from the south to the northeast. Although these dividing mountain ranges can also affect local weather and climate, they are smaller in height than the Southern Alps. A number of high elevation volcanoes are clearly visible throughout the North Island, including Mount Taranaki in the west and Mount Tongariro and Ruapehu in the central region. The LHI is calculated across the majority of the coastal North Island and limited coastal regions in the South Island. The MHI is calculated for the majority of the remainder of the North Island, although the HHI is calculated near the high elevation central volcanic region. Finally, the HHI is calculated in widespread regions of the Southern Alps. The CHI is calculated only where the LHI and MHI are calculated,

and not where the HHI is calculated.

The FWI is a fire behaviour index that represents the wildland fire intensity for a reference fuel type, although it is also commonly used as an indicator of fire danger (Lawson and Armitage, 2008). The FWI is derived from two intermediate fire behaviour indices known as the Initial Spread Index (ISI) and Build Up Index (BUI). The ISI represents the expected rate of forward fire spread and the BUI represents the fuel available for combustion. The ISI is derived from the wind speed and Fine Fuel Moisture Code (FFMC), whereas the BUI is derived from the Duff Moisture Code (DMC) and Drought Code (DC). The FFMC, DMC and DC are fuel moisture indices that are calculated once daily based on the air temperature, relative humidity, wind speed and 24-hr rainfall at 1200 NZST. They are calculated iteratively, such that their value on a given day is directly dependent on the previous day's value. The FFMC represents the ease of ignition and flammability of fine fuels, the DMC represents the expected fuel consumption in duff layers and moderately sized fuels, and the DC represents the seasonal drought effect on deep organic layers and large sized fuels. An FWI value of greater than or equal to either 17 or 32 represents a "Very High" or "Extreme" fire danger day, respectively, for forested regions in New Zealand (Alexander, 1994, 2008).

The fire weather climatology developed by Pearce (2003) and Pearce et al. (2011b) was used initialise the modelled FFMC, DMC and DC on 31 July 2009. Derived values of the fuel moisture indices were taken from 82 weather station sites across New Zealand and a nearest neighbour algorithm was used to assign initial values to each WRF model grid cell over land. The modelled air temperatures, relative humidities, wind speeds and 24-hr rainfall at 1200 NZST on 1 August 2009 were combined with the initial FFMC, DMC and DC values to calculate the full set of fuel moisture and fire behaviour indices on 1 August 2009.

The FWI has an approximately exponential frequency distribution and varies significantly in time and space across New Zealand (Pearce et al., 2011b). The long-term average FWI is typically highest to the east of the dividing mountain ranges in the North Island and South Island, and lowest to the west. For example, the long-term average number of Very High or Extreme FWI fire season days ranges from a minimum of 0.0 and 1.2 days at the West Coast and Southland stations, respectively, to a maximum of 34.2 and 27.8 days at the Marlborough and Canterbury stations, respectively. The three weather stations with the highest long-term average number of Very High or Extreme FWI fire season days are Awatere Valley, Woodbourne Aero and Tara Hills with 65.8, 60.1 and 55.5 days, respectively. Very High or Extreme fire danger classes are therefore relatively common in some regions of New Zealand, particularly where the mean annual rainfall is low.

3.4 Behaviour of Weather Variables

This section presents and discusses the behaviour of atmospheric properties used to derive the HI, CHI and FWI. Simpson et al. (2013b) previously determined that WRF typically underpredicted the air temperatures and relative humidities, and overpredicted the wind speeds on extreme fire weather days across most of New Zealand. Renwick (2011) has previously investigated the relationship between synoptic weather types, which are dynamically associated with the phase of the El Niño Southern Oscillation (ENSO) and the polarity of the Southern Annular Mode (SAM), and daily climate anomalies of the daily maximum air temperature and rainfall. The 2009/10 fire season coincided with El Niño conditions and predominantly negative polarity of the SAM.

Figure 3.2a shows the season-averaged mean daily maximum air temperature across New Zealand. There is significant spatial variability in the mean air temperatures across both the South Island and North Island, with warmer temperatures in the North Island than the South Island as expected. In the North Island, the mean air temperatures are warmest between 18–20°C in the north and in isolated regions eastwards of the dividing mountain ranges. In the South Island, the mean air temperatures are warmest in central regions directly eastwards of the Southern Alps. The high air temperatures to the east of mountainous terrain could be associated with the thermal effects of foehn winds. Foehn winds occur relatively frequently in the South Island in the non-winter months and are known locally as the "Canterbury Northwester" (McGowan and Sturman, 1996). The mean air temperatures are coldest in the high elevation mountainous terrain of the Southern Alps and can be lower than 2°C.

Figure 3.2b shows the season-averaged mean daily maximum wind speed across New Zealand. There are a number of isolated regions running parallel to and directly eastwards of high relief mountains in the Southern Alps that have high mean wind speeds exceeding 45 km h^{-1}. These high wind speed regions could be associated with atmospheric interactions with topography, such as the development of mountain lee waves and associated downslope windstorms. The mean wind speeds are typically less than 33 km h^{-1} in the northwestern South Island and in the central and northern North Island. There is an isolated region of relative high wind speeds in the southern South Island near the Tararua Range.

Figures 3.2c and 3.2d show the season-averaged mean daily minimum relative humidity and 24-hr rainfall at 1200 NZST across New Zealand. In the South Island, the mean relative humidities are lowest eastwards of the Southern Alps, particularly in the central South Island where it is typically ∼40–50 %. In contrast the mean relative humidities are typically ∼65–80 % on the western side of the Southern Alps and are highest in the southwestern Fiordland region. There is comparatively little spatial variation in the

mean relative humidities across the North Island, where they are typically ∼50–65 %. The spatial variability in the mean rainfall follows a similar although more identifiable pattern as the spatial variability in the mean relative humidity. The mean rainfall was significantly higher on the western side of the Southern Alps than throughout the rest of New Zealand, which is associated with orographic lifting of the prevailing westerlies. The rain shadow cast by the Southern Alps across the eastern South Island is clearly visible, with low mean rainfalls of less than 2 mm per day across the central eastern South Island. There are three isolated regions of relatively high mean rainfall in the North Island, which correspond to high elevation regions surrounding Mount Taranaki, Mount Ruapehu and the Tararua Range. Throughout the rest of the North Island, the mean rainfall is typically ∼2–6 mm per day.

Figure 3.3 shows the time series of the daily maximum air temperature and wind speed, daily minimum relative humidity and 24-hr rainfall at 1200 NZST at the WRF model grid cells closest to the Kaitaia, Christchurch and Hokitika weather stations. There is an expected distinct seasonality in the air temperatures at each location, which are typically higher in the summer months i.e. December, January and February. The inter-daily and inter-weekly variations in the air temperature are significantly higher at Christchurch than at Kaitaia or Hokitika. There is limited seasonality in the wind speeds at each location. There is a distinct seasonality in the relative humidities at Kaitaia, which are lower in the summer months, and Hokitika, which are higher in the summer months. There is a distinct seasonality in the rainfall at Kaitaia, which is lower in the summer months, although not at Christchurch. The inter-monthly rainfall is highly variable at Hokitika, with comparatively dry months in August, December and January.

Figure 3.4 shows the season-averaged mean daily maximum temperature lapse rate between 850 and 700 hPa, and the dew point depression at 850 hPa across New Zealand. The mean lapse rates are highest directly eastwards of the Southern Alps in the central and northeastern South Island. In isolated regions the mean lapse rate can exceed 11.0°C, which is the value required for the atmospheric stability index, HA, to equal a maximum value of 3. The mean lapse rates are also higher on the eastern side of the North Island dividing mountain ranges relative to the western side. These high mean lapse rates are likely associated with atmospheric processes over mountainous terrain, such as mountain lee wave development. The very different spatial patterns of the mean relative humidity at 2 m above ground level and the dew point depression at 850 hPa indicate that the season-averaged humidities are very different near the surface and aloft. The mean dew point depressions are highest in the northern North Island, where they are typically higher than 20°C, and lowest in the southern South Island and in the Southern Alps, where they are typically lower than 14°C. These results suggest that the dew point depressions are commonly higher than 13°C across most of New Zealand, which is value

required for the atmospheric humidity index, HB, to equal to a maximum value of 3. The high degree of spatial variability in mean dew point depressions could be related to differences in air masses over New Zealand.

3.5 Behaviour of Fire Weather Indices

This section presents and discusses the season-averaged spatial and temporal variability of the modelled daily maximum HI and CHI, and the daily FWI. Simpson et al. (2013b) previously determined that WRF typically overpredicted the CHI and the number of extreme fire weather days, based on the FWI, across most of New Zealand.

Figures 3.5a and 3.5b show the season-averaged mean daily maximum HI and CHI across New Zealand. The spatial variability in the HI and CHI are similar, with low values in the Southern Alps and high values on the eastern side of mountainous terrain in the central and northeastern South Island, and southeastern North Island. The mean HI and CHI values are typically lower than 4.0 and 4.8 in the Southern Alps, respectively, and higher than 4.6 and 6.6 in the central eastern South Island, respectively. The high mean HI and CHI values in the central South island are associated with the previously discussed high mean temperature lapse rates. In contrast, the high mean HI and CHI values in the southeastern North Island are associated with a combination of moderate mean temperature lapse rates and moderate to high mean dew point depressions. The moderate HI and CHI values in the northern North Island are associated with low mean temperature lapse rates and high mean dew point depressions.

Figures 3.5c and 3.5d show the season-averaged standard deviation of the daily maximum HI and CHI across New Zealand. The standard deviations of the HI and CHI share in common a number of features, but can also differ from each other significantly. The standard deviations of the HI and CHI are low in the western and northern North Island, and high directly eastwards of the dividing mountain ranges in the eastern North Island. There is a narrow isolated region in the central to northeastern South Island for which the standard deviations are high for both the HI and CHI. However, throughout much of the central and southern South Island the standard deviations for both the HI and CHI are notably different.

Figure 3.6 shows the season-averaged mean and standard deviations of the daily ISI, BUI and FWI across New Zealand. The mean ISI, BUI and FWI values are lowest to the west of the Southern Alps and highest directly to the east in the central South Island. This spatial pattern is reasonably consistent with the spatial variability in the mean air temperatures, relative humidities, wind speeds and rainfall discussed earlier. In the North Island, the mean ISI and FWI values are higher on the eastern side of the dividing mountain ranges than on the western side. The mean BUI values are relatively high in

both the northern North Island and eastwards of the dividing mountain ranges. The spatial patterns in the standard deviations of the ISI, BUI and FWI closely resemble the equivalent spatial patterns in the mean values, which suggests that regions with high mean index values also experience high temporal variability.

Figure 3.7 shows the time series of the daily maximum HI and CHI, and daily FWI at the WRF model grid cells closest to the Kaitaia, Christchurch and Hokitika weather stations. The inter-monthly variation is similar between the HI and CHI values at each location and there is no significant seasonality. However, there seems to be more considerable inter-daily and inter-weekly variability in the HI and CHI, which could be associated with the synoptic meteorology. In contrast there is an apparent seasonality in the FWI at Kaitaia and Christchurch, which higher monthly values from November to February. There are nine days for which the FWI exceeds 50 at Christchurch, indicating extreme fire weather conditions. Eight of these days are associated with northwesterly foehn winds, whereas the other day is associated with southerly winds and occurs in between two of the foehn days. The inter-daily and inter-weekly variability in the FWI is much higher at Christchurch than at either Kaitaia or Hokitika, which further demonstrates the highly variable nature of near-surface fire weather conditions in the eastern South Island.

Figure 3.8a shows the season-averaged percentage number of days for which the daily maximum HI is equal to its maximum value of six across New Zealand. The percentage is typically less than 5 % across most of New Zealand, although it can be significantly higher than this directly eastwards of mountainous terrain in the North Island and South Island. There is a long and narrow region stretching from the central to northeastern South Island where the percentage is typically higher than 20 % and can exceed 40 %. These results demonstrate that there is no saturation of the HI in New Zealand like that seen in southern Australia. Werth and Werth (1998) identified a significant positive correlation between the elevation of a weather station and the frequency of high HI values. However, based on Figure 3.8a there is no similar correlation in New Zealand and instead the frequency of high index values appears to be most closely associated with atmospheric processes over mountainous terrain.

Figure 3.8b shows the season-averaged percentage number of days for which the daily FWI is greater than or equal to 32 across New Zealand. In the North Island, the percentage is less than 5 % to the west of the dividing mountain ranges, whereas it is typically ∼5–10 % to the east. In the South Island, the percentage is typically less than 5 % in the south and northwest, and to the west of the Southern Alps. In contrast, it is typically ∼10–20 % eastwards of the Southern Alps and there are isolated regions in which the percentage can exceed 20 %, which indicates relatively frequent extreme fire weather conditions at these locations. However, it should be cautioned that these

results could significantly overpredict the number of extreme FWI days, particularly in the eastern South Island (Simpson et al., 2013b).

Figure 3.9 shows the variation of the season-averaged mean fire weather indices with surface elevation for WRF model grid cells over land. The mean daily maximum HHI values are systematically lower than the mean LHI and MHI values at equivalent surface elevations below 300 and 1000 m, respectively. This indicates that there are systematic biases in the HI at surface elevations above 1000 m, where the HHI is used. Additionally, there is a decrease in the minimum mean daily maximum MHI and CHI values with increasing surface elevation, which is not seen for the LHI or HHI. This decrease is predominantly due to a decrease in the dew point depressions at 850 hPa with increasing surface elevation. In comparison, there is a marked variation of the mean ISI, BUI and FWI with surface elevation. Although there is a wide range of mean ISI, BUI and FWI values at elevations below ∼1000 m, the frequency of high mean index values tends to decrease with increasing surface elevation. These results demonstrate that the season-averaged fire weather conditions are typically less severe in mountainous terrain across New Zealand.

3.6 Fire Weather Associated with Wildland Fires

There were a total of 3,858 recorded wildland fires during the 2009/10 New Zealand fire season. There were 39 wildland fires that burned an area greater than 5 ha and information is available on the day, geographical location, dominant fuel type and total area burned for 36 of these fires. This information was provided by the National Rural Fire Authority in New Zealand for this study. Figure 3.10a shows the location and approximate area burned for these 36 fires. The fires were divided relatively evenly between the North Island and South Island, although there was a cluster of 12 fires in the far northern North Island. There were relatively few major fires in the central eastern South Island, despite its more severe fire weather conditions, which could be related to predominantly agricultural land use of this region. The spatial distribution of these wildland fires demonstrates the importance of other aspects of the fire environment, including the vegetation characteristics and topography, as well as complex social factors, for major fire occurrence in New Zealand.

The fire weather conditions associated with each wildland fire were calculated using WRF model output from the corresponding model grid cell. It is necessary to consider daily measures of fire weather conditions as only the day of each fire is known. This limitation means that the presented daily measures of fire weather conditions could differ significantly from the actual fire weather conditions associated with each wildland fire. In addition, there are known systematic biases in the modelled fire weather conditions,

so a comparison with nearby available weather station data is planned in future work. The modelled fire weather conditions associated with each wildland fire are presented in Table 3.2. Although only the fire weather conditions are shown for the day of each fire, the antecedent fire weather conditions are also likely to be important for their role in modifying fuel conditions.

The majority of the wildland fires occurred in low altitude regions below 300 m and only one fire occurred at an altitude above 1000 m. This result suggests that the CHI is calculable for most large wildland fires in New Zealand. The wildland fires occurred under a broad range of near-surface fire weather conditions, with daily maximum air temperatures ranging from 10.0 to 28.4°C, daily minimum relative humidities ranging from 23.8% to 74.9% and daily maximum wind speeds ranging from 22.2 to 103.9 km h^{-1}. The 24-hr rainfall at 1200 NZST was greater than 1 mm for three of the fires, which had corresponding low FWI values of less than 5. The wildland fires also occured under a broad range of FWI values, ranging from 0.4 to 60.9, which reflects the broad range in the near-surface atmospheric properties. The FWI values were greater than 32, representing extreme fire weather conditions, at six of the wildland fires, which were also typically associated with either low relative humidities or high wind speeds, or a combination of both. The HI was equal to either four or five for 29 of the wildland fires and was only equal to six for two fires.

Figure 3.10b shows the daily maximum CHI and daily FWI associated with the 36 wildland fires. There is no apparent statistical relationship between the wildland fire size and either the CHI or FWI. In addition, there is no obvious relationship between the CHI and FWI values associated with these wildland fires, although the FWI values are higher than 30 on the three occasions that the CHI is higher than 10. It is interesting to note that the largest recorded wildland fire of the 2009/10 fire season was associated with relatively low CHI and FWI values, which again indicates the importance of external factors to the weather in wildland fire growth.

3.7 Summary and Conclusions

The WRF mesoscale model was used to investigate the behaviour of fire weather indices and their associated atmospheric properties for the 2009/10 New Zealand wildland fire season. The fire weather indices included in the analysis were the Haines Index (HI), Continuous Haines Index (CHI) and New Zealand Fire Weather Index (FWI). The atmospheric properties considered in the analysis included the near-surface air temperature, relative humidity, wind speed and rainfall, and the aloft air temperature lapse rate between 850 and 700 hPa, and the dew point depression at 850 hPa. The behaviour of these fire weather variables were primarily analysed using season-averaged means and

standard deviations, and time series of the daily values at three locations in distinct fire climates.

The analysis demonstrated that there was significant spatial variability in each season-averaged fire weather index and their associated atmospheric properties throughout New Zealand, particularly in or near mountainous terrain. Although these results are broadly consistent with previous climatological studies (Heydenrych et al., 2001; Gosai et al., 2003; Pearce, 2003; Gosai et al., 2004; Griffiths, 2004; Pearce et al., 2011b), they provide a higher spatial resolution dataset than has previously been considered, at the expense of a longer timescale. It is clear from these results that atmospheric processes over mountainous terrain, such as foehn winds and mountain lee waves, can significantly influence inter-monthly and seasonal fire weather conditions throughout New Zealand. Further research is required to extend this analysis to a climatologically significant timescale and to investigate how specific atmospheric processes over complex terrain can affect fire weather conditions across New Zealand. The fire weather conditions were more spatially uniform across the North Island, which indicates that regional reanalysis data could be used to construct a fire weather climatology for this region. However, the high degree of spatial variability in the fire weather conditions throughout the South Island suggests that regional reanalysis may not be at a sufficient spatial resolution to capture this variability. It may therefore be necessary to use NWP mesoscale modelling to construct a fire weather climatology for the South Island.

The HI and CHI were found to behave similarly to each other throughout New Zealand, which was expected given their mathematical similarities (Mills and McCaw, 2010). The analysis demonstrated that there was no specific requirement for the greater determination of the HI at the upper end of the scale, unlike in Australia, which was a primary motivating factor using the CHI instead of the HI. In addition, unlike the HI, the CHI does not have a high elevation variant so should therefore not be used over altitudes of $\sim$1000 m above sea level. This prohibits use of the CHI across widespread regions of the Southern Alps, and the volcanic regions and dividing mountain ranges of the North Island. In contrast, the HI can be calculated throughout New Zealand, although the HHI values were found to be systematically lower than the MHI and LHI at equivalent heights below 1000 m. The resulting negative bias in the HI at high altitudes could affect its utility in these regions. However, only one of the 36 major wildland fires occurred at an altitude over 1000 m above sea level, which suggests that these elevation related issues for the CHI and HI are not overly limiting in an operational context. It would be valuable to re-define the HI or CHI in terms of terrain-following coordinates, in order to remove the limitation of using fixed pressure levels. In addition, there was no apparent correlation between either the HI or CHI with surface elevation, which is contrast to results presented by Werth and Werth (1998).

The model output was used to estimate the fire weather conditions associated with 36 of the largest recorded wildland fires in the 2009/10 fire season. Most of the fires occurred in low altitude coastal regions and the CHI was calculable for all but one wildland fire. The fires occurred under a broad range of fire weather conditions and, for this small sample size, there were no apparent statistical relationships between the fire size and fire weather indices. This and other studies look for relationships between fire size and fire weather indices because higher index values could be expected to result in a higher flammability of fuels or higher potential for extreme fire behaviour. However, the fire size depends on many other factors external to weather, including the fuel conditions and arrangement, fire suppression efforts and terrain. It would be more useful to examine relationships between specific details of fire behaviour, such as sudden changes in fire intensity or forward spread direction, with fire weather indices. However, there is limited observational data available on specific aspects of fire behaviour, whereas the fire size can be easily measured post-fire.

Without information on other aspects of fire behaviour associated with these wildland fires, it is not possible to ascertain any statistical relationships between the fire weather conditions and fire behaviour in this study. Further research is needed to identify relationships between various aspects of fire behaviour and fire weather in New Zealand. This can be achieved through consideration of wildland fires that have more detailed information available on specific aspects of fire behaviour. Given the relatively small annual number of large wildland fires in New Zealand, such an analysis would span a number of fire seasons. This would coincide with the previously discussed extension of the analysis of fire weather conditions to climatologically significant timescales. Additional case studies of fire weather conditions associated with extreme fire behaviour in New Zealand's endemic fuel types would also be valuable.

At present the FWI is the primary tool used in fire weather and climate assessment throughout New Zealand. However, the FWI only considers the near-surface atmospheric conditions and is therefore unable to fully represent the three-dimensional nature of atmosphere-fire interactions. It is therefore recommended that fire weather indices that consider atmospheric properties aloft, such as the HI and CHI, be considered for operational use in New Zealand to provide an additional measure of the fire weather conditions. However, this study has highlighted several issues associated with use of either HI or CHI in New Zealand, and further research is required to more thoroughly examine their suitability for operational use in New Zealand. In particular further research is needed to identify the precise cause of the high season-averaged HI and CHI directly eastwards of the Southern Alps.

Table 3.1: Equations used to evaluate the atmospheric stability index, HA, and humidity index, HB, for the Low, Mid and High Haines Index

HI	Atmospheric Stability			Atmospheric Humidity		
Variant	Calculation	Condition	HA	Calculation	Condition	HB
Low	T_{950} - T_{850}	$< 4°C$	1	T_{850} - D_{850}	$< 6°C$	1
		$\geq 4°C$ and $< 8°C$	2		$\geq 6°C$ and $< 10°C$	2
		$\geq 8°C$	3		$\geq 10°C$	3
Mid	T_{850} - T_{700}	$< 6°C$	1	T_{850} - D_{850}	$< 6°C$	1
		$\geq 6°C$ and $< 11°C$	2		$\geq 6°C$ and $< 13°C$	2
		$\geq 11°C$	3		$\geq 13°C$	3
High	T_{700} - T_{500}	$< 18°C$	1	T_{700} - D_{700}	$< 15°C$	1
		$\geq 18°C$ and $< 22°C$	2		$\geq 15°C$ and $< 21°C$	2
		$\geq 22°C$	3		$\geq 21°C$	3

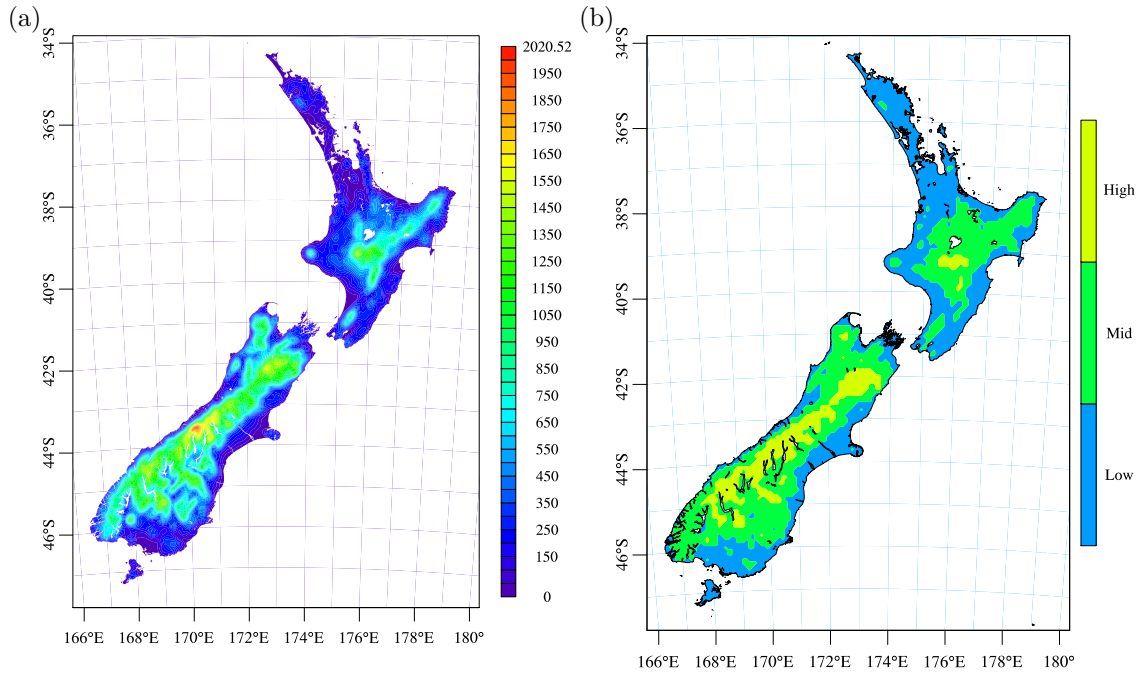

Figure 3.1: Contour plots showing the modelled (a) surface elevation (m) and (b) Haines Index boundaries. In (b) the "Low" regions have an elevation below 300 m, "Mid" regions have an elevation between 300 and 1000 m and "High" regions have an elevation above 1000 m.

Table 3.2: Wildland fire properties and modelled fire weather conditions for the 36 wildland fires considered in this study. The weather variables calculated are the daily maximum air temperature (T_A) and wind speed (W_S), daily minimum relative humidity (RH) and 24-hr rainfall at 1200 NZST (R_{24H}). The elevation categories, based on those presented in Figure 3.1b, show which variant of the Haines Index is relevant. The fire weather indices calculated are the daily maximum LHI, MHI, HHI and CHI, and the daily FWI. FWI values higher than 32.0 are shown in bold font as they represent extreme fire weather conditions.

Date	Size (ha)	T_A (°C)	RH (%)	W_S (km h^{-1})	R_{24H} (mm)	Elevation	LHI	MHI	HHI	CHI	FWI
10-08-09	10.4	13.4	64.0	23.5	0.0	Low	5	4	5	7.3	6.5
28-08-09	85.0	12.8	62.2	58.4	3.7	Mid	-	5	3	5.1	4.8
15-09-09	19.0	12.9	64.8	25.3	4.1	Low	5	5	5	8.5	0.4
23-10-09	915	13.0	55.0	33.4	0.0	Low	4	4	2	3.6	1.1
31-10-09	8.50	17.4	43.3	30.4	0.0	Low	5	4	4	4.5	9.3
02-11-09	9.00	10.0	65.4	45.9	0.3	High	-	-	3	-	8.5
16-11-09	8.00	14.8	46.7	34.4	0.0	Low	4	3	4	2.8	9.0
21-11-09	37.5	16.8	74.9	62.4	0.0	Low	4	5	5	7.3	20.2
26-11-09	541	14.8	48.2	51.5	0.4	Mid	-	4	4	4.7	**35.7**
05-12-09	8.62	18.0	38.4	26.8	0.0	Mid	-	4	2	4.8	8.0
09-12-09	5.00	23.8	43.6	28.6	0.0	Low	5	5	4	8.4	19.6
11-12-09	6.50	28.4	35.3	31.4	0.0	Low	5	5	3	9.2	17.9
15-12-09	6.20	17.1	42.6	31.2	8.4	Low	5	5	4	6.3	4.5
18-12-09	5.00	21.4	42.2	103.9	0.0	Mid	-	6	6	11.7	**35.6**
19-12-09	11.0	23.2	38.6	25.1	0.0	Low	5	5	4	7.5	24.4
23-12-09	5.00	17.4	63.7	22.2	0.0	Low	5	5	4	7.0	19.4
24-12-09	8.26	15.5	45.9	29.2	0.0	Low	5	5	4	9.6	14.6
28-12-09	12.2	25.5	23.0	27.4	0.0	Low	6	5	3	7.1	0.4
01-01-10	5.00	20.3	38.0	31.1	0.0	Low	5	5	5	8.9	21.0
01-01-10	8.00	15.3	68.1	24.2	0.1	Low	4	5	4	8.4	4.1
04-01-10	5.00	20.3	26.5	50.0	0.0	Low	5	5	4	7.8	**60.9**
26-01-10	82.0	24.9	52.8	24.6	0.0	Low	3	3	2	3.0	20.2
03-02-10	39.9	20.8	66.0	45.3	0.0	Low	4	5	4	7.1	**32.8**
07-02-10	6.90	18.1	55.0	28.9	0.0	Low	4	5	4	6.1	18.2
07-02-10	32.5	17.6	63.7	22.2	0.0	Low	4	5	4	7.3	14.4
10-02-10	30.4	17.0	71.1	29.8	0.0	Low	5	5	4	5.6	12.1
10-02-10	125	21.6	46.4	27.3	0.1	Low	4	4	4	4.8	27.1
18-02-10	11.6	18.2	63.9	36.1	0.3	Low	3	4	2	2.5	15.2
21-02-10	72.0	15.6	74.6	37.4	0.0	Low	4	5	4	7.6	6.9
22-02-10	78.0	25.2	23.8	43.4	0.0	Mid	-	5	5	10.3	**56.2**
24-02-10	44.0	24.1	28.1	37.3	0.0	Mid	-	6	5	11.7	**33.3**
27-02-10	198	16.6	65.4	58.7	0.0	Low	4	5	5	8.3	24.4
08-03-10	15.0	17.9	38.4	24.2	0.0	Low	5	5	4	5.7	0.5
13-03-10	117	18.4	43.0	26.8	0.1	Low	4	5	4	8.7	0.6
17-03-10	54.0	18.7	53.9	27.9	0.0	Low	4	5	5	9.8	2.1
20-03-10	10.0	19.3	57.4	31.3	0.3	Low	3	3	4	2.4	15.8

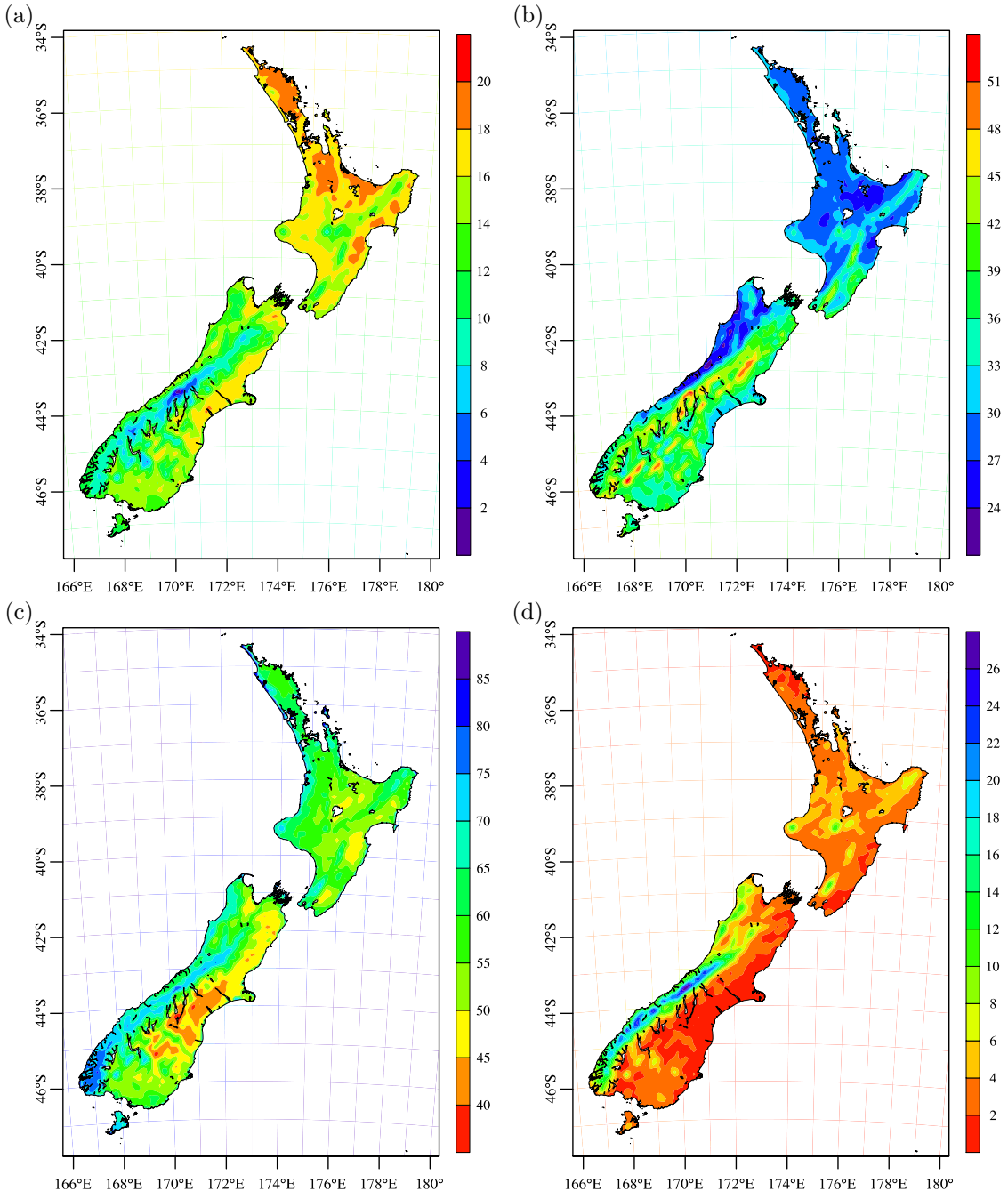

Figure 3.2: Contour plots showing the season-averaged mean modelled (a) daily maximum air temperature (°C), (b) daily maximum wind speed (km h^{-1}), (c) daily minimum relative humidity (%) and (d) daily rainfall (mm).

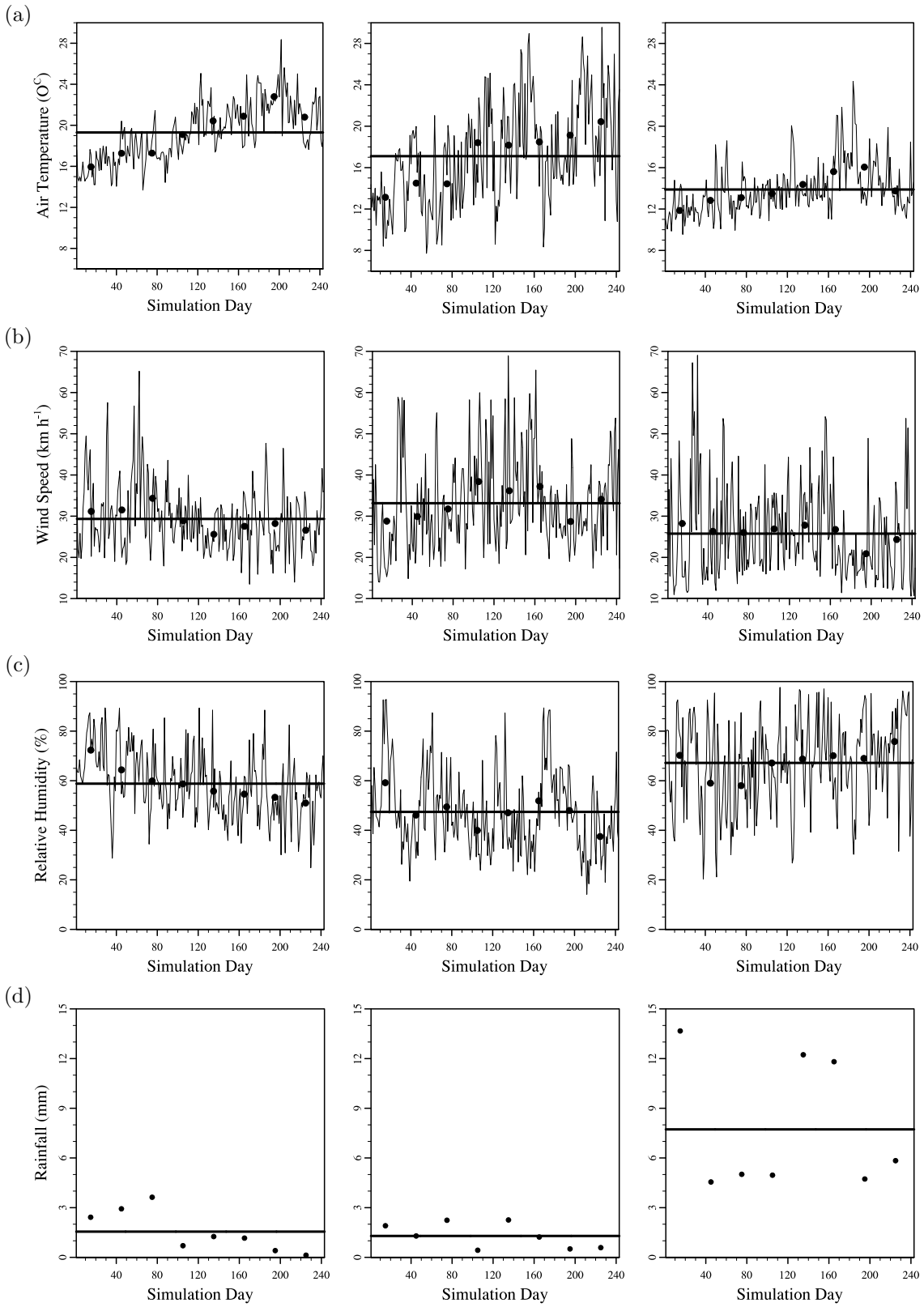

Figure 3.3: Time series plots showing the modelled (a) daily maximum air temperature, (b) daily maximum wind speed, (c) daily minimum relative humidity and (d) monthly mean 24-hr rainfall at the WRF model grid cells closest to the Kaitaia (left), Christchurch (middle) and Hokitika (right) weather stations. The horizontal black lines indicate the season-averaged mean at each model grid cell and the black circular markers show the monthly moving average.

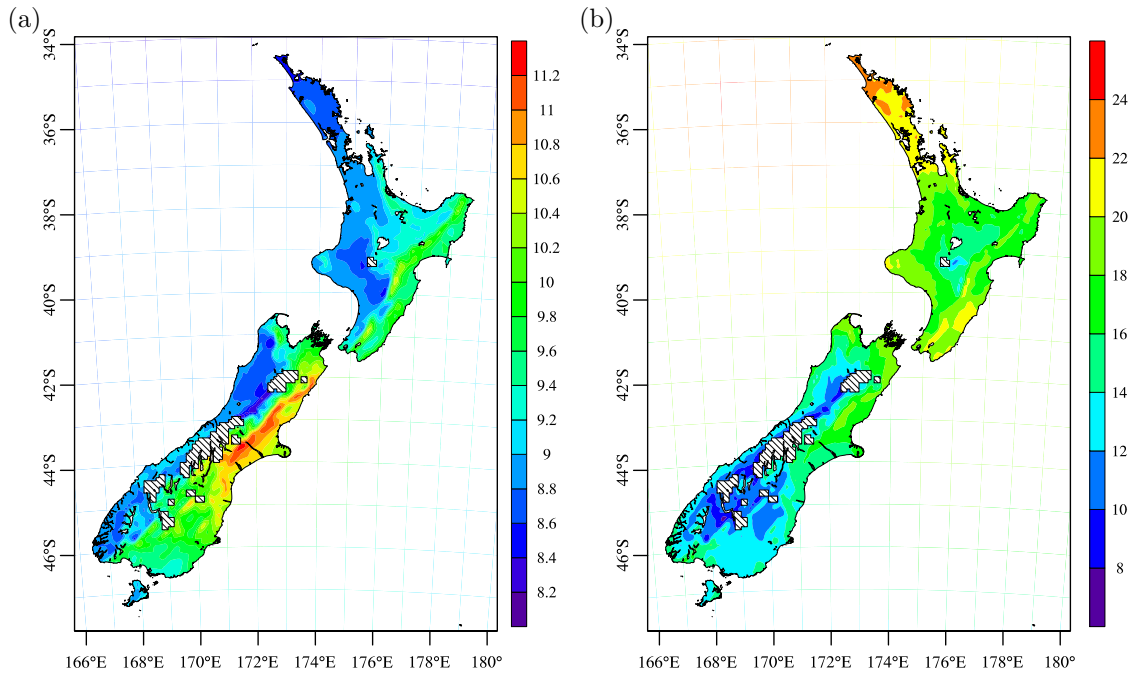

Figure 3.4: Contour plots showing the season-averaged mean modelled daily maximum (a) air temperature lapse rate between 850 and 700 hPa (°C) and (b) dew point depression at 850 hPa (°C). A dashed fill pattern is used in regions where the mean value is undefined.

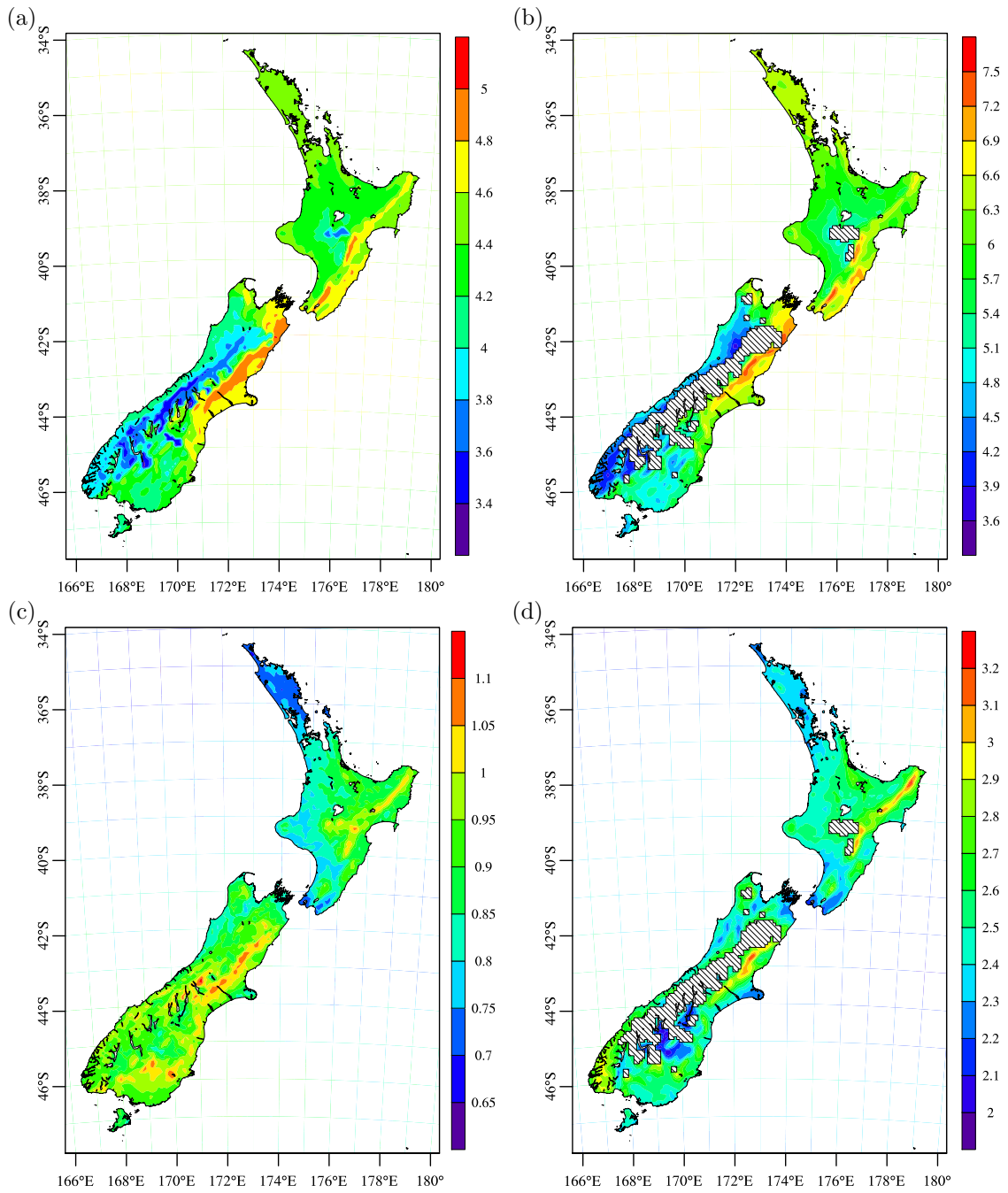

Figure 3.5: Contour plots showing the season-averaged mean (a,b) and standard deviation (c,d) of the modelled daily maximum (a,c) HI and (b,d) CHI. A dashed fill pattern is used in regions where the mean value is undefined.

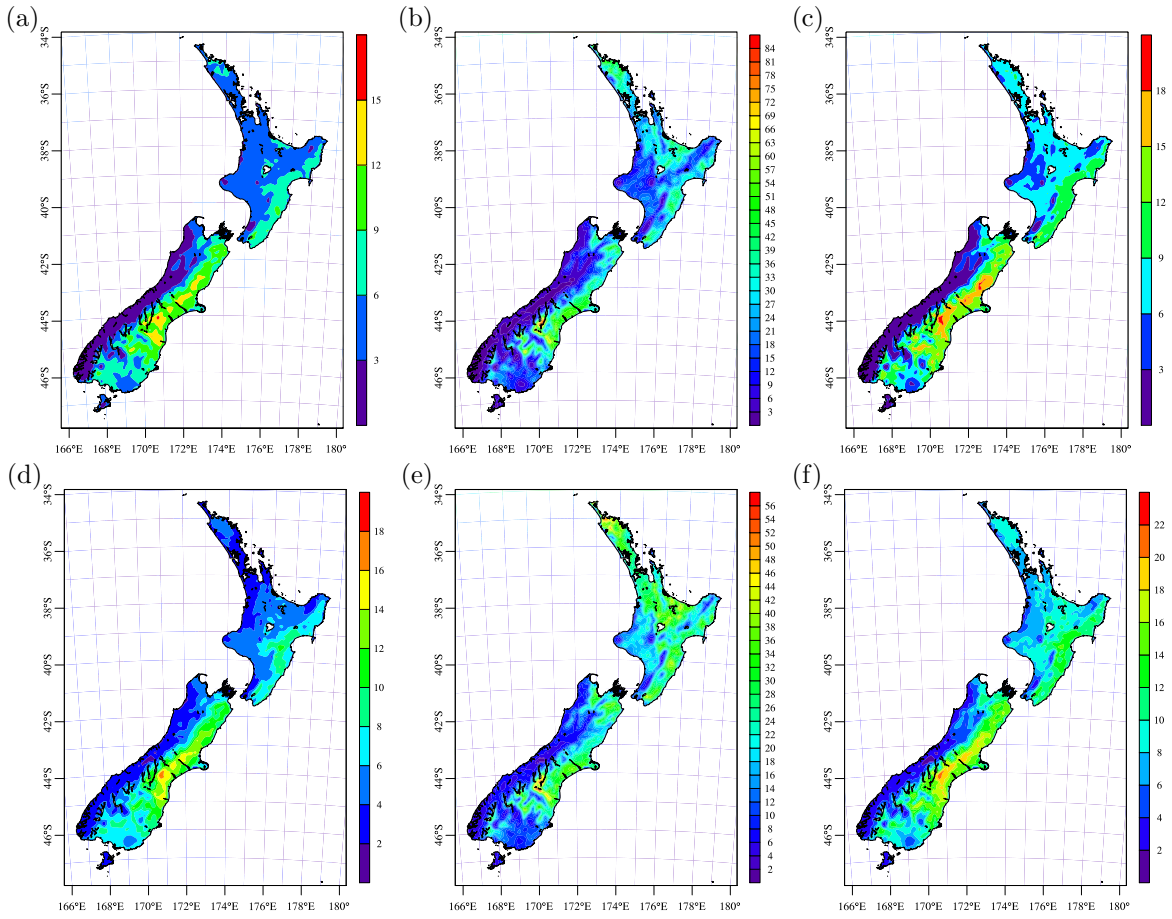

Figure 3.6: Contour plots showing the season-averaged mean (a,b,c) and standard deviation (d,e,f) of the modelled daily maximum (a,d) ISI, (b,e) BUI and (c,f) FWI.

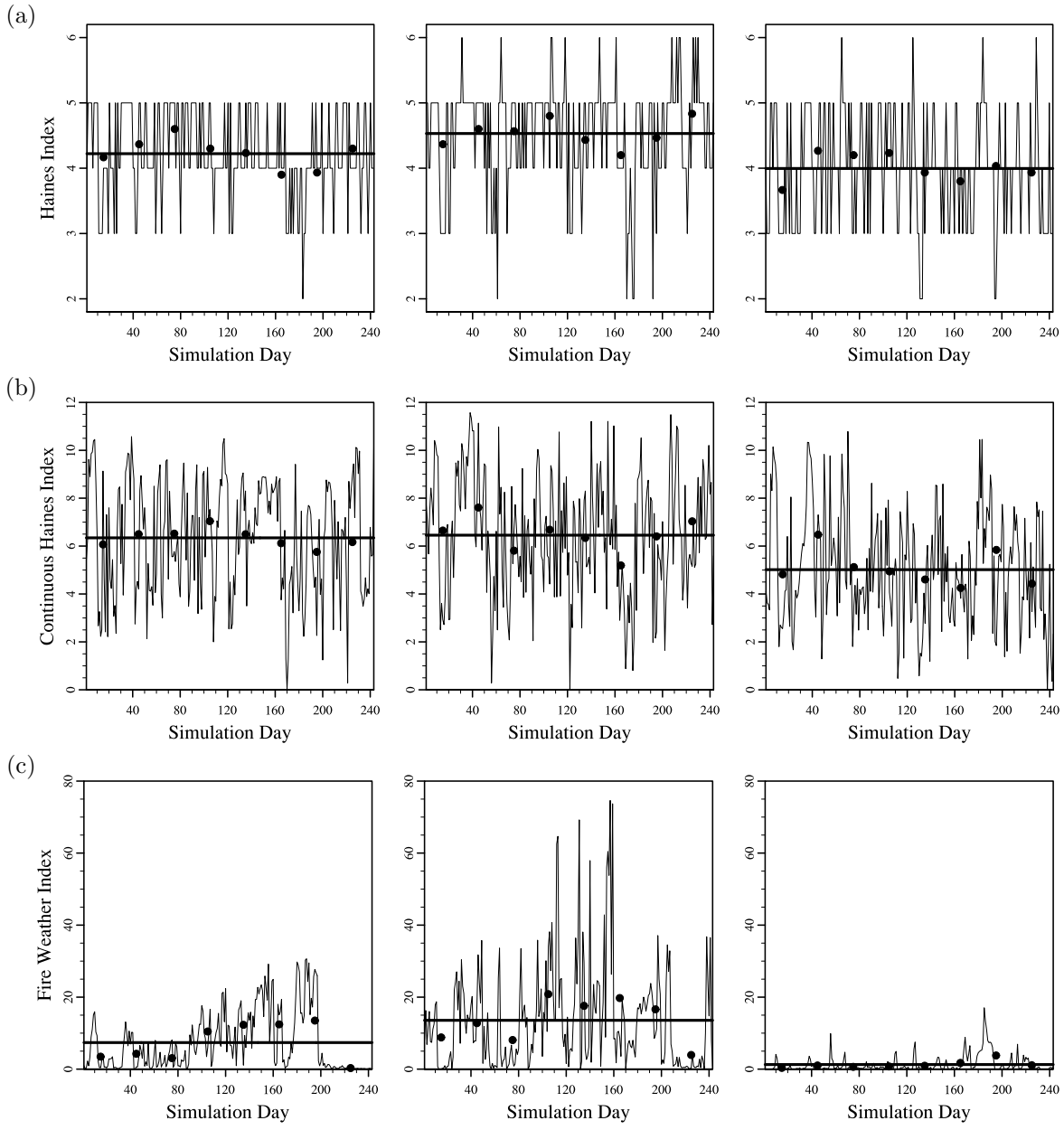

Figure 3.7: Time series plots showing the modelled (a) daily maximum HI, (b) daily maximum CHI and (c) daily FWI at the WRF model grid cells closest to the Kaitaia (left), Christchurch (middle) and Hokitika (right) weather stations. The horizontal black lines indicate the season-averaged mean at each model grid cell and the black circular markers show the monthly moving average.

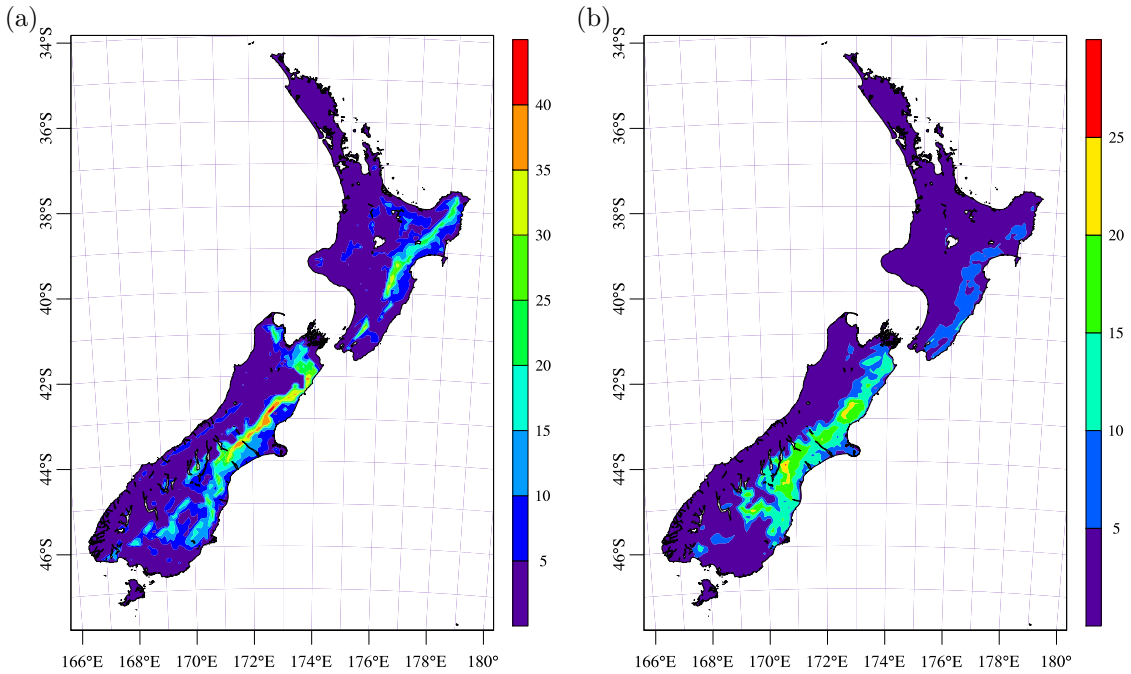

Figure 3.8: Contour plots showing the percentage number of days for which the modelled (a) daily maximum HI is equal to six and (b) daily FWI is greater than 30.

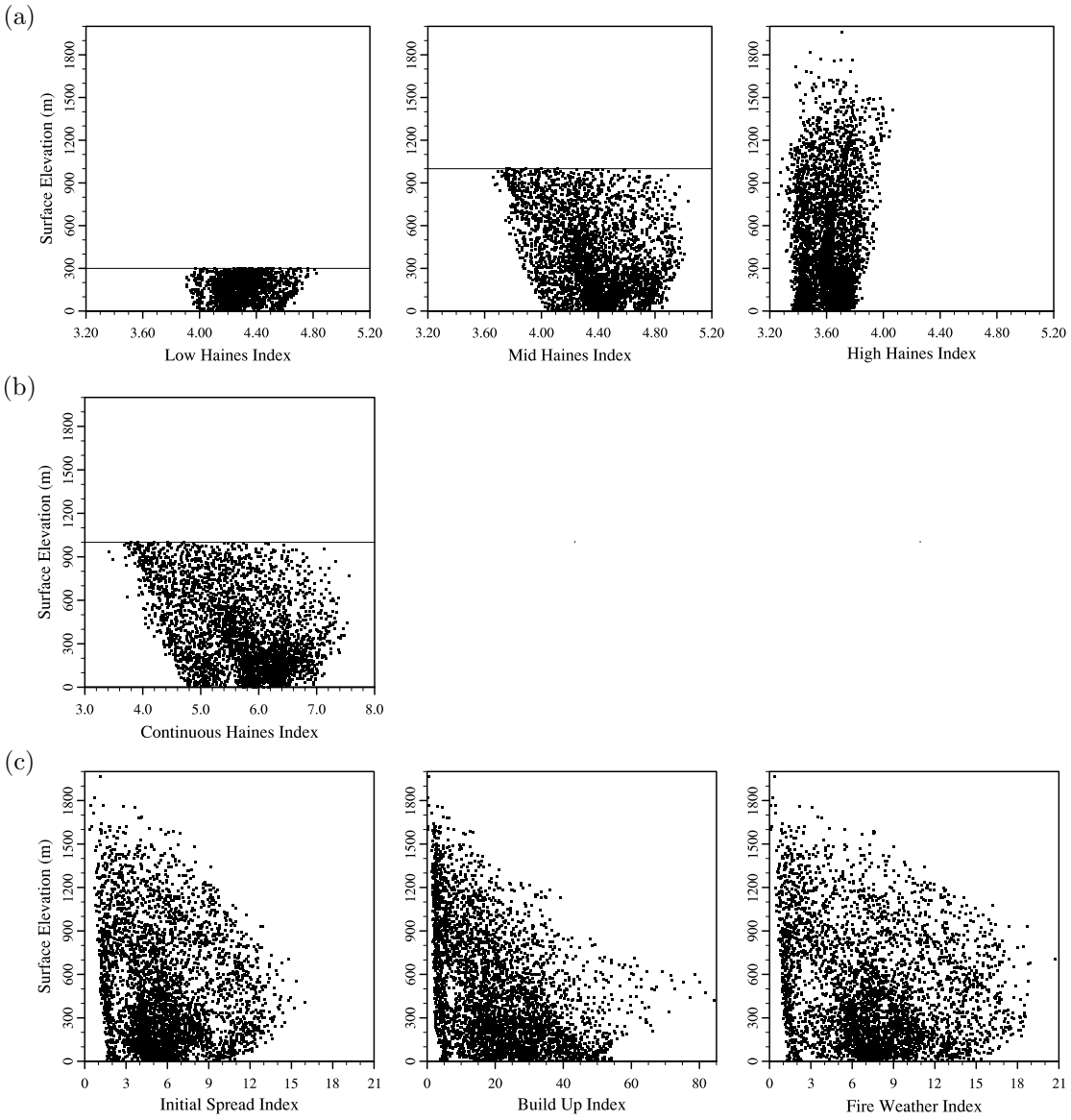

Figure 3.9: Scatter plots showing the surface elevation and season-averaged mean modelled (a) LHI, MHI and HHI, (b) CHI and (c) ISI, BUI and FWI at each WRF model grid cell over land. The LHI and MHI are not calculated at surface elevations above 300 and 1000 m, respectively, and the CHI is not calculated at surface elevations above 1000 m.

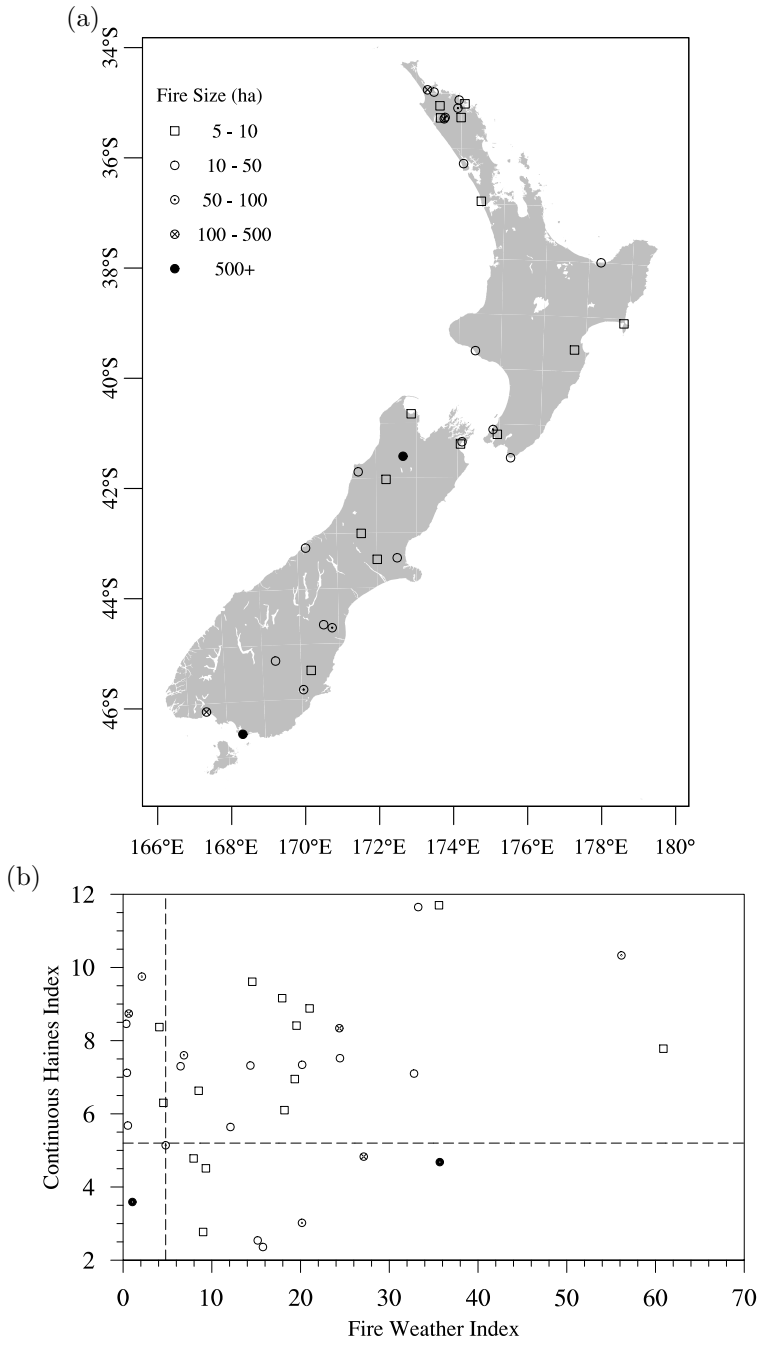

Figure 3.10: (a) Map plot showing the geographical location and approximate size of the 36 wildland fires. (b) Scatter plot showing the modelled daily maximum CHI and daily FWI associated with the 36 wildland fires. The horizontal and vertical dashed lines indicate the season-averaged and nationally-averaged median modelled daily maximum CHI and daily FWI.

Chapter 4

Fire Weather of an Extreme Foehn Event in South Island, New Zealand

C. C. Simpson[A], A. P. Sturman[A], P. Zawar-Reza[A] and H. G. Pearce[B]

[A] Department of Geography, University of Canterbury, Christchurch, New Zealand
[B] Rural Fire Research Group, Scion, Christchurch, New Zealand

Abstract

On 6 February 2011 the South Island of New Zealand experienced synoptically driven northwesterly flow associated with a pressure gradient across the Southern Alps. The interaction of the synoptic flow and the Southern Alps resulted in northwesterly foehn winds in the lee of the mountains, which was modelled using the Weather Research and Forecasting (WRF) atmospheric model. The atmosphere was stable upwind of the Southern Alps and resulted in orographic blocking of lower-level winds along the west coast. Mountain waves developed in the northwesterly flow over the Southern Alps and had a direct influence on fire weather conditions in the lee of the mountains. A hydraulic jump along the foothills of the Canterbury Plains resulted in a downslope windstorm with wind speeds exceeding 80 km h^{-1}. Further south, mountain wave amplification effects resulted in large amplitude waves that directly influenced the near-surface wind speeds and atmospheric stability aloft. The thermal effect of the foehn event resulted in peak near-surface air temperatures over 35°C and relative humidities below 40 % in the eastern coastal South Island. The New Zealand Fire Weather Index indicated that the near-surface fire weather conditions were extreme across widespread regions of the eastern South Island. In contrast, the Continuous Haines Index indicated that the severity of the fire weather conditions aloft was highly variable spatially and closely associated with the mountain wave characteristics. It was typically high in the hydraulic jump region and low where there

were large amplitude mountain waves. The subsequent passage of a cold front on 7 February 2011 brought a marked reduction in fire weather severity across the South Island due to the associated moderate widespread rainfall.

4.1 Introduction

The South Island of New Zealand is situated in the southern mid-latitudes and therefore experiences prevailing westerly synoptic winds. The Southern Alps mountain range extends ∼450 km from the southwest to the northeast of the South Island, as shown in Figure 4.1, and has a significant influence on the weather and climate of the South Island (Sturman et al., 1999). Foehn winds are common in the South Island, aside from in the winter months, and are locally known as either the "Canterbury Northwester", "Northwester" or simply "Nor'wester" (McGowan and Sturman, 1996). The foehn winds are northwesterly in direction and are typically associated with increased air temperatures and wind speeds, and decreased relative humidities on the eastern side of the Southern Alps. Foehn-like winds also occur on the eastern side of the dividing mountain ranges in the North Island. However, their thermal effect is typically smaller than the Northwester due to the lower elevation of the North Island dividing mountain ranges.

Kidson (1932), Lamb (1975), McGowan and Sturman (1996) and McGowan et al. (2002) have previously studied the spatial and temporal characteristics of the Northwester, which is also known to modify local wind systems in the Southern Alps and eastwards of the mountains (McKendry et al., 1985, 1988; McGowan, 2003). In addition, the Northwester is associated with dust transport and wind erosion in the Southern Alps (McGowan et al., 1996; McGowan, 1997). The atmospheric properties upwind of the Southern Alps and subsequent orographic blocking by the mountains have been investigated for a number of Northwesters (McCauley and Sturman, 1999; Wratt et al., 1996). These studies collectively provide valuable information on the characteristics of the Northwester, although little attention has previously been given to its influence on fire weather and climate in the South Island.

Foehn winds are a relatively common meteorological phenomenon globally and are commonly referred to by their local names, such as the Chinook (Brinkmann, 1970), Sundowner (Blier, 1998) and Santa Ana (Raphael, 2003) winds in North America. International studies of foehn winds often consider the associated atmospheric processes over mountainous terrain, such as mountain wave development, downslope windstorms and orographic blocking (Brinkmann, 1971, 1974; Hoinka, 1985; Smith, 1985; Heimann, 1997; Drobinski et al., 2001). The study of foehn winds is therefore closely associated with that of mountain meteorology (Barry, 1992) and remains an active area of research internationally.

Foehn winds are typically associated with an increase in air temperatures and wind speeds, and a decrease in relative humidities on the leeward side of the mountains. Foehn winds can therefore significantly influence fire weather and climate in the lee of mountainous terrain (Whiteman, 2000; Sharples, 2009). For example, the Santa Ana and Sundowner winds are known to influence fire weather in California (Blier, 1998; Westerling et al., 2004) and the frequency of occurrence of Santa Ana winds is expected to rise given future climate projections (Miller and Schlegel, 2006). In Australia, foehn-like winds can result in elevated fire weather severity in Tasmania (Fox-Hughes, 2012) and southeastern Australia (Sharples et al., 2010b).

This study aims to investigate the fire weather associated with an extreme foehn event that occurred on 6 February 2011 in the South Island of New Zealand. This study links the spatial and temporal variations in fire weather to atmospheric processes over compex terrain, such as mountain wave development and orographic blocking. The next section discusses the methods applied throughout this study and is followed by a discussion of the synoptic meteorology of the Northwester. The following two sections discuss the characteristics of the associated orographic blocking and mountain wave development, and the resulting spatial and temporal variations in fire weather conditions across the South Island. Finally, the study is summarised and presented alongside a number of conclusions in the closing section.

4.2 Methods

4.2.1 Fire Weather Assessment

Fire weather can be assessed through consideration of fire weather indices and weather variables that are associated with wildland fire behaviour. Fire weather indices typically aim to summarise the fire weather conditions using a numerical rating system, although they differ from each other in their choice of considered weather variables. The fire weather indices considered in the analysis are the New Zealand Fire Weather Index (FWI) and Continuous Haines Index (CHI). The weather variables considered in the analysis are the air temperature, relative humidity, rainfall, wind speed and wind direction. These weather variables were chosen as they are each associated with wildland fire behaviour (Potter, 2012a) and are collectively used to derive the hourly FWI (Van Wagner, 1977).

The FWI is a fire behaviour index that represents the expected fire intensity for a reference fuel type and is the primary index used in fire weather assessment throughout New Zealand. The FWI is an important component of the New Zealand Fire Danger Rating System (Anderson, 2005), which is based on the Canadian Forest Fire Danger Index (Van Wagner, 1987; Stocks et al., 1989; Lawson and Armitage, 2008) and has been specifically modified for use in New Zealand (Fogarty et al., 1998; Anderson, 2005).

The FWI is derived from the air temperature, relative humidity, wind speed and rainfall at or below 10 m above ground level and an FWI value of greater than or equal to 30 indicates extreme near-surface fire weather conditions for forested regions (Alexander, 1994, 2008).

The CHI (Mills and McCaw, 2010) is a stand-alone fire weather index that is based on the widely used Haines Index (Haines, 1988). The CHI is calculated through the summation of an atmospheric stability index, which is calculated based on air temperature lapse rate between 850 and 700 hPa, and a humidity index, which is calculated based on the dew point depression at 850 hPa. Higher values of the air temperature lapse rate or dew point depression result in higher CHI values. It has previously been suggested that the CHI could be used operationally alongside the FWI in New Zealand (Simpson et al., 2013a). However, due to the use of fixed atmospheric pressure levels it is not calculated at surface elevations above 1000 m. Throughout this study the CHI is calculated using NWP model output only, due to a lack of available weather station measurements of the vertical profiles of the air and dew point temperatures.

4.2.2 Numerical Weather Prediction Model

The numerical weather prediction (NWP) model used in this study is version 3.4 of the Weather Research and Forecasting (WRF) model (Skamarock et al., 2008). The WRF model was chosen for this study as it is widely used in the scientific community and has previously been applied to investigating fire weather in New Zealand (Simpson et al., 2013b,a). The simulation covers a five-day period from 1200 NZST on 3 February 2011 to 1200 NZST on 8 February. The modelled hourly air temperatures and relative humidities are taken at 2 m above ground level, whereas the modelled hourly wind speeds are taken at 10 m above ground level.

A two-way nested three domain configuration is used to model synoptic and mesoscale weather processes across New Zealand. The three domains have a horizontal grid spacing of 18, 6 and 2 km, respectively, and a computational domain of 120×120, 193×193 and 391×391 grid points, respectively. The first domain covers all of mainland New Zealand and extends far out into the Pacific Ocean and Tasman Sea. The second domain covers all of the South Island and a fraction of the North Island, whereas the third domain covers only the South Island. The three domains share an identical configuration of 50 vertical levels, which extend from a height of ∼16 m above ground level to a fixed model pressure top of 10 hPa. Four-dimensional data assimilation is used to nudge the first domain at six-hourly intervals using the National Centers for Environmental Prediction (NCEP) Final Analyses (FNL).

WRF utilises fully compressible non-hydrostatic equations and has a mass-based terrain-following coordinate system. The microphysics are represented by a single-

moment six-class scheme with mixed-phase processes (Hong and Lim, 2006). The sub-grid scale effects of convective or shallow clouds are modelled in the first domain using a modified Kain-Fritsch scheme (Kain, 2004). The surface layer and planetary boundary layer are represented by the Eta schemes (Janjic, 1990, 1996, 2002). The heat and moisture fluxes over land are provided by the Noah Land Surface Model (Chen and Dudhia, 2001), which has soil temperature and moisture in four layers, fractional snow cover and frozen soil physics. The short-wave and long-wave radiation are represented by a simple short-wave radiation scheme (Dudhia, 1989) and the Rapid Radiative Transfer Model (Mlawer et al., 1997), respectively. A gravity wave damping layer (Klemp et al., 2008) is used in the top 2 km to prevent unphysical wave reflection off the upper boundary. The main model time steps are 30, 10 and ∼3.3 s for the three domains, respectively, with time integration performed using a third-order Runge-Kutta scheme (Wicker and Skamarock, 2002). This physics and dynamics configuration is broadly similar to that used in previous WRF studies on fire weather in New Zealand (Simpson et al., 2013b,a).

4.2.3 Weather Station Data

The analysis in this study considers observed fire weather conditions at the Christchurch, Tara Hills and Hokitika weather stations, the locations of which are shown in Figure 4.1. These three stations were chosen as they are expected to experience different fire weather conditions associated with the foehn event. Hokitika is located west of the Southern Alps where heavy orographic rainfall is expected. Christchurch and Tara Hills are located east of the Southern Alps, where high air temperatures and wind speeds, and low relative humidities are expected. However, Tara Hills could experience different fire weather conditions due to its more southerly and inland location.

The observational data were obtained from the National Climate Database, which is operated by the National Institute of Water and Atmospheric Research (NIWA), and includes the hourly air temperatures, relative humidities, wind speeds, wind directions and rainfall. There are no missing data for the period from 1200 NZST on 3 February 2011 to 1200 NZST on 8 February. The air temperatures and relative humidities were measured at 1.2 m above ground level, whereas the wind speeds were measured at 10 m above ground level.

4.3 Synoptic Meteorology

Figure 4.2 shows the mean sea level pressure (MSLP) analyses issued by the Bureau of Meteorology, Australia, for the Australia and New Zealand region from 4 to 7 February 2011. At 1200 NZST on 4 February the remnants of Tropical Cyclone Yasi as a tropical low was located over northern Australia, and high pressure systems were located south-

west of Australia and northwest of New Zealand. The high pressure system southwest of Australia had a peak central pressure of 1034 hPa at 1200 NZST on 4 February and moved eastwards from 4 to 7 February across the Great Australian Bight. The high pressure system northwest of New Zealand had a central pressure of 1023 hPa at 1200 NZST on 4 February and its location and central pressure did not change significantly by 1200 NZST on 6 February. From 4 to 7 February, a pair of cold fronts moved from the Great Australian Bight eastwards across Tasmania and then the South Island of New Zealand.

Figure 4.3 shows the modelled MSLP and 10 m horizontal wind conditions for the New Zealand region from 4 to 7 February. At 1200 NZST on 6 February, a combination of high pressure to the north and northeast, low pressure to the southwest and an approaching cold front resulted in a strong synoptic pressure gradient from northeast to southwest across the South Island. This resulted in northwesterly synoptic flow across the South Island. Orographic blocking of the lower-level northwesterly winds by the Southern Alps resulted in the development of a lee trough in the eastern South Island and flow splitting around the South Island. The passage of the cold front through the South Island on 7 February brought predominantly southwesterly flow and eliminated the pressure gradient across the South Island.

Figure 4.4 shows the time series of the MSLP difference between the model grid cells nearest to the Hokitika and Christchurch weather stations from 0000 NZST on 5 February to 0000 NZST on 8 February. These weather stations are located at similar latitudes on either side of the Southern Alps and the cold front passed over them at similar times. The pressure gradient across the Southern Alps began to intensify early on 5 February and increased from $\sim$2 to 7 hPa by 0000 NZST on 6 February. On 6 February the MSLP difference varied from $\sim$8 to 10 hPa as a result of the orographic blocking by the Southern Alps. The MSLP difference dropped sharply starting at 2300 NZST on 6 February due to the passage of the cold front, reaching $\sim$0 hPa by 0600 NZST on 7 February.

Figure 4.5 shows the modelled 500 hPa geopotential height and horizontal wind conditions for the New Zealand region from 4 to 7 February. The 500 hPa geopotential height decreased with increasing latitude and the latitudinal gradient was strongest across the South Island throughout the four-day period. At 1200 NZST on 4 and 5 February, the prevailing westerly winds aloft were predominantly zonal across New Zealand and the wind speeds typically increased with increasing latitude. At 1200 NZST on 6 February, there was a northwesterly jet stream across the South Island, with higher wind speeds upstream of the Southern Alps and lower wind speeds downstream. At 1200 NZST on 7 February, the northwesterly jet stream westwards of the South Island weakened and changed to a predominantly westerly direction, whereas to the east the jet stream

strengthened and changed to a predominantly northwesterly direction.

4.4 Orographic Blocking and Mountain Waves

Figure 4.6 shows the modelled 10 m horizontal wind streamlines for the South Island region at 1200 NZST on 6 and 7 February. At 1200 NZST on 6 February, there was northwesterly synoptic flow across the Tasman Sea, which subsequently interacted with the Southern Alps. Orographic blocking by the Southern Alps resulted in the development of a northeasterly barrier flow along the central west coast of the South Island. There was also limited flow splitting around the north and south of the South Island through the Cook and Foveaux Straits, respectively. The resulting gap flow through the Cook Strait had a northerly to northeasterly direction close to the eastern coastline of the South Island, athough it did not modify the wind direction inland over the Canterbury region. At 1200 NZST on 7 February, the passing cold front brought predominantly southwesterly flow over the Tasman Sea and Pacific Ocean. The wind direction was southerly over the Canterbury Plains, although the wind direction was less clear over land throughout the rest of the South Island.

Figure 4.7 shows the modelled vertical wind velocity 2 km above sea level for the South Island region at 1200 NZST on 6 February and 0000 NZST on 7 February. At 1200 NZST on 6 February, mountain waves associated with the foehn event had developed over the Southern Alps. In the central South Island the mountain waves did not propagate far downstream, whereas further south the mountain waves propagated far downstream and out over the Pacific Ocean. At 0000 NZST on 7 February, the frontal zone was located over the central South Island and there were no mountain waves behind it, due to the associated change in air mass. Figure 4.8 clearly shows cloud formations associated with both the mountain waves and cold front in MODIS satellite imagery on 6 and 7 February.

Figure 4.9 shows two vertical cross-sections of the modelled potential temperature across the South Island region at 1200 NZST on 6 February. The cross-sections are located over the Canterbury and Otago regions and are aligned approximately parallel to the northwesterly foehn winds. There are two hydraulic jumps in the Canterbury cross-section, with one along the central Southern Alps and one along the foothills of the Canterbury Plains. Hydraulic jumps such as these are commonly associated with severe downslope winds. The potential temperature was weakly stratified along the Canterbury Plains below $\sim$800 m above ground level, which indicates that the planetary boundary layer was well mixed in this layer and capped by mountain waves. In the Otago cross-section the northwesterly flow encountered a number of widely spaced mountain peaks and the mountain waves propagated far downstream out over the Pacific Ocean. Mountain wave amplification effects were seen over land in the eastern half of the Otago

cross-section and the potential temperature was weakly stratified only within ∼60 km of the east coast up to a height of ∼800 m above ground level. As the upstream potential temperature lapse rate was similar in both cross-sections, the differences in mountain wave characteristics between the Canterbury and Otago regions must be associated with the different terrain profiles and incoming wind speeds.

A more detailed assessment of the mountain wave properties is beyond the scope of this thesis, but would likely follow the procedures used in other studies (Smith et al., 2008). For example, the phase relationships between the horizontal and vertical wave velocities, and the potential temperatures could be investigated in detail. This would help in confirming that the stability and winds, and the associated waves are consistent with dynamics theory.

4.5 Fire Weather

Figure 4.10 shows the spatial variability in modelled fire weather conditions across the South Island at 1200 NZST on 6 February. The air temperatures were over 30°C in isolated coastal regions of the northeastern and central South Island. The relative humidities followed a similar spatial pattern to the air temperatures and were typically less than 50 % where the air temperatures were higher than 30°C. There was significant spatial variability in the relative humidities, which were high (low) to the west (east) of the Southern Alps. The apparent line separating high and low relative humidities approximately followed the mid point of the Southern Alps. There was heavy rainfall across the central and southern west coast, with modelled 24-hr rainfall in excess of 250 mm in isolated regions. The heavy rainfall indicates that despite orographic blocking of lower-level winds, there was still orographic lifting of the northwesterly synoptic flow over the Southern Alps.

There were alternating bands of high and low wind speeds across the central and southern South Island, which were aligned approximately parallel to the southwest to northeast orientation of the Southern Alps. These wind speed bands are therefore likely to be associated with the large amplitude mountain waves seen in Figure 4.9c. The wind speeds were highest along the foothills of the Canterbury Plains, where they exceeded 80 km h^{-1}, and are associated with the hydraulic jump seen in Figure 4.9b. Immediately downstream of the foothills of the Canterbury Plains are three distinct low wind speed regions, which are associated with the transition from high to low wind speeds at the hydraulic jump. The FWI values were close or equal to zero westwards of the Southern Alps due to the heavy rainfall and high relative humidities. In contrast, the FWI values were higher than 30 across widespread regions eastwards of the Southern Alps, indicating extreme fire weather conditions.

The CHI values were moderate to high in the central and northeastern South Island and comparatively low further south. Figure 4.11 shows Skew–T Log–P diagrams at the model grid cells nearest to the Christchurch and Tara Hills weather stations, which are located in regions of comparatively high and low CHI values, respectively, at 1200 NZST on 6 February. The air temperature lapse rate between 850 and 700 hPa is ∼10 and 5°C km^{-1} at Christchurch and Tara Hills, respectively, and the dew point depression at 850 hPa is ∼22 and 6°C, respectively. The CHI value is therefore higher at Christchurch due to the higher temperature lapse rate and dew point depression aloft. The difference in temperature lapse rate between the two locations is likely to be related to the difference in mountain wave characteristics between Canterbury and Otago. The vertical potential temperature lapse rate between 850 and 700 hPa was higher downstream of the hydraulic jump in the Canterbury cross-section than in the large amplitude mountain waves in the Otago cross-section.

As the CHI only considers the atmospheric layer between 850 and 700 hPa, it does not account for the extremely dry air at 500 hPa seen at Christchurch in Figure 4.11a. This could be an important limitation of the CHI if a wildland fire's pyro-convective plume extends up to a height of 500 hPa and vertical return circulations close to the plume bring this dry air down to the surface near to or ahead of the fire. Any such dry air that is brought to the surface would act to increase the flammability of the vegetation, particularly fine fuels. Thermodynamic analysis of Figure 4.11a indicates that the convection temperature at Christchurch was ∼42°C, or approximately 13°C higher than the modelled near-surface air temperature. If heat added to the atmosphere by a wildland fire is sufficient to lift the near-surface air dry adiabatically in the pyro-convective plume to the convection condensation level, this would likely initiate free convection up to the tropopause and allow the plume to interact with the dry air at 500 hPa. However, the situation is complicated by the facts that combustion also adds moisture to the pyro-convective plume, which will affect its buoyancy, and turbulent mixing and entrainment in the mixed layer can diffuse the pyro-convection plume and its associated vertical return circulations.

Figure 4.12 shows the spatial variation in modelled fire weather conditions across the South Island at 1200 NZST on 7 February. Eastwards of the Southern Alps, the air temperatures were ∼10 to 20°C colder than at 1200 NZST on 6 February. The relative humidities were typically higher than 80 % within ∼300 km of the frontal zone and less than 70 % further south. The 24-hr rainfall was higher than 10 mm across most of the central and southern South Island and exceeded 250 mm in isolated regions west of the Southern Alps. The isolated regions of heavy rainfall were associated with the foehn event, whereas the widespread moderate rainfall was associated with the passing cold front. The wind speeds were relatively uniform across the South Island behind the

frontal zone and were typically less than 30 km h^{-1}. The FWI values were uniformly close to or equal to zero behind the frontal zone due to a combination of the reduced air temperatures and wind speeds, increased relative humidities and moderate widespread rainfall.

The CHI values were uniformly low aross the South Island behind the frontal zone. Figure 4.13 shows Skew–T Log–P diagrams at the model grid cells nearest to the Christchurch and Tara Hills weather stations at 1200 NZST on 7 February. The air temperature lapse rate between 850 and 700 hPa is ∼0 and 3°C km^{-1} at Christchurch and Tara Hills, respectively. The dew point depression at 850 hPa is ∼0°C at both Christchurch and Tara Hills, indicating the air at this level is saturated. The cold front passage brought a change in wind direction below ∼2 and 3 km at Christchurch and Tara Hills, respectively. At both locations the post-frontal cold air mass was capped by a potential temperature inversion above 1.5 and 2.5 km, respectively.

Figure 4.14a shows the time series of the observed air temperatures at the Christchurch, Tara Hills and Hokitika weather stations from 0000 NZST on 5 February to 0000 NZST on 8 February. On 5 February, the diurnal variation in air temperature was greatest at Tara Hills and comparatively low at Christchurch and Hokitika. At 2200 NZST on 5 February the diurnal variation in air temperature was reversed at Christchurch and Tara Hills, which marked the onset of the foehn's thermal effect. The air temperature increased from 17 to 35°C at Christchurch and 23 to 32°C at Tara Hills by 1500 NZST on 6 February. These daily maximum air temperatures exceeded the climatological averages for February from 1981–2010, which are 21.9 and 23.3°C at Christchurch and Tara Hills, respectively. The passing cold front resulted in a rapid decrease in air temperatures after 2200 NZST at Tara Hills and 0100 NZST on 7 February at Christchurch. The air temperature showed little variation at Hokitika on 6 February and dropped only a few degrees with the passage of the cold front after 0700 NZST on 7 February.

Figure 4.14b shows the time series of the observed relative humidities at the Christchurch, Tara Hills and Hokitika weather stations from 0000 NZST on 5 February to 0000 NZST on 8 February. On 5 February, the relative humidity exhibited a diurnal variation at each station that was inversely associated with the air temperature, with a daily minimum of ∼30 and 70 % at Tara Hills and Christchurch, respectively. As with the air temperature, the diurnal variation in relative humidity was reversed due to the onset of the foehn's thermal effect at 2200 NZST on 5 February. The relative humidity decreased to a daily minimum of ∼40 % by 1300 NZST on 6 February at Tara Hills and ∼30 % by 1800 NZST at Christchurch. The passage of the cold front resulted in a rapid increase in relative humidities after 2200 NZST on 6 February at Tara Hills and 0100 NZST on 7 February at Christchurch. The relative humidity was ∼100 % at Hokitika on 6 February due to the heavy rainfall.

Figures 4.14c and 4.14d shows the time series of the observed wind conditions at the Christchurch, Tara Hills and Hokitika weather stations from 0000 NZST on 5 February to 0000 NZST on 8 February. The wind direction changed from southeasterly to approximately northwesterly at 1600 NZST at Tara Hills and coincided with a sudden increase in wind speeds, marking the onset of the foehn winds. The wind direction changed from approximately northeasterly to northwesterly at 1000 NZST at Christchurch and also coincided with a sudden increase in wind speeds, marking the onset of the foehn winds at this coastal location. The wind speeds were highly variable at Tara Hills and Christchurch throughout 6 February, although they were typically higher than throughout 5 February. The daily maximum hourly wind speeds were ∼45 km h^{-1} at 1200 NZST on 6 February at Tara Hills and ∼50 km h^{-1} at 1900 NZST at Christchurch. The passage of the cold front brought a marked change in wind direction in the final hours on 6 February at Tara Hills and 0200 NZST at Christchurch. At Hokitika, the orographic blocking of the northwesterly foehn winds by the Southern Alps resulted in a northerly to northeasterly barrier flow forming at around 1100 NZST on 5 February. This barrier jet was associated with moderate wind speeds and persisted until around 0600 NZST on 7 February, after which time the passage of the cold front resulted in a change to southwesterly flow.

Figure 4.14e shows the time series of the FWI derived from observed weather conditions at the Christchurch, Tara Hills and Hokitika weather stations from 0000 NZST on 5 February to 0000 NZST on 8 February. At Christchurch, the FWI was relatively low until 0900 NZST on 6 February, after which time it increased to a daily maximum of ∼75 at 1900 NZST. At Tara Hills, the FWI was relatively low until 1500 NZST on 5 February, after which time it increased to a daily maximum of ∼55 at 1200 NZST on 6 February. At Christchurch and Tara Hills the timing of the sudden increase in the FWI and the daily maximum value coincided with the observed wind conditions. The FWI values were higher than 30, indicating extreme near-surface fire weather conditions, for a combined period of ∼10 hr at both Tara Hills and Christchurch. The passage of the cold front resulted in a sudden decrease in the FWI towards zero by 0000 NZST on 7 February at Tara Hills and 1000 NZST at Christchurch.

Figure 4.14f shows the time series of the modelled CHI at the model grid cells nearest to the Christchurch and Tara Hills weather stations from 0000 NZST on 5 February to 0000 NZST on 8 February. Prior to the foehn event, the CHI peaked locally at a value of ∼5 at 0900 NZST on 5 February at Christchurch. After 1600 NZST, the CHI increased from ∼5 to 9 by 0000 NZST on 6 February and was predominantly above 8 throughout 6 February. In the first half of 6 February, the CHA and CHB contributed relatively evenly towards the high CHI values. In the second half of 6 February, the CHB increased and became the dominant contributor towards the high CHI values, whereas the CHA

decreased. As the CHB is an indicator of atmospheric humidity aloft, this suggests that the drying effect of the foehn event contributed most significantly towards the high CHI values at Christchurch. The CHI was low at Tara Hills on 6 February, due to the weak air temperature lapse rate between 850 and 700 hPa and dew point depression at 850 hPa seen in Figure 4.11b. The passage of the cold front resulted in a sharp drop of the CHI towards zero at both locations.

4.6 Summary and Conclusions

This case study has investigated the fire weather conditions associated with an extreme foehn event on 6 February 2011 across the South Island of New Zealand. The synoptic situation led to northwesterly synoptic flow across the South Island on 6 February and the northwesterly foehn winds were associated with widespread extreme fire weather conditions across the eastern South Island. Orographic blocking of the lower-level northwesterly synoptic flow resulted in a northeasterly barrier flow along the central west coast and flow splitting around the north and south of the South Island through the Cook and Foveaux Straits. The resulting gap flow through the Cook Strait did not modify the local winds across the eastern South Island like in some previous Northwester events (McKendry et al., 1985). The synoptic situation and orographic blocking are similar to that observed in some previous Northwester events (McGowan and Sturman, 1996; McCauley and Sturman, 1999).

Mountain waves developed in the northwesterly synoptic flow over the Southern Alps and their characteristics varied markedly across the South Island due to the varying terrain and upstream wind profiles. There was limited downstream propagation of mountain waves over Canterbury and a hydraulic jump along the foothills of the Canterbury Plains. Trapped lee waves propagated far downstream over Otago and wave amplification effects were seen due to the widely spaced and numerous mountain peaks. The trapped lee waves have the potential to modify pyro-convective plume dynamics and therefore also wildland fire behaviour. For example, if the upward velocity portion of a mountain wave passes over a pyro-convective plume that has developed vertically to the top of the well-mixed surface layer, this could locally enhance vertical plume development and vertical return circulations. Local enhancement of the vertical plume development could more directly influence fire behaviour through its effects on the near-surface inflow at the base of the plume. In contrast, the downward velocity portion would locally suppress vertical plume development, although it could promote enhanced vertical return circulations outside of the plume. The precise impact of these passing mountain waves on wildland fire behaviour would be a useful topic for further research.

Both the northwesterly foehn winds and mountain waves significantly influenced the

fire weather conditions in the lee of the Southern Alps. The combination of high air temperatures and wind speeds, and low relative humidities resulted in widespread extreme near-surface fire weather conditions across the eastern South Island. Both the FWI and CHI were at a maximum along the foothills of the Canterbury Plains, due to the high wind speeds in excess of 80 km h^{-1} and high air temperature lapse rate between 850 and 700 hPa associated with the hydraulic jump. The large amplitude mountain waves across the southern South Island significantly influenced the horizontal wind conditions down to 10 m above ground level. The apparent absence of high wind speeds due to topographic channelling in the Southern Alps, such as that observed by McGowan and Sturman (1996), could be associated with the coarse spatial resolution of the model. When compared with the fire weather climatology of the South Island (Pearce et al., 2011b), this Northwester event constitutes an extreme fire weather event.

The passage of the cold front over the South Island brought a southerly change in wind direction on the eastern side of the Southern Alps that was similar to previously studied southerly changes (Sturman et al., 1990). The change in wind direction below a height of 2 km is important as approximately ninety degree changes in wind direction are widely known to lead to potentially dangerous changes in wildland fire behaviour, in particular the rate and direction of forward spread (Cheney et al., 2001). In this case the wind direction changed by approximately ninety degrees at Christchurch around two hours before the FWI dropped below 30 due to the rainfall associated with the frontal zone. This two hour period represents a dangerous fire weather situation for fire fighters and further research is needed to identify the relationship of the wind directions and FWI during Northwester events.

The results demonstrated the difference in behaviour of the FWI and CHI in response to the Northwester event. The FWI indicated widespread extreme near-surface fire weather conditions across widespread regions of the eastern South Island. In contrast, the CHI only indicated high fire weather severity aloft in the central and northeastern South Island and low severity further south. The CHI appeared to be more sensitive to the spatial variations in mountain wave characteristics than the FWI, which is intuitive given that the CHI partly measures the atmospheric stability aloft. In addition, the layer of extremely dry air at 500 hPa was not accounted for by the CHI, which only considers the layer between 850 and 700 hPa. This could be an important limitation in situations where there is significant vertical atmosphere-fire interactions.

The fire weather conditions associated with Northwester events could significantly influence wildland fire behaviour in the eastern South Island. The sudden and simultaneous increase in air temperatures and decrease in relative humidities at the onset of the foehn's thermal effect, which can occur at a time distinct from the sudden change in wind conditions, could result in a sudden intensification of fire behaviour. The combina-

tion of high peak air temperatures and wind speeds, and low relative humidities, could influence important aspects of fire behaviour, such as the fine fuel flammability and the forward rate of fire spread. The highly variable wind speeds in the lee of the mountains are associated with the turbulent well-mixed planetary boundary layer and the large amplitude mountain waves and could influence fire behaviour in an unpredictable and complex manner. The downslope windstorms associated with the hydraulic jump and the southwesterly wind direction change associated with the passing cold front represent dangerous fire weather situations for fire fighters. The high air temperature lapse rates and dew point depressions between 850 and 700 hPa indicate that vertical atmosphere-fire interactions could influence fire behaviour in the central South Island. If a wildland fire were to interact vertically with the very dry layer at 500 hPa, this could also lead to a dangerous fire weather situation for fighters. Further research is needed to investigate the fire behaviour of major wildland fires that have occurred in the lee of the Southern Alps during Northwester events.

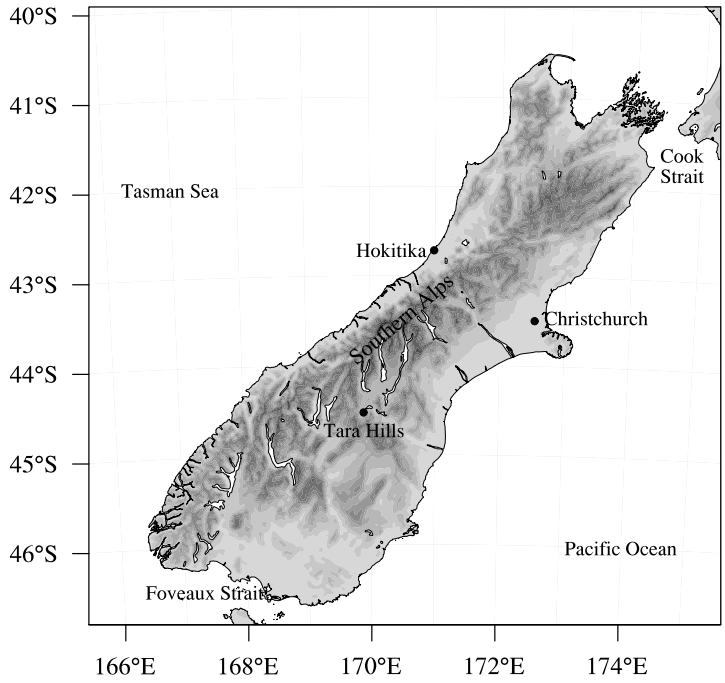

Figure 4.1: Locations and names of the three weather stations and important geographical features of the South Island, New Zealand.

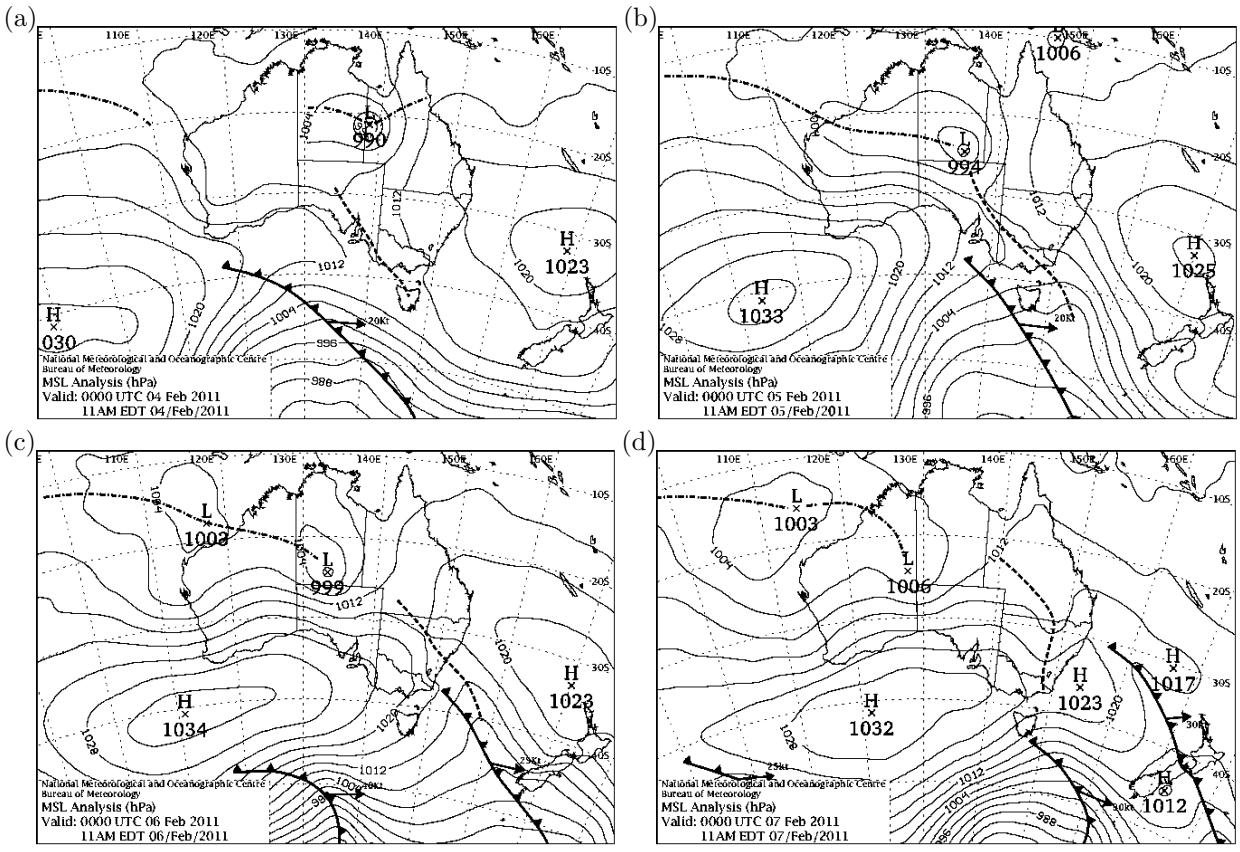

Figure 4.2: MSLP maps issued by the Bureau of Meteorology, Australia, for the Australia and New Zealand region at 1200 NZST on 4 to 7 February 2011. The MSLP is contoured at an interval of 4 hPa.

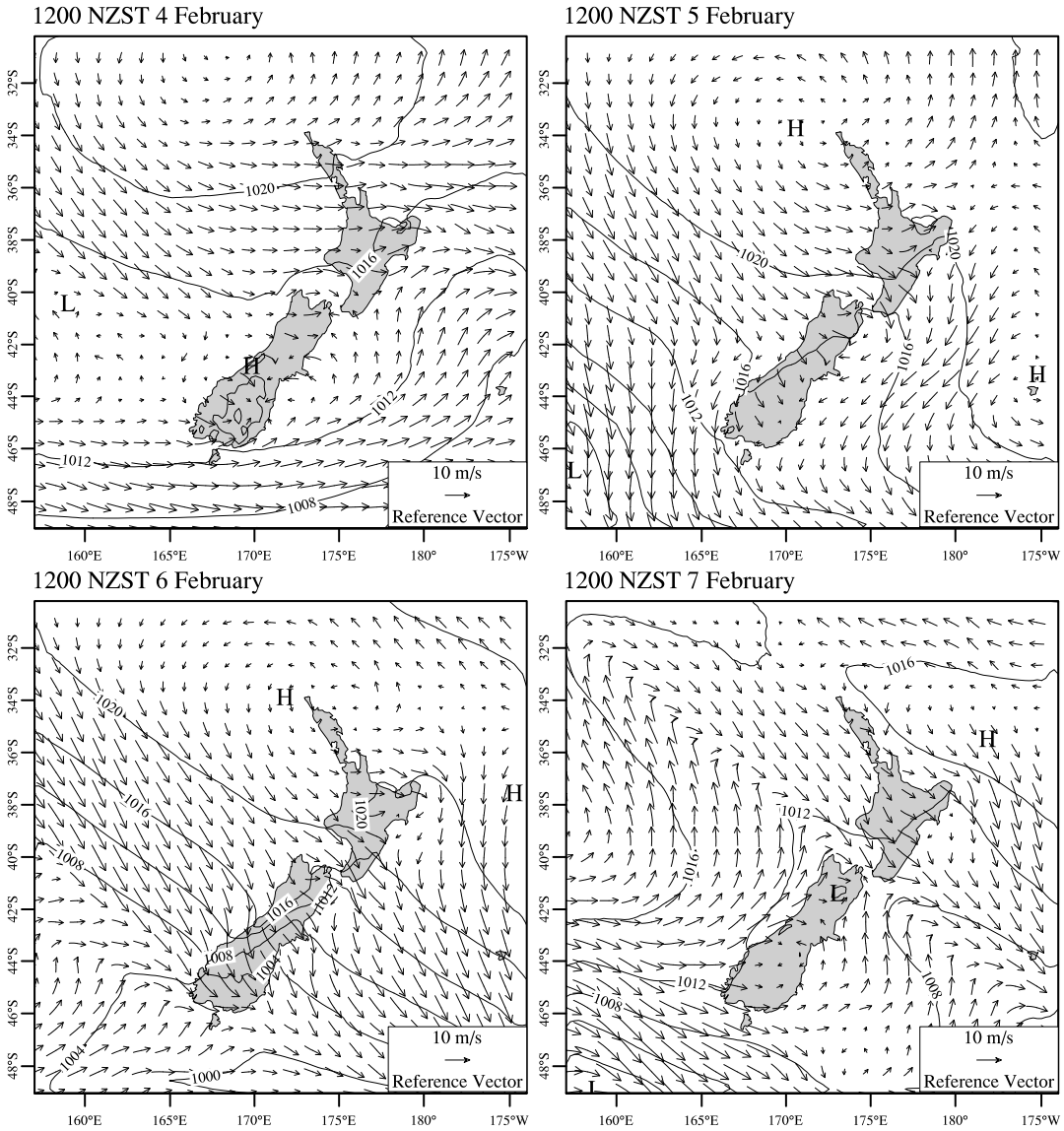

Figure 4.3: Modelled MSLP contours and 10 m horizontal wind vectors at 1200 NZST on 4 to 7 February 2011. The wind vector length scales linearly with wind speed and the reference wind vector represents a wind speed of 10 m s^{-1}. The MSLP is contoured at an interval of 4 hPa and the model horizontal grid spacing for this domain is 18 km.

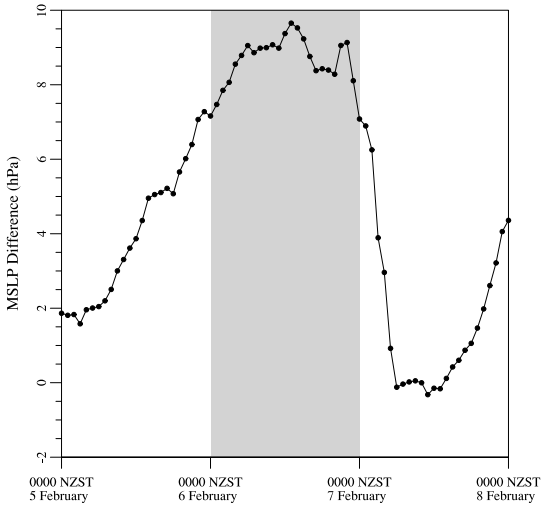

Figure 4.4: Time series of modelled MSLP difference (hPa) between Hokitika and Christchurch from 5 to 8 February 2011. Positive values indicate that MSLP is higher at Hokitika than Christchurch.

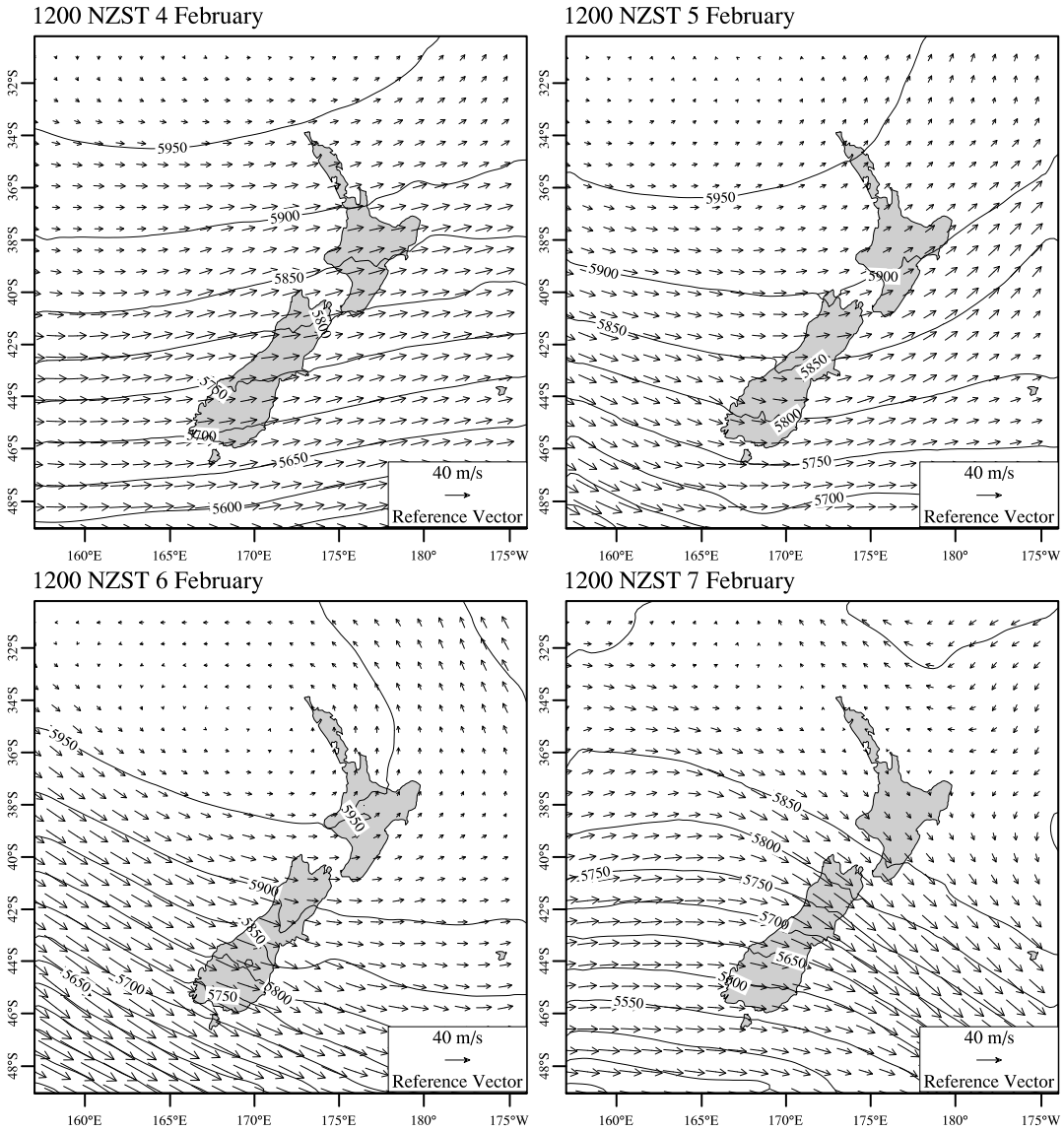

Figure 4.5: Modelled 500 hPa geopotential height contours and horizontal wind vectors at 1200 NZST on 4 to 7 February 2011. The wind vector length scales linearly with wind speed and the reference wind vector represents a wind speed of 40 m s^{-1}. The 500 hPa geopotential height is contoured at an interval of 50 m and the model horizontal grid spacing for this domain is 18 km.

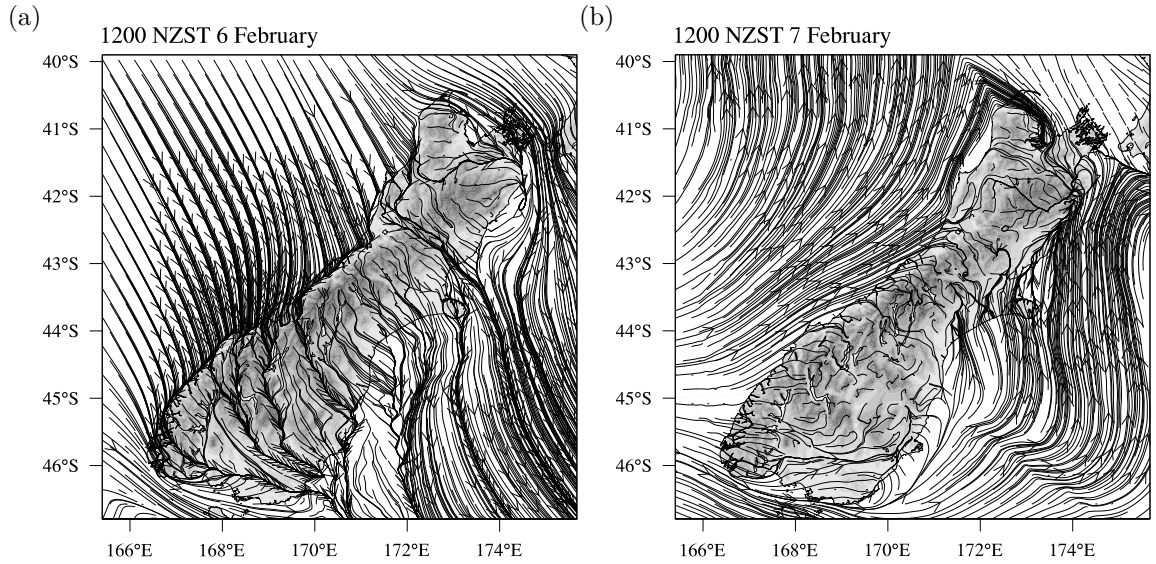

Figure 4.6: Modelled 10 m horizontal flow streamlines across the South Island region at (a) 1200 NZST on 6 February and (b) 1200 NZST on 7 February 2011.

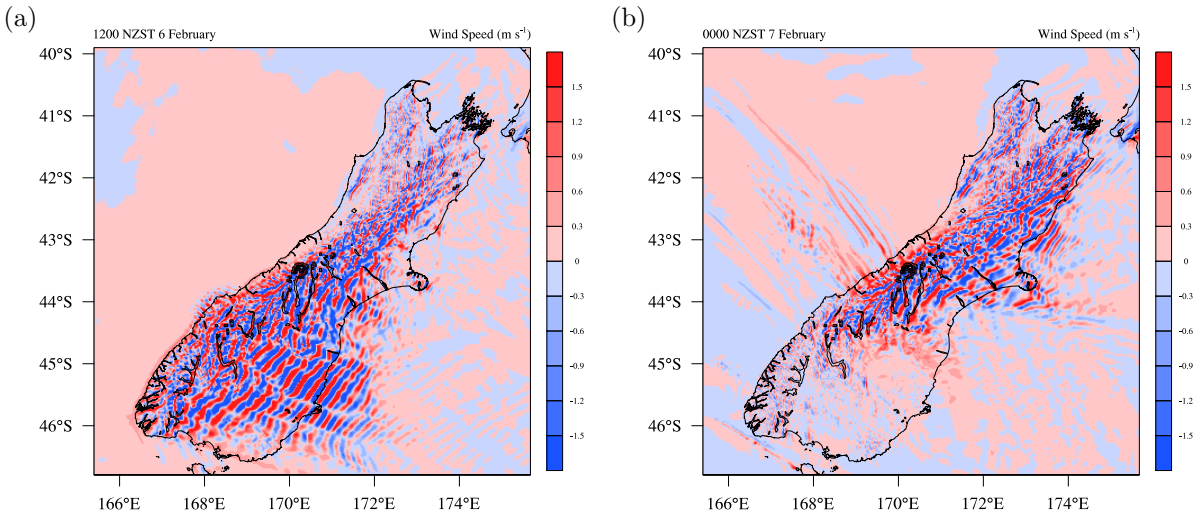

Figure 4.7: Modelled vertical wind velocity contours at a height of 2 km at (a) 1200 NZST on 6 February and (b) 1200 NZST on 7 February 2011. The model horizontal grid spacing of this domain is 2 km.

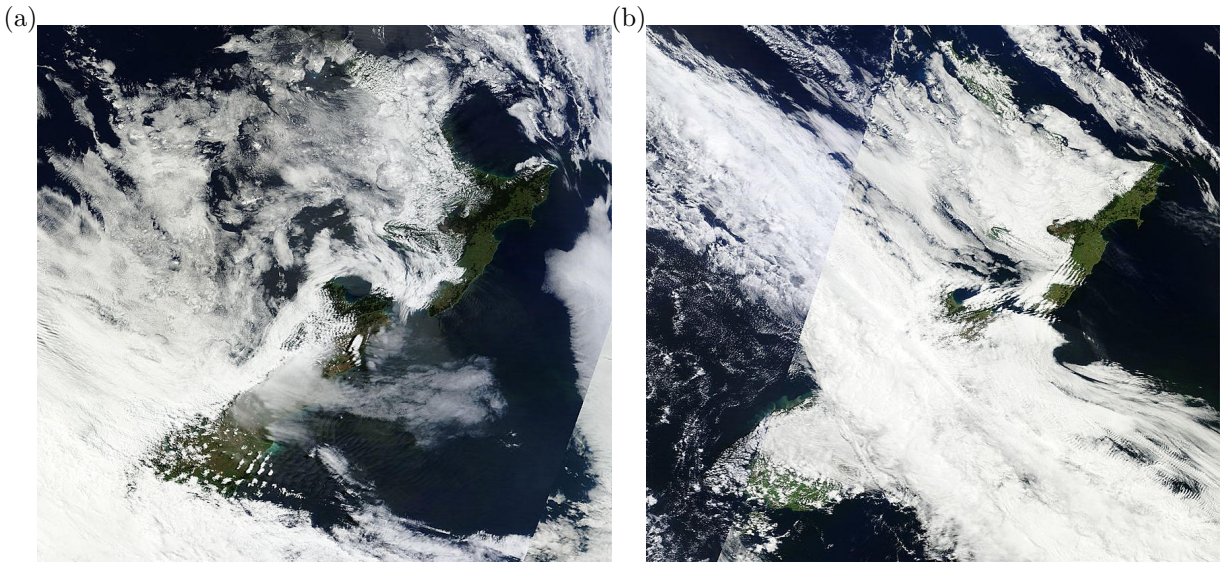

Figure 4.8: MODIS satellite composite images of New Zealand taken at (a) 1415, 1550 and 1555 NZST on 6 February, and (b) 1320, 1325, 1455 and 1500 NZST on 7 February.

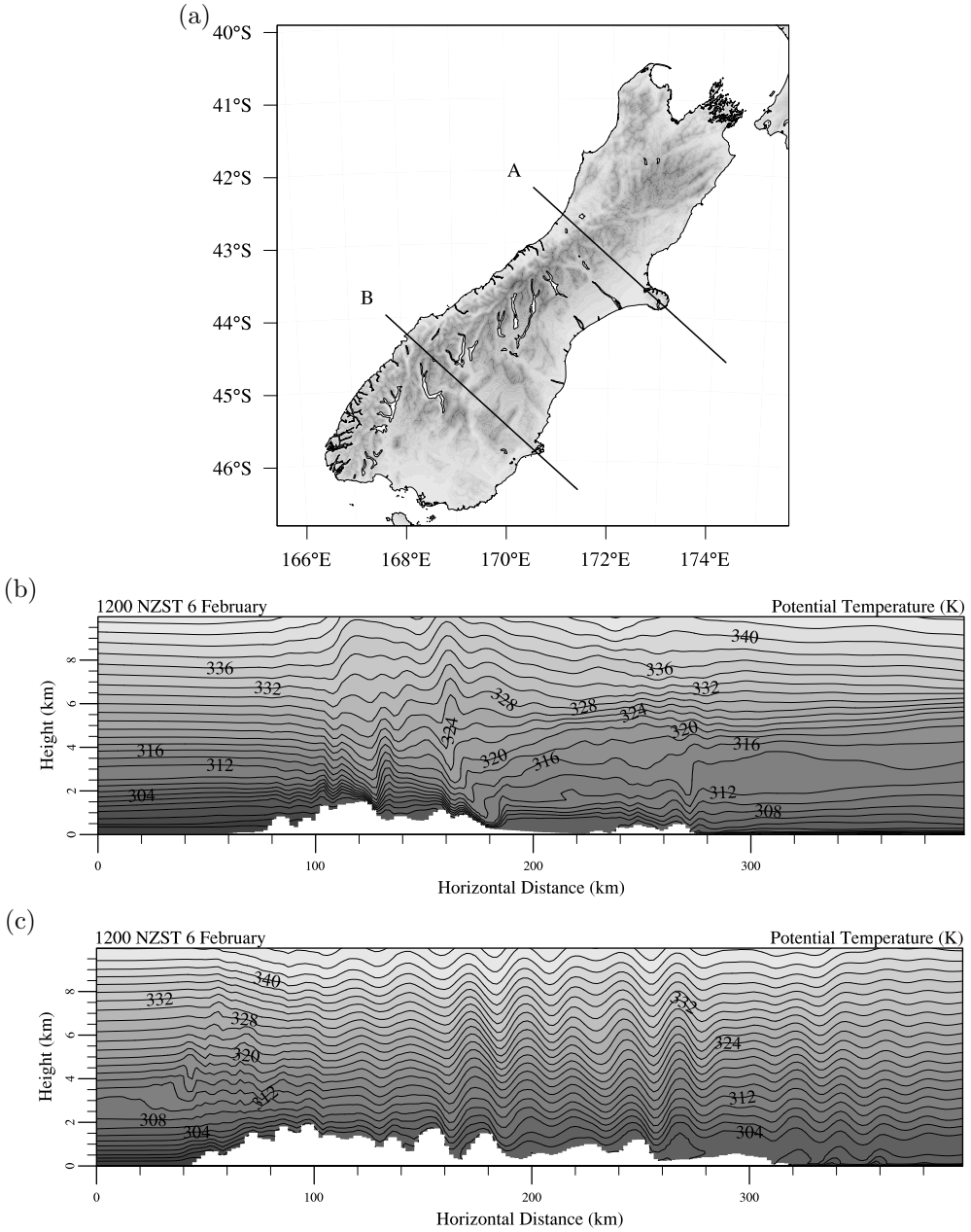

Figure 4.9: (a) Location of two vertical cross-sections of modelled potential temperature across the South Island. The A and B cross-sections were extracted for 1200 NZST on 6 February 2011 and located over the (b) Canterbury and (c) Otago regions.

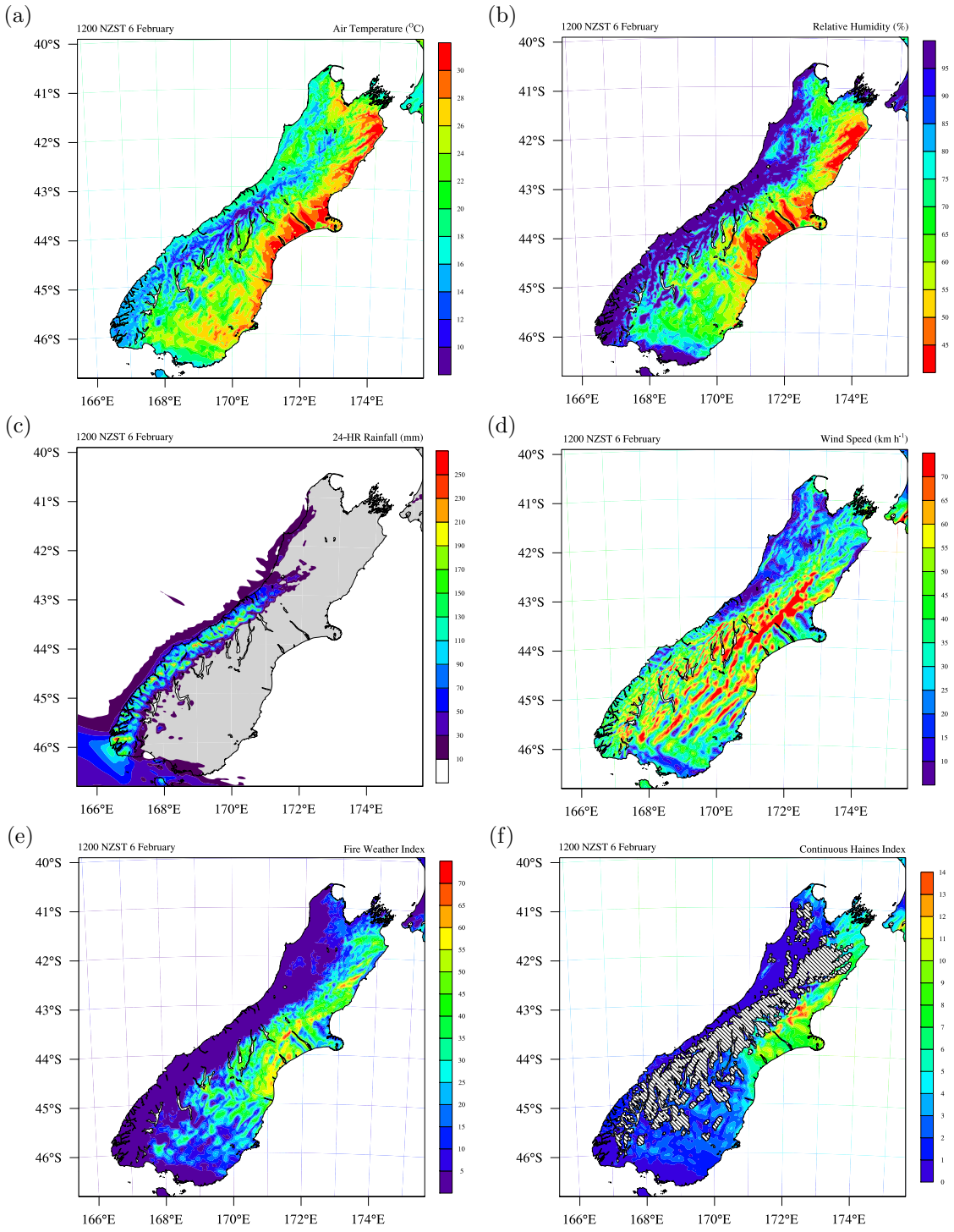

Figure 4.10: Modelled fire weather variables for the South Island region at 1200 NZST on 6 February 2011. The fire weather variables included are the (a) air temperature (b) relative humidity (c) 24-hr rainfall (d) wind speed (e) FWI and (f) CHI. In (c) regions over land with zero rainfall are shaded grey. In (f) regions for which the surface elevation is above 1000 m are contoured using a dashed pattern, because the CHI is undefined in these regions.

(a)

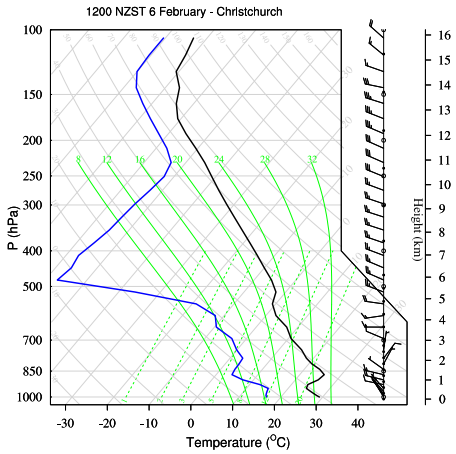

(b)

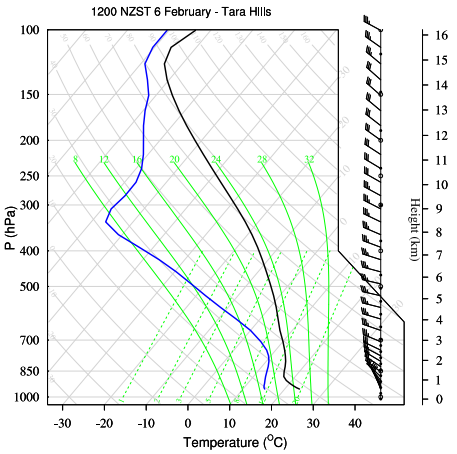

Figure 4.11: Skew–T Log–P diagrams for model output at 1200 NZST on 6 February at (a) Christchurch and (b) Tara Hills. The wind vectors are given at each of the model vertical levels.

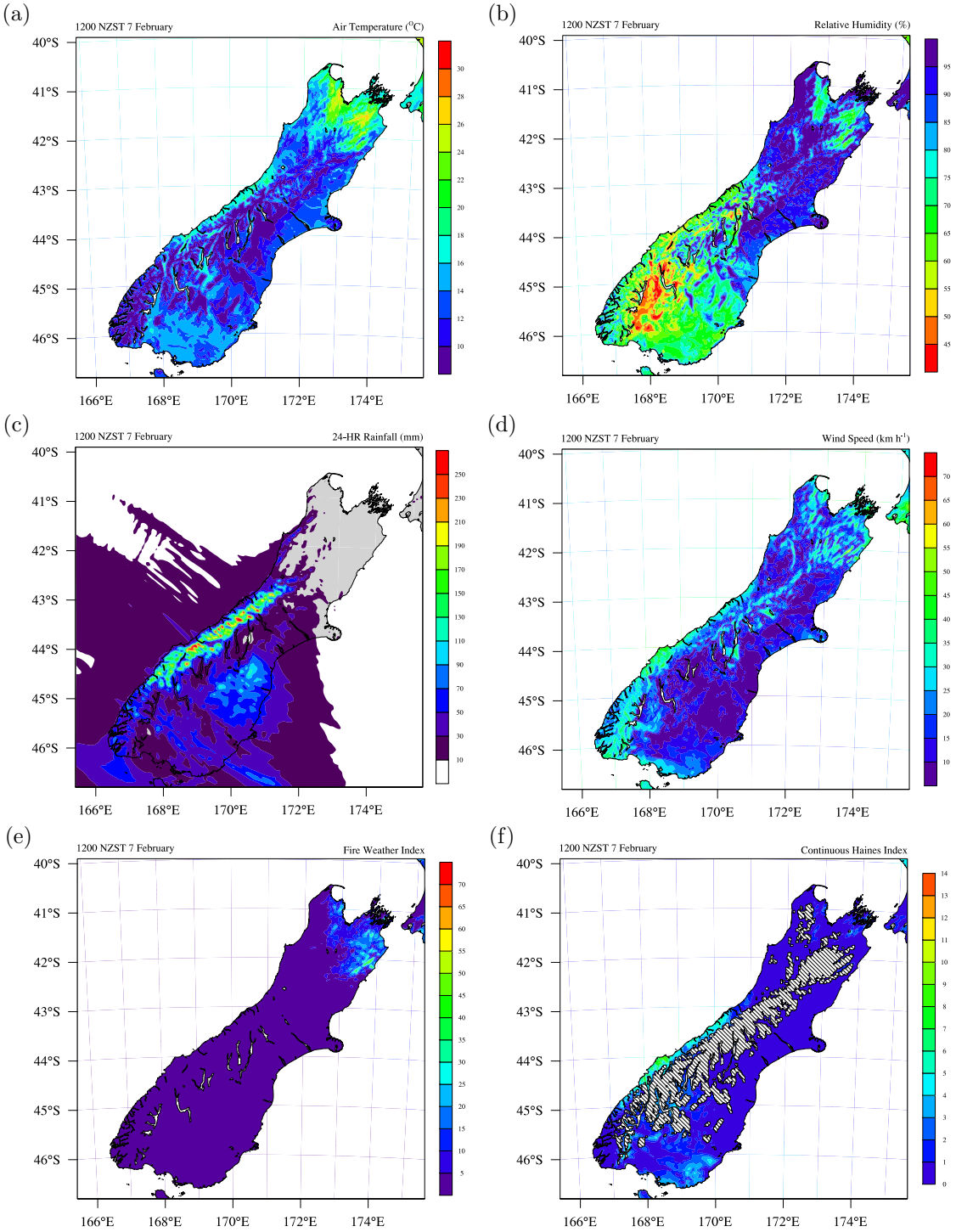

Figure 4.12: Same as in Figure 4.10, but instead at 1200 NZST on 7 February 2011.

(a)

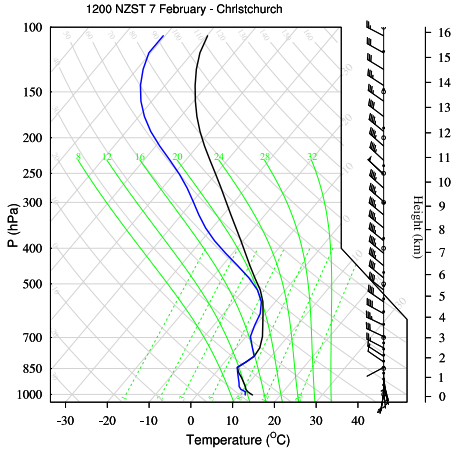

(b)

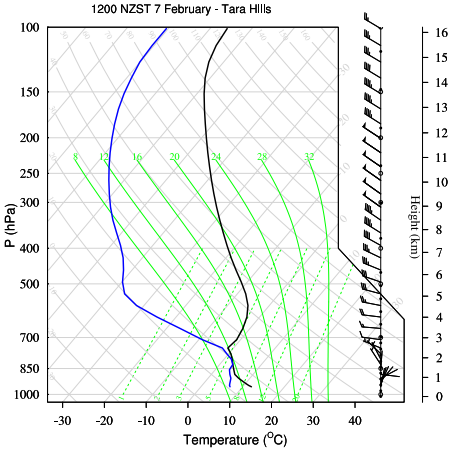

Figure 4.13: Same as in Figure 4.11, but instead at 1200 NZST on 7 February 2011.

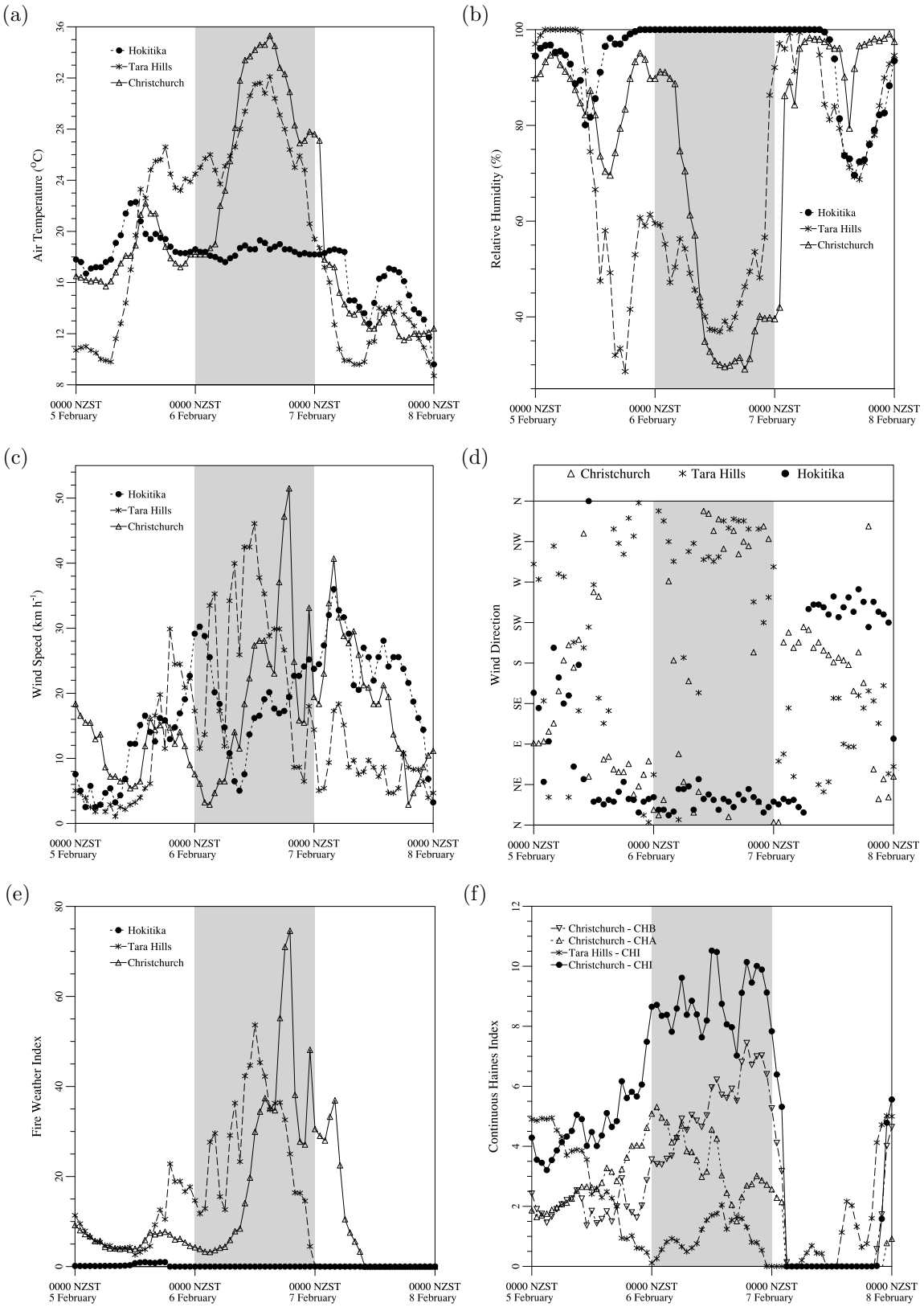

Figure 4.14: Time series of hourly fire weather at Christchurch, Tara Hills and Hokitika from 5 to 7 February 2011. The variables included are the (a) air temperature (b) relative humidity (c) wind speed (d) wind direction (e) FWI and (f) CHI. Modelled data are used in (f), whereas observational data are used in the remaining plots. In (f) the modelled CHA and CHB at Christchurch are shown in addition to the CHI, whereas only the CHI at Tara Hills is shown, and Hokitika is not included.

Chapter 5

Large Eddy Simulation of Atypical Wildland Fire Spread on Leeward Slopes

Colin C. Simpson[A], Jason J. Sharples[B], Jason P. Evans[C], Matthew F. McCabe[D]

[A] Department of Geography, University of Canterbury, Christchurch, New Zealand
[B] School of Physical, Environmental and Mathematical Sciences, University of New South Wales at Canberra, Canberra, Australia
[C] Climate Change Research Centre, Faculty of Science, University of New South Wales, Sydney, Australia
[D] Department of Civil and Environmental Engineering, University of New South Wales, Sydney, Australia

Abstract

The WRF-Fire coupled atmosphere-fire modelling system was used to investigate atypical wildland fire spread on steep leeward slopes through a series of idealised numerical simulations. The simulations are used to investigate both the leeward flow characteristics, such as flow separation, and the fire spread from an ignition region at the base of the leeward slope. The fire spread was considered under varying fuel type and with atmosphere-fire coupling both enabled and disabled. When atmosphere-fire coupling is enabled and there is a high fuel mass density, the fire spread closely resembles that expected during fire channelling. Specifically, the fire spread is initially dominated by upslope spread to the mountain ridge line at an average rate of 2.0 km h^{-1}, followed by predominantly lateral spread close to the ridge line at a maximum rate of 3.6 km h^{-1}. The intermittent rapid lateral spread occurs when updraft-downdraft interfaces, which are associated with strongly circulating horizontal winds at the mid-flame

height, move across the fire perimeter close to the ridge line. The updraft-downdraft interfaces are formed due to an interaction between the strong pyro-convection and the terrain-modified winds. Through these results, a new physical explanation of fire channelling is proposed.

5.1 Introduction

A wildland fire is capable of exhibiting highly complex behaviour in response to multi-scale interactions between the fire and the local fire environment, namely the fuel, weather and topography. It has previously been identified that terrain-modified atmospheric conditions, particularly in complex terrain, can significantly affect fire spread and behaviour (Sharples, 2009; Sharples et al., 2010a). This paper investigates a fire spread phenomenon referred to as 'fire channelling', in which atmosphere-terrain-fire interactions are believed to play an important role. McRae (2004) first noted this phenomenon, which he referred to as 'lee-slope channelling', through the presence of atypical fire spread patterns in multispectral line-scan data from the Canberra 2003 bushfires. A study by Sharples et al. (2010c) investigated fire channelling at the laboratory scale, through a series of combustion tunnel experiments, and confirmed the incidence of atypical lateral fire spread across a leeward slope, apparently driven by an interaction between the wind, the terrain and the fire.

Previous studies have identified a number of important distinguishing features of fire channelling (Sharples and McRae, 2011; Sharples et al., 2011, 2012). These features include rapid lateral fire spread across the the top of a steep leeward slope in a direction approximately perpendicular to the synoptic wind conditions. The upwind edge of the lateral spread is constrained by a major break in topographic slope, such as a mountain ridge line. There is an extension of the active flaming zone downwind of the synoptic flow, possibly through a process such as spotting. Additional features include darker smoke and vigorous convection associated with the laterally advancing flanks of the fire. The rapid lateral fire spread indicates that fire channelling may pose a significant danger to fire fighter and civilian safety.

Sharples et al. (2012) have previously determined that a number of environmental conditions are necessary for fire channelling. The leeward slope angle of the mountain should be greater than $\sim 25^\circ$ and the topographic aspect and synoptic wind direction should be within $\sim 40^\circ$ of each other. The synoptic wind speed should also be greater than $\sim$25–30 km h^{-1}, which allows for flow separation in the lee of the mountain. This study postulated that fire channelling occurs due to an interaction between the fire and a lee rotor, which is formed through leeward flow separation. It was further conjectured that the lateral fire spread is driven by thermal expansion of the air within the lee rotor as heat is added to it from the fire, with the resulting lateral atmospheric flow effectively

following a path of least resistance.

An important step in this study is to use a numerical weather prediction model to investigate the nature of the atmospheric flow in the lee of a mountain. A number of studies have previously investigated turbulent flow for environmental conditions and atmospheric scales similar to that considered in this paper (Schär and Durran, 1997; Allen and Brown, 2002; Doyle and Durran, 2002, 2007; Ding et al., 2003; Pathirana et al., 2003; Hertenstein and Kuettner, 2005; Sheridan and Vosper, 2006; Ayotte, 2008; Katurji et al., 2011). Many of these studies used a large eddy simulation model to investigate the nature of the atmospheric flow. Based on the results of these studies, it is evident that the nature of the leeward atmospheric flow is closely associated with many environmental conditions, including the atmospheric stability, surface roughness, upstream wind conditions and the geometric properties of the terrain.

Another important step in this study is to simulate the fire spread across the leeward slope of a mountain using a coupled atmosphere-fire model. Over the past two decades, a number of studies have used coupled atmosphere-fire modelling to investigate fire spread, fire behaviour and atmosphere-fire interactions. Previous studies focussing on fire spread across flat terrain have been able to reproduce a number of physically realistic fire spread features (Heilman and Fast, 1992; Clark et al., 1996b,a, 2004; Cunningham et al., 2005; Cunningham and Linn, 2007; Mell et al., 2007; Sun et al., 2009). These modelled features include the parabolic fire shape that typically develops under the influence of light uniform winds. Previous studies focussing on fire spread across non-flat terrain have similarly yielded useful results (Heilman, 1992; Linn et al., 2002, 2007; Clark et al., 2004; Coen, 2005).

The aim of this paper is to perform a series of idealised numerical simulations that allow for an evaluation of the fire channelling hypothesis forwarded by Sharples et al. (2012) and facilitate a detailed analysis of the physical mechanisms responsible for driving the lateral fire spread associated with fire channelling. The numerical modelling system used to perform these numerical simulations is described in the next section. The results of the two-dimensional (2D) and three-dimensional (3D) atmospheric simulations of flow over a mountain are presented in the following two sections. The results of the simulations of fire spread across the leeward slope of a mountain are presented in the subsequent section. A summary of the study is presented in conjunction with a number of conclusions in the final section.

5.2 Numerical Models

5.2.1 Atmospheric Model

The atmospheric model used in this study is version 3.3 of the Weather Research and Forecasting model (WRF) (Skamarock et al., 2008). It is used in a highly idealised large eddy simulation (LES) configuration that is well suited to studying turbulent atmospheric flow on length scales of tens to hundreds of metres. The model explicitly resolves the large-scale atmospheric eddies, whereas the effects of subgrid-scale motions on the resolved turbulence are modelled using a subfilter-scale stress model. The model uses fully compressible nonhydrostatic equations with a mass-based terrain-following coordinate system. The model is used in both a 2D and 3D configuration.

The model domain is configured to capture the turbulent flow in the lee of a mountain at high resolution. In both the 2D and 3D simulations, the west-east dimension (x-axis) has an extent of 30 km. In the 2D simulations, the south-north dimension (y-axis) is three grid points wide with cyclic boundary conditions, whereas in the 3D simulations it has an extent of 5 km. The horizontal grid spacing in both the 2D and 3D simulations is 50 m. The model top in each simulation is initially set to 10 km, with an initial vertical grid spacing of 50 m. However, due to the use of terrain-following sigma coordinates, the model top, and therefore also the vertical grid spacing, varies in time with the atmospheric pressure. However, the model top descends no more than a few hundred metres in any simulation and the vertical grid spacing is therefore always in the range of 47–50 m. The model grid cells are therefore approximately isotropic throughout the duration of each simulation. The atmospheric model has a computational domain of 600×3×200 and 600×100×200 (x,y,z) grid points in the 2D and 3D simulations, respectively. This model domain setup is similar to that considered in previous WRF LES studies (Mirocha et al., 2010; Kirkil et al., 2012).

The lateral boundary conditions are specified using a one-dimensional input sounding. The surface pressure is 1000 hPa and the surface moisture mixing ratio is zero. The vertical profiles of the vapour mixing ratio, horizontal wind conditions and potential temperature are also specified. The vapour mixing ratio and y-axis wind velocity are zero at all heights. The horizontal wind conditions at the western lateral boundary are set as a temporally uniform incoming westerly wind field, which varies with height according to:

$$U(z) = \begin{cases} 20 \times \left(\frac{z}{200}\right)^2 & z \leq 200 \\ 20 & z > 200 \end{cases} \tag{5.1}$$

where $U(z)$ is the wind speed (m s^{-1}) and z is the height (m). Moreover, this vertical

wind profile is used to define the initial wind conditions over the entire domain.

A total of three different vertical profiles of the potential temperature, which represent a stable, neutral and unstable atmosphere, are used in this study. In the stable atmosphere, the potential temperature is initially equal to 280 K at the surface and increases linearly to 320 K at a height of 10 km. In the neutral atmosphere, the potential temperature is initially equal to 290 K at all heights, including the surface. In the unstable atmosphere, the potential temperature is initially 290 K at the surface and decreases linearly to 280 K at a height of 5 km, with a constant potential temperature of 280 K above a height of 5 km. The constant potential temperature lid on the unstable atmosphere acts to prevent the model top from descending to a very low height above the surface.

In each simulation there is a mountain with a triangular profile, with a height of approximately 1 km, located within the model domain. The mountain starts 10 km to the east of the western lateral boundary and the windward slope has an inclination angle of 20°, giving a windward slope width of 2.75 km. The mountain ridge line is therefore located 12.75 km to the east of the western lateral boundary, which limits any physical connection between the terrain-induced turbulence and the western lateral boundary. The leeward slope has an inclination angle of either 25° or 35°, giving a leeward slope width of 2.14 or 1.43 km. The mountain is flattened slightly at the ridge line, with the highest two model grid points set to the same height. This ensures that there is no sudden change from positive to negative topographic gradient between adjacent model grid points.

The model is used in a highly idealised configuration, with many of the model physics schemes disabled, including the microphysics, longwave radiation, shortwave radiation, urban surface physics, planetary boundary layer and cumulus parameterisations. The MM5 surface layer scheme, which is based on Monin-Obukhov similarity, is enabled as surface friction is important for generating the near-surface vertical wind shear. Diffusion in physical space is calculated using the velocity stress tensor and eddy viscosities are calculated using a 3D prognostic 1.5-order turbulence closure. A Rayleigh damping scheme (Klemp et al., 2008), with a damping timescale of 10 s, is used in the top 3 km of the model to absorb upward propagating gravity wave energy. All lateral boundary conditions other than the cyclic boundary conditions used in the y-axis for the 2D simulations are open radiative. The main model time integration in WRF is performed using a third-order Runge-Kutta scheme and the primary time step chosen here is 0.1 s. The secondary time step is a time-split small step for acoustic and gravity wave modes, and is equal to one eighth of the primary time step. The initial 30 min of each simulation is considered the spin-up period and is not included in any calculation of the time-averaged variables discussed below.

5.2.2 Coupled Atmosphere-Fire Model

The wildland fire spread model used in this study is SFIRE (Mandel et al., 2011), which is distributed with version 3.3 of WRF. The resulting coupled atmosphere-fire model is referred to as WRF-Fire.

The level set method is used to numerically track the temporally evolving wildland fire perimeter as it spreads through the model domain. In this method, an auxillary function, known as the level set function, is used to represent the closed curve of the two-dimensional fire perimeter. The spatially and temporally variable fire spread rate is calculated using the Rothermel equation (Rothermel, 1972):

$$S = R_0 \ (1 + \phi_W + \phi_S) \tag{5.2}$$

where S is the rate of spread, R_0 is the base rate of spread in the absence of wind or slope, ϕ_W is the wind correction factor and ϕ_S is the slope correction factor. The base rate of spread is calculated based upon the local fuel conditions. The slope correction factor is calculated based on the local terrain slope, θ, which is determined from the SFIRE model surface elevations. The wind correction factor is calculated based upon the wind conditions at an estimated mid-flame height. This mid-flame height varies between fuel types and the wind conditions are vertically interpolated to this mid-flame height using an assumed ideal logarithmic wind profile.

The SFIRE model is a two-dimensional model and its computational domain matches the horizontal extent of the three-dimensional WRF model domain. The SFIRE model grid was chosen to have a subgrid ratio of five to one relative to the WRF model, resulting in a horizontal grid spacing of 10 m and a computational domain of 3000×500 (x,y) grid points. The SFIRE model has the same terrain configuration as the WRF model, although it is defined at a higher spatial resolution to match the subgrid ratio. There are a total of 13 different fuel types available in the model, which are based upon the 13 Anderson fuel categories (Anderson, 1982). The parameterised properties unique to each fuel type include the initial mass loading, fuel depth, surface area to volume ratio, moisture content of extinction and rate of mass loss following ignition. A homogeneous fuel type is assigned across the entire model domain, such that there is no computational restriction on where the fire can spread.

The fire perimeter is ignited at the end of the 30-min atmospheric spin-up period. The fire perimeter is ignited out to a distance of 50 m in all directions away from a south-north line of 400 m in length. This south-north line is centred on the middle of the y-axis and is located 13.7 km to the east of the western lateral boundary. This represents an ignition location near to the base of the leeward slope, which emulates the laboratory experiments described in Sharples et al. (2010c). The fire is initially ignited

at the southern tip of the south-north line and then spreads to the northern tip over a period of a few minutes. Following this ignition process, the fire is allowed to spread freely thoughout the model domain for the remainder of the simulation. The asymmetric fire ignition results in asymmetric behaviour in the atmospheric model when two-way coupling is enabled between the SFIRE and WRF models.

The two-way atmosphere-fire coupling between the SFIRE and WRF models is achieved through the release of latent and sensible heat from SFIRE to WRF. The sensible and latent heat flux densities, ϕ_h and ϕ_q (W m^{-2}), released in time interval $(t, t{+}\Delta t)$ are calculated as:

$$\phi_h = \frac{F(t) - F(t + \Delta t)}{\Delta t} \frac{1}{1 + M_f} \omega_l h \tag{5.3}$$

$$\phi_q = \frac{F(t) - F(t + \Delta t)}{\Delta t} \frac{M_f + 0.56}{1 + M_f} \omega_l L \tag{5.4}$$

where $F(t)$ is the fuel fraction at a time t, ω_l is the total fuel load (kg m^{-2}), h is the heat content of dry fuel (J kg^{-1}), M_f is the fuel particle moisture content, 0.56 is the estimated mass ratio of the water output from the combustion to the dry fuel, and L is the specific latent heat of condensation of water at 0°C, used for nominal conversion of moisture into heat (Mandel et al., 2011). For each kilogram of fuel combusted in the SFIRE model, a total of 17.43 MJ of sensible heat is released into the lower levels of the WRF model at the corresponding location. The latent heat flux density is considerably much smaller than the corresponding sensible heat flux density for all fuel types tested in this paper. The sensible and latent heat fluxes are distributed throughout the WRF vertical levels using an exponential decay function. This release of heat into the WRF model has the capacity to modify the local atmospheric conditions. Any such modification of the horizontal wind conditions at the mid-flame height will subsequently influence the local fire spread rate. Therefore, the WRF-Fire coupled atmosphere-fire model is capable of directly modelling atmosphere-terrain-fire interactions. However, this two-way atmosphere-fire coupling can be switched off by not passing on the latent and sensible heat fluxes from the SFIRE model to the WRF model.

5.3 Two-Dimensional Atmospheric Simulations

In this section the results of six 2D simulations of atmospheric flow over a triangular mountain are presented. Details of the setup used in each simulation are provided in Table 5.1. Each 2D simulation has a unique name derived from three properties: dimensionality ("2D"), atmospheric stability ("S" for stable, "N" for neutral and "U" for

unstable) and leeward slope angle ("25" or "35"). These simulations are used to investigate the leeward atmospheric flow under different atmospheric stability and leeward slope angle conditions.

Figure 5.1 shows the temporal evolution of the upstream vertical potential temperature profiles for the 2DS35, 2DN35 and 2DU35 simulations, respectively. The neutral profile shows no change with time, whereas the stable and unstable profiles become slightly more stable and unstable, respectively, with time. The atmospheric stability profiles are therefore relatively constant in time.

5.3.1 Stable Atmosphere

The 2DS25 and 2DS35 simulations have a stable atmosphere, which allows for the development of mountain waves in the lee of the mountain. The Brunt-Väisälä frequency in these two simulations is $\sim$0.01 s^{-1}, which corresponds to a predicted wavelength of $\sim$10 km. This wavelength is significantly longer than the leeward slope width and implies that the mountain waves will likely have little direct effect on the flow conditions close to the leeward slope.

Figure 5.2 shows the time-averaged potential temperature for the 2DS35 simulation. Mountain waves are seen to develop in the lee of the mountain, with an amplitude of several hundred metres and a wavelength close to the 10 km predicted using the Brunt-Väisälä frequency. The mountain waves extend up to the bottom of the Rayleigh damping layer, which is located at a height of $\sim$7 km. Although not shown specifically, the mountain wave characteristics in the 2DS25 simulation are very similar.

Figure 5.3 shows the time-averaged horizontal wind velocity for the 2DS25 and 2DS35 simulations. It is evident that there is a high degree of similarity between the wind conditions in these two simulations. The westerly flow is seen to accelerate up the windward slope, reaching a peak velocity of $\sim$20–24 m s^{-1} at the mountain peak. There is a region of flow separation at the base of the windward slope, which is not unexpected given the stable atmosphere. Rapid deceleration of the westerly flow is seen as it moves down the leeward slope, which results in flow separation in the lee of the mountain. This region of flow separation starts at a height of $\sim$600 m on the leeward slope and extends eastwards out to a distance of $\sim$2 km downstream of the mountain. The acceleration and deceleration of the flow as it moves upslope and downslope is most likely due to the pressure gradient encountered by the flow as it lifts and descends across the mountain.

Also of interest in Figure 5.3 is another region of flow separation located directly beneath the first mountain wave crest, which is $\sim$6–12 km downstream of the mountain. Doyle and Durran (2002) have previously shown that rotors can form under mountain wave crests, resulting in flow separation. The downstream location of this flow separation region confirms the above statement that the wavelength of the mountain waves is too

long for the waves to directly influence the flow conditions across the leeward slope.

Figure 5.4a shows the instantaneous horizontal vorticity and wind conditions at a time of 60 min for the 2DS35 simulation. The horizontal vorticity, η_y, is a useful quantity for diagnosing flow circulation and is calculated as:

$$\eta_y = \frac{\partial U}{\partial z} - \frac{\partial W}{\partial x} \tag{5.5}$$

where U and W are the horizontal and vertical wind velocities, respectively. Positive and negative vorticity indicate clockwise and counterclockwise flow rotation, respectively.

Figure 5.4a demonstrates that the flow separation at the top of the leeward slope is associated with periodic vortex shedding in the lee of the mountain. The deceleration of the flow at the top of the leeward slope results in the development of a quasi-permanent region of strong positive vorticity at a height of 800–900 m, which extends out eastwards for 2 km from the leeward slope. Lee rotors are periodically generated beneath this quasi-permanent positive vorticity region. The rotors have an initial horizontal and vertical extent slightly less than the mountain height and are seen to detach from the mountain and propagate downstream with the westerly flow. The downstream movement of these rotors is seen to be closely associated with the mountain waves and the stable atmosphere acts to limit any increase in their vertical extent. This vortex shedding process is responsible for quasi-periodic changes in the flow direction from the base of the leeward slope up to a height of ∼700 m.

5.3.2 Neutral Atmosphere

Figure 5.5 shows the time-averaged horizontal wind velocity for the 2DN25 and 2DN35 simulations. As with the stable atmosphere simulations, there is acceleration of the westerly flow as it moves upslope, with a peak velocity at the mountain peak, and rapid deceleration of the flow at the top of the leeward slope, resulting in flow separation downstream of the mountain. There is a high degree of similarity between the two neutral simulations, however there are some important differences in the flow separation between the stable and neutral atmosphere simulations. First, no mountain waves develop in the neutral atmosphere and consequently there is no flow separation associated with mountain waves downstream of the mountain. Second, there is no flow separation at the base of the windward slope in the neutral atmosphere. Third, the leeward flow separation region in the neutral atmosphere seems to be lifted slightly from the surface across the leeward slope at heights under ∼400 m. Fourth, the leeward flow separation region extends ∼6 km downstream in the neutral atmosphere, which is ∼4 km further than in the stable atmosphere.

Figure 5.4b shows the horizontal vorticity and wind conditions at a time of 60 min

for the 2DN35 simulation. The vortex shedding process is qualitatively similar to that described above for the 2DS35 simulation. However, in the neutral atmosphere the lee rotors have a greater initial horizontal and vertical extent and they propagate downstream free of any influence from mountain waves.

5.3.3 Unstable Atmosphere

Figure 5.6 shows the time-averaged potential temperature for the 2DU35 simulation. No mountain waves develop in the lee of the mountain due to the unstable atmosphere. The potential temperature is at a maximum at the top of the leeward slope, where the rapid flow deceleration occurs, and is seen to decrease with both height and distance downstream of the mountain. The roughness of the potential temperature contour lines in the lee of the mountain suggests that the flow becomes more turbulent with height further downstream of the mountain. This result implies that the unstable atmosphere acts to vertically lift the lee rotors as they propagate downstream of the mountain.

Figure 5.7 shows the time-averaged horizontal wind velocity for the 2DU25 and 2DU35 simulations. There is a high degree of similarity between the two simulations and the acceleration and deceleration of the upslope and downslope flow is qualitatively similar to that discussed for the stable and neutral atmosphere simulations. In the unstable atmosphere there is greater acceleration of the upslope flow than in the stable and neutral atmospheres, with a peak velocity of $\sim$40 m s^{-1} at the mountain peak. The leeward flow separation region in the unstable atmosphere simulations starts at a height of $\sim$700 m on the leeward slope and extends $\sim$4 km downstream of the mountain. As with the neutral atmosphere simulations, there is a slight uplift of the flow separation region above the surface at the base of the leeward slope.

Figure 5.4c shows the horizontal vorticity and wind conditions at a time of 60 min for the 2DU35 simulation. The vortex shedding process is qualitatively similar to that described for the 2DS35 and 2DN35 simulations. The lee rotors in this simulation have a greater initial horizontal and vertical extent than in either the neutral or stable atmosphere simulations. As the lee rotors propagate downstream, they are lifted due to the unstable atmosphere and grow in vertical extent. As these rotors extend vertically, they eventually break down into a number of smaller-scale sub-rotors.

5.4 Three-Dimensional Atmospheric Simulations

In this section the results of three 3D simulations of atmospheric flow over a triangular ridge line are presented. Details of the setup used in each simulation are provided in Table 5.1. The above analysis of the 2D simulations shows that, for the range of conditions tested, the atmospheric stability plays a more important role than does the leeward

slope angle in the leeward flow separation. Therefore, the 3D simulations use a fixed leeward slope angle of 35° and the atmospheric stability is varied. Each 3D simulation has a unique name derived from three properties: dimensionality ("3D"), atmospheric stability ("S", "N" or "U") and leeward slope angle ("35"). These simulations are used to investigate the important differences between the leeward flow in two and three dimensions.

Figure 5.8 shows the time-averaged potential temperature on a vertical cross-section for the 3DS35 and 3DU35 simulations. It is evident that there is a high degree of similarity between the equivalent 2D and 3D simulations. The mountain waves formed in the stable atmosphere have a wavelength of ∼10 km and an amplitude of several hundred metres. There are no mountain waves in the unstable atmosphere, and the potential temperature is at a maximum at the top of the leeward slope and decreases with height and distance downstream of the mountain.

Figure 5.9 shows the time-averaged horizontal velocity on a vertical cross-section for the 3DS35, 3DN35 and 3DU35 simulations. As in the equivalent 2D simulations, there is acceleration of the flow as it moves up the windward slope, reaching a peak velocity at the mountain peak, and rapid deceleration and flow separation across much of the leeward slope and extending some distance downstream of the mountain. However, there are some important differences between the equivalent 2D and 3D simulations. First, the flow separation is typically weaker and more spatially confined in the 3D simulations. Second, the flow separation is not lifted slightly above the surface as it was in the neutral and unstable 2D simulations. Third, the time-averaged horizontal velocity in the 3D simulations has a higher degree of spatial variability, as shown by the rougher horizontal velocity contour lines.

Figure 5.10 shows the horizontal vorticity and wind conditions at a time of 60 min on a vertical cross-section for the 3DS35, 3DN35 and 3DU35 simulations. The horizontal vorticity is calculated identically to how it was calculated for the 2D simulations. As in the equivalent 2D simulations, a quasi-permanent region of strong positive vorticity develops at the top of the leeward slope and extends out eastwards ∼1 km from the leeward slope. However, there are no large-scale lee rotors and the leeward flow is instead dominated by chaotic fine-scale features. The 3D turbulence is therefore subject to energy cascade down to smaller-scales than was seen in 2D.

Doyle and Durran (2007) have previously considered some of the important differences between the 2D and 3D atmospheric turbulence downstream of a mountain. They found that the 2D turbulence is steadier and greater in spatial extent, whereas the 3D turbulence is more chaotic and fine-scale. They proposed that processes such as tilting and stretching of vortical structures between different directional components may be important in 3D. The differences between the turbulence seen in these 2D and 3D sim-

ulations are consistent with this previous study, however the tilting and stretching of vortical structures is not specifically considered in this study. Sharples et al. (2012) postulated that fire channelling occurs due to an interaction between the fire and a lee rotor, with thermal expansion of the rotor due to the addition of heat from the fire. However, the absence of large-scale lee rotors in the 3D simulations does not fully support this hypothesis and suggests that it is overly simplistic.

5.5 Coupled Atmosphere-Fire Simulations

In this section the results of four WRF-Fire simulations of fire spread on a leeward slope are presented. Details of the setup used in each simulation are provided in Table 5.1. Each simulation has a unique name derived from two properties: atmosphere-fire coupling ("FC" for atmosphere-fire coupling or "FN" for no atmosphere-fire coupling), and fuel type ("F05" for brush fuel type or "F13" for heavy logging slash fuel type). By comparing simulations with the atmosphere-fire coupling enabled or disabled, a direct evaluation of the importance of atmosphere-fire interactions on the fire spread can be made. The "F05" and "F13" fuel types are based upon the "Brush (2 feet)" and "Heavy Logging Slash" Anderson fuel categories (Anderson, 1982) and were chosen as they have very different fuel properties.

5.5.1 Fire Spread on Leeward Slope

Figure 5.11a shows the fuel fraction remaining at times of 60, 90 and 120 min for the FCF05 simulation. Between 30 and 60 min, the fire spreads predominantly upslope asymmetrically and comes within 20 m of the mountain ridge line. As the fuel conditions and leeward slope angle are constant, this fire spread asymmetry must be due to a combination of the turbulent mid-flame wind conditions and the asymmetric fire ignition pattern. Between 60 and 90 min, the fire spreads in a predominantly lateral direction and there is no fire spread west of the ridge line due to the strong westerly flow across the ridge line. Between 90 and 120 min, the fire spread is still predominantly lateral, with some fire spread downslope of the ignition region. By 120 min, the fire perimeter has a maximum south-north and west-east extent of $\sim$1.7 and 1.3 km, respectively.

Figure 5.11b shows the fuel fraction remaining at times of 60, 90 and 120 min for the FNF05 simulation. Between 30 and 60 min, the fire spreads both laterally and upslope, and the fire perimeter is approximately elliptical. Between 60 and 90 min, the fire spreads upslope to the mountain ridge line, but there is no further westward spread due to the strong westerly winds across the windward slope. The fire spread during this period is therefore predominantly lateral, in particular to the north. Between 90 and 120 min, the fire spread is still predominantly lateral, with some fire spread downslope

of the ignition region. By 120 min, the fire perimeter has a maximum south-north and west-east extent of around ∼2.0 and 1.3 km, respectively.

The similarity between the fire spread in these two simulations suggests that atmosphere-fire interactions do not play a significant role in the FCF05 simulation. Instead, the fire spread is primarily driven by the steep slope and the turbulent wind conditions at the mid-flame height. The only possible exception to this is the initial 30-min period of predominantly upslope fire spread after ignition. The upslope fire spread occurs at a faster rate in the coupled simulation, which indicates that the pyro-convection must influence the wind conditions across the leeward slope at the mid-flame height. The lateral fire spread does not seem to be closely associated with the distance from the mountain ridge line, which implies that the lateral fire spread seen is not consistent with fire channelling.

Figure 5.11c shows the fuel fraction remaining at times of 60, 90 and 120 min for the FCF13 simulation. Between 30 and 60 min, the fire spreads predominantly upslope at an average rate of ∼2.0 km h^{-1}. By 60 min, the fire perimeter is approximately elliptical and extends up to 100 m west of the mountain ridge line. Between 60 and 90 min, the fire spread is dominated by lateral spread both northwards and southwards directly to the east of the ridge line. The northwards and southwards lateral spread occurs at an average rate of ∼1.9 and 1.0 km h^{-1}, respectively. Between 90 and 120 min, the fire spread is still dominated by lateral spread close to the ridge line at an average rate of ∼1.0 km h^{-1}. By 120 min, the fire perimeter has a highly asymmetric shape, with a maximum south-north extent of ∼2.8 km directly to the east of the ridge line.

Figure 5.11d shows the fuel fraction remaining at times of 60, 90 and 120 min for the FNF13 simulation. Between 30 and 60 min, the fire spreads predominantly upslope up to a height of ∼800 m on the leeward slope, which is well below the mountain ridge line. By 60 min the perimeter is approximately circular with a diameter of ∼1.0 km. Between 60 and 90 min, the fire spreads both upslope and laterally, however the westward spread does not extend beyond the mountain ridge line. Between 90 and 120 min, the fire spreads in a predominantly lateral direction, however there is also limited fire spread to the west of the ridge line and downslope from the ignition region. By 120 min, the fire perimeter is approximately elliptical, with a maximum south-north and west-east extent of ∼1.9 and 1.4 km, respectively.

The fire spread seen in the FNF13 and FNF05 simulations is very similar. This suggests that the fire spread is more closely associated with the slope angle and wind conditions than with the fuel conditions. The fire spread seen in the FCF13 simulation is very different to the other three simulations and shares in common a number of characteristics with the fire spread expected during fire channelling. The rapid lateral fire spread occurs intermittently in both directions across the leeward slope in close proximity to the mountain ridge line. The fire spread seen to the west of the mountain ridge

line, however, is not typically seen during fire channelling. The downwind extension of the active flaming zone expected during fire channelling is not seen in this simulation. However, this can be explained by the absence of spotting in the WRF-Fire model, which likely plays an important role in the downwind extension of the active flaming zone. A direct comparison of the FCF13 and FNF13 simulations indicates that the atmosphere-fire interactions play an important role in the fire spread for this fuel type. It is likely that the rapid lateral fire spread seen close to the ridge line results from a modification of the mid-flame wind conditions by pyro-convection.

5.5.2 Dynamical Atmosphere-Fire Interactions

The previously discussed differences in the fire spread seen between the heavy logging slash and brush fuel type simulations is likely to be closely associated with the pyro-convection and the resulting atmosphere-terrain-fire interactions. The heavy logging slash fuel type has a significantly higher fuel depth and density than does the brush fuel type, giving it a higher fuel mass per unit area and a higher corresponding sensible and latent heat release rate.

Figure 5.12a shows the time-varying total heat release rate from the fire for the FCF05 and FNF05 simulations. The heat release rate is very similar between the two simulations, which further demonstrates that the atmosphere-fire interactions do not significantly influence the fire spread in the FCF05 simulation. Figure 5.12b shows the time-varying total heat release rate from the fire for the FCF13 and FNF13 simulations. The total heat release rate is approximately an order of magnitude larger for the heavy logging slash fuel type, which is closely associated with its higher fuel depth and density. Between 50 and 90 min, the heat release rate is higher in the coupled simulation, which implies that the atmosphere-fire interactions make a significant difference to the fire spread prior to the fire perimeter first reaching the mountain ridge line at a time of $\sim$56 min. The FCF13 simulation has a local and global maximum in the total heat release rate at times of $\sim$64 and 75 min, respectively. These correspond to the times at which there is significant lateral fire spread in close proximity to the mountain ridge line.

Figure 5.13 shows the potential temperature anomalies and wind conditions at a time of 56 min on a vertical cross-section for the FCF13 simulation. The potential temperature anomalies are a useful indicator of pyro-convection and are calculated relative to the vertically averaged potential temperature upstream of the mountain. A pyro-convective plume, which is tilted eastwards by the westerly flow, is visible downstream of the mountain up to a height of 4 km. There are positive anomalies, associated with ongoing combustion, across much of the leeward slope, extending from the fire ignition region to the mountain ridge line. The pyro-convection is at a maximum directly eastwards of the ridge line and results in strong upslope flow across much of the leeward

slope. This upslope flow associated with the pyro-convection contributes to the high average upslope fire spread rate between 30 and 60 min. Strong horizontal convergence between the windward and leeward slope flows is seen at the ridge line, which results in a strong updraft near the ridge line. The downstream wind conditions indicate that there is an extensive turbulent wake downstream of the pyro-convective plume. The pyro-convective plume dissipates quickly with distance away from the mountain, indicating that there is a high level of mixing and entrainment of mean flow with the plume. The pyro-convective plume dynamics may have important implications for downstream transport of firebrands, however this is not specifically considered in this study.

Figure 5.14 shows the fire perimeter, vertical wind velocities taken at a height of ∼16 m, and the horizontal wind conditions taken at the mid-flame height, at a time 60, 66 and 72 min for the FCF13 simulation. By 60 min, the fire has spread westwards from the ignition region to ∼100 m west of the mountain ridge line. By this time the fire spread has been predominantly upslope, driven partly by the strong easterly flow associated with the pyro-convection. A downdraft region is visible ∼100 m to the south of the fire perimeter and directly to the east of the ridge line. This downdraft region is in close proximity to the base of the pyro-convective plume, which extends across much of the fire area. The inflow and outflow associated with these updraft and downdraft regions interact to form a region of counterclockwise rotating flow at the mid-flame height in close proximity to the southern flank of the fire. Between 60 and 66 min, this updraft-downdraft interface moves across the southern flank of the fire perimeter and the associated counterclockwise rotating flow acts to spread the fire in a lateral direction close to the ridge line. Between 66 and 72 min, this lateral fire spread continues at an average rate of ∼3.6 km h^{-1} and ignites an area of ∼12 ha. This rapid lateral spread rate is therefore significantly higher than the average upslope spread rate of 2.0 km h^{-1} between 30 and 60 min. By 72 min the updraft-downdraft interface moves inside the fire perimeter and the lateral spread rate rapidly decreases to nearly zero.

5.6 Summary and Conclusions

The atypical wildland fire spread phenomenon known as "fire channeling" has been investigated through a series of idealised two and three-dimensional numerical simulations. These simulations were performed using the WRF-Fire coupled atmosphere-fire numerical model and provide important new insights into the physical processes responsible for the lateral fire spread seen during fire channelling.

The 2D atmospheric flow over a triangular mountain was investigated under varying atmospheric stability and leeward slope angle conditions. In each simulation there was acceleration of the flow as it moved up the windward slope and rapid deceleration of the

flow as it moved down the leeward slope. This acceleration and deceleration of the flow is most likely due to the pressure gradient encountered by the flow as it moves across the mountain. The rapid leeward flow deceleration resulted in flow separation across much of the leeward slope and several kilometres downstream of the mountain. This flow separation was associated with the periodic formation of large-scale rotors in the lee of the mountain, which were then seen to detach from the mountain and propagate downstream. In a stable atmosphere, mountain waves were seen to develop in the lee of the mountain, with associated flow separation under the first downstream mountain wave crest. The wavelength of these mountain waves was, however, too long for any direct effect of the mountain waves on the flow across the leeward slope. For the range of conditions tested, it was found that the leeward flow behaviour was more closely associated with the atmospheric stability than with the leeward slope angle.

The 3D atmospheric flow over a triangular mountain was investigated under varying atmospheric stability conditions. The atmospheric flow features seen in the 3D simulations were found to be broadly similar to the flow features of the equivalent 2D simulations, but with some important differences. First, the instantaneous horizontal vorticity indicated that the 3D flow was dominated by chaotic fine-scale features, with an absence of the large-scale lee rotors seen in 2D. Second, the flow separation close to the leeward slope was typically weaker and more spatially confined in the 3D simulations. These results are consistent with the previous study by (Doyle and Durran, 2007), who identified that 3D tilting and stretching of vortical structures may explain these differences, although this is not specifically tested in this study. The absence of large-scale lee rotors in the 3D simulations allows this study to refute the fire channeling hypothesis proposed by Sharples et al. (2012), which depends upon their existence.

The fire spread across a leeward slope was investigated for two different fuel types and with the atmosphere-fire coupling switched either on or off. The two fuel types considered were based on the brush and heavy logging slash Anderson fuel categories (Anderson, 1982). The patterns of fire spread in the coupled and non-coupled brush fuel type simulations were very similar, indicating that the atmosphere-fire interactions did not play an important role in the fire spread for this fuel type. This was supported by examination of the total fire heat release rate, which was very similar for the two simulations and low in both cases, suggesting little pyro-convection. The fire spread was very different between the coupled and non-coupled heavy logging slash fuel type simulations and in the coupled simulation was found to closely resemble that expected during fire channelling. The fire spread was initially predominantly upslope until it reached the mountain ridge line, after which the fire spread was dominated by intermittent rapid lateral spread in close proximity to the ridge line. The atmosphere-fire interactions were found to make an important difference to the fire spread for the heavy logging slash fuel

type, with a noticeable increase in the total heat released from the fire for the coupled simulation.

The intermittent rapid lateral fire spread seen in the coupled heavy logging slash fuel type simulation was found to be driven by a process where an updraft-downdraft interface moved across the fire perimeter. The inflow and outflow associated with these updrafts and downdrafts resulted in either clockwise or counterclockwise flow rotation at the mid-flame height near the northern and southern flanks of the fire, respectively. When an updraft/downdraft interface moved across the fire perimeter, the associated rotating flow acted to significantly increase the lateral spread rate up to 3.6 km h^{-1} close to the mountain ridge line for a period of a few minutes. When compared with the average spread rate of $\sim$2.0 km h^{-1} during the initial run up the leeward slope with the upslope wind, this lateral spread rate is significantly higher. This result is important given that the upslope spread is traditionally assumed to yield the highest rates of spread. The formation of these updraft-downdraft interfaces results from an interaction of the pyro-convection and the terrain-modified winds though precise mechanisms remain to be investigated. This proposed physical process shares some characteristics in common with the description of the generation of fire whirls on leeward slopes given by Countryman (1971), who proposed that fire whirls are likely to develop where there is significant convection and also eddies in the atmospheric flow. The dynamics of the convective plume seen in the coupled simulation suggest that spotting could result in the transport of firebrands downstream of the mountain. Such a spotting process could explain the downwind extension of the active flaming zone typically seen during fire channelling.

This study has provided a number of important new insights into the fire channelling phenomenon. First, this study has shown that it is possible to simulate the fire channelling phenomenon using the WRF-Fire coupled atmosphere-fire model. Second, the study has provided important new insights into the physical processes that may be driving the atypical fire spread seen during fire channelling. Future work will incorporate additional coupled atmosphere-fire simulations to better understand the environmental conditions, such as fuel type, terrain configuration and atmospheric stability, required for fire channelling to occur. The atypical fire spread seen in these simulations suggests that the fire channelling phenomenon has particular relevance to fire management and fire fighter safety.

Table 5.1: Name and model configuration of each of the numerical simulations.

Simulation Name	2D or 3D	Leeward Slope (°)	Atmospheric Stability	Simulation Time (hr)	Fuel Type	Two-Way Coupling
2DS35	2D	35	Stable	4	-	-
2DN35	2D	35	Neutral	4	-	-
2DU35	2D	35	Unstable	4	-	-
2DS25	2D	25	Stable	4	-	-
2DN25	2D	25	Neutral	4	-	-
2DU25	2D	25	Unstable	4	-	-
3DS	3D	35	Stable	2	-	-
3DN	3D	35	Neutral	2	-	-
3DU	3D	35	Unstable	2	-	-
FCF05	3D	35	Neutral	2	5	Y
FNF05	3D	35	Neutral	2	5	N
FCF13	3D	35	Neutral	2	13	Y
FNF13	3D	35	Neutral	2	13	N

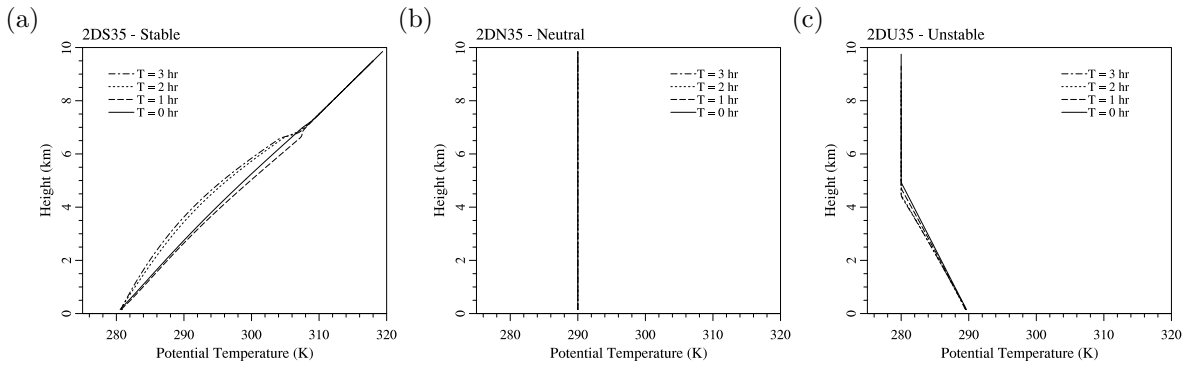

Figure 5.1: Vertical profiles of the potential temperature at the western lateral boundary for the (a) 2DS35 (b) 2DN35 and (c) 2DU35 simulations. In each plot the instantaneous vertical potential temperature profile is shown at times of 0, 1, 2 and 3 hr.

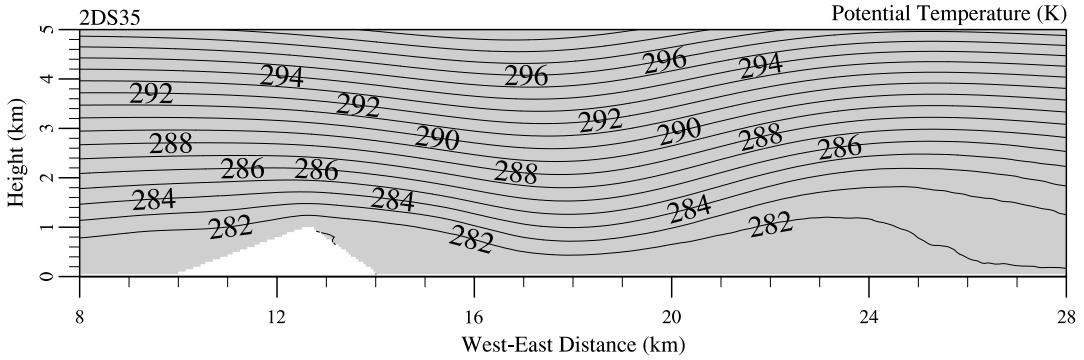

Figure 5.2: Contour line plots of the time-averaged potential temperature for the 2DS35 simulation. The contour line interval in (a) and (b) is 1 K. A subset of the full model domain is shown in (a) and (b), with white shading used to represent the mountain.

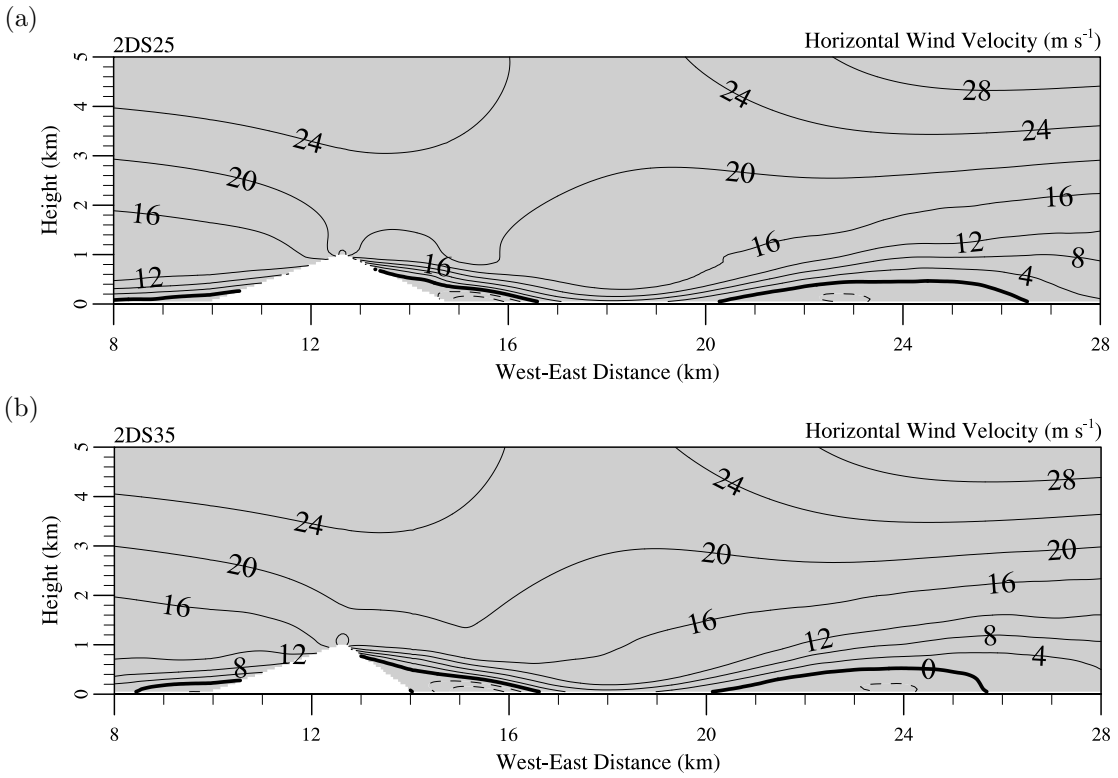

Figure 5.3: Contour line plots of the time-averaged horizontal wind velocity for the (a) 2DS25 and (b) 2DS35 simulations. The contour line interval in (a) and (b) is 4 m s^{-1}. The solid contour lines indicate westerly winds and the dashed contour lines indicate easterly winds. The thick solid black line indicates a horizontal velocity of zero. A subset of the full model domain is shown in (a) and (b), with white shading used to represent the mountain.

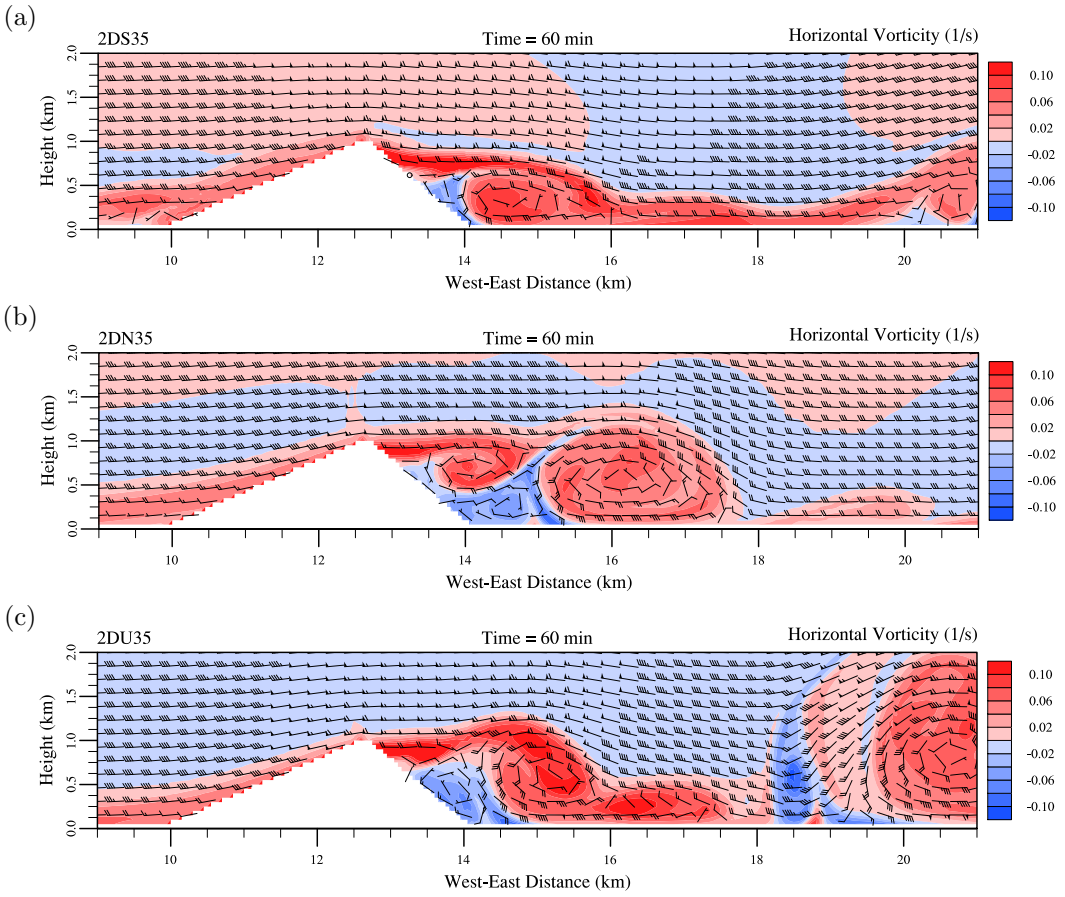

Figure 5.4: Instantaneous horizontal vorticity contour and wind barb plots at a time of 60 min for the (a) 2DS35 (b) 2DN35 and (c) 2DU35 simulations. The horizontal vorticity has a contour interval of 0.02 s^{-1}. The wind conditions are determined using the west-east and vertical wind components. Standard weather map wind barbs are used to indicate the wind speed in knots and the direction, with each full feather indicating an additional 10 knots in wind speed. A subset of the full model domain is shown in each plot, with white shading used to represent the mountain.

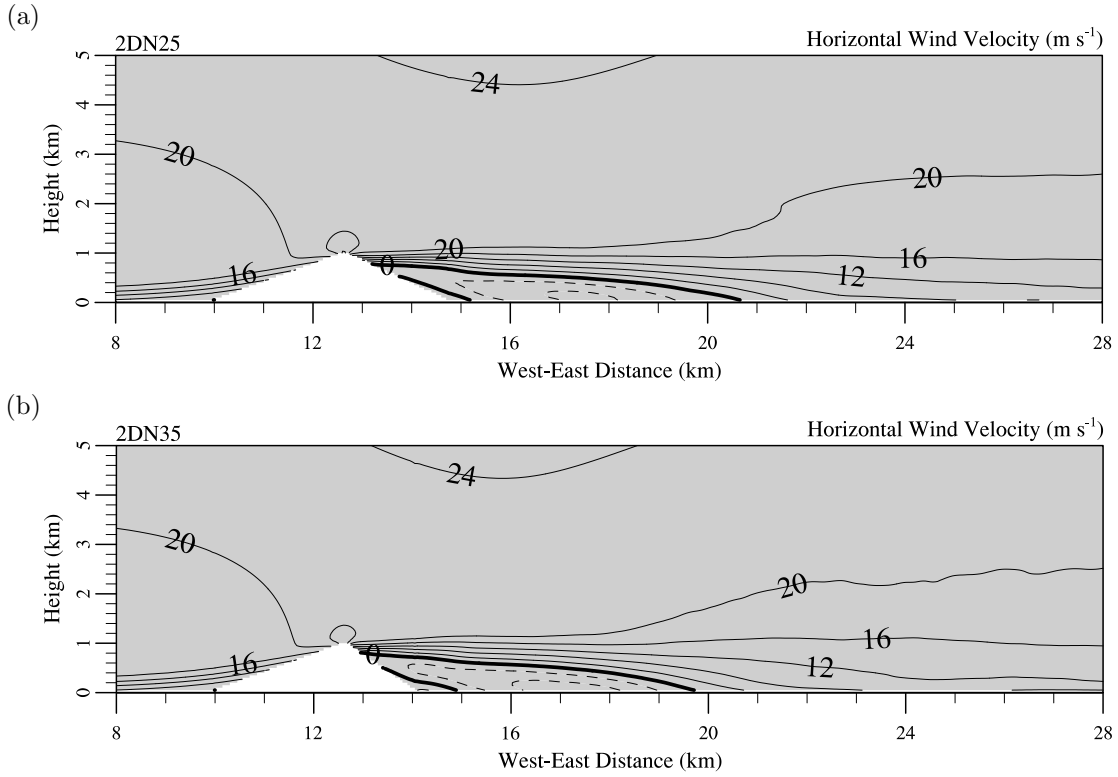

Figure 5.5: As in Figure 5.3, but for the (a) 2DN25 and (b) 2DN35 simulations.

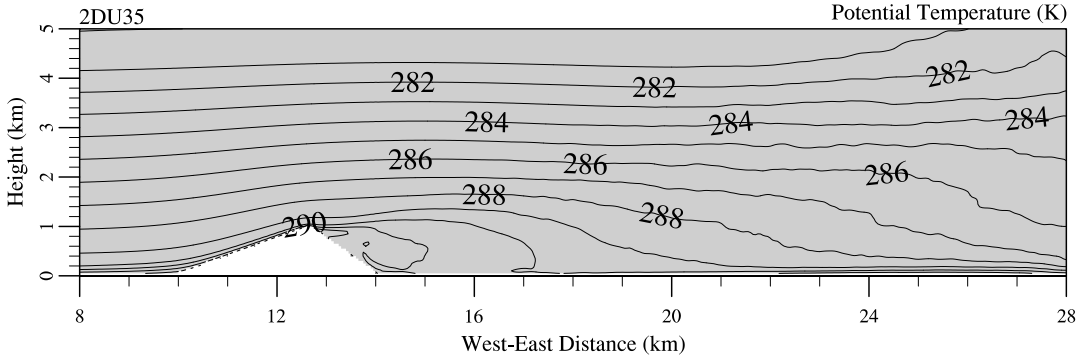

Figure 5.6: As in Figure 5.2, but for the 2DU35 simulation.

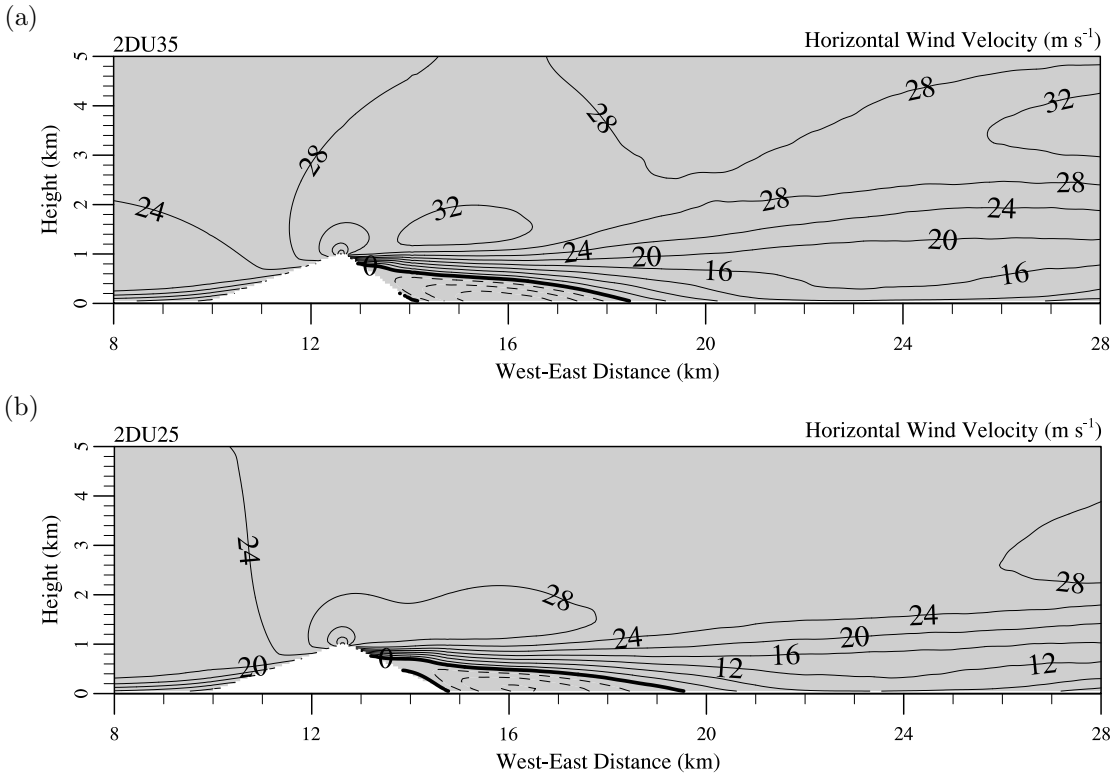

Figure 5.7: As in Figure 5.3, but for the (a) 2DU25 and (b) 2DU35 simulations.

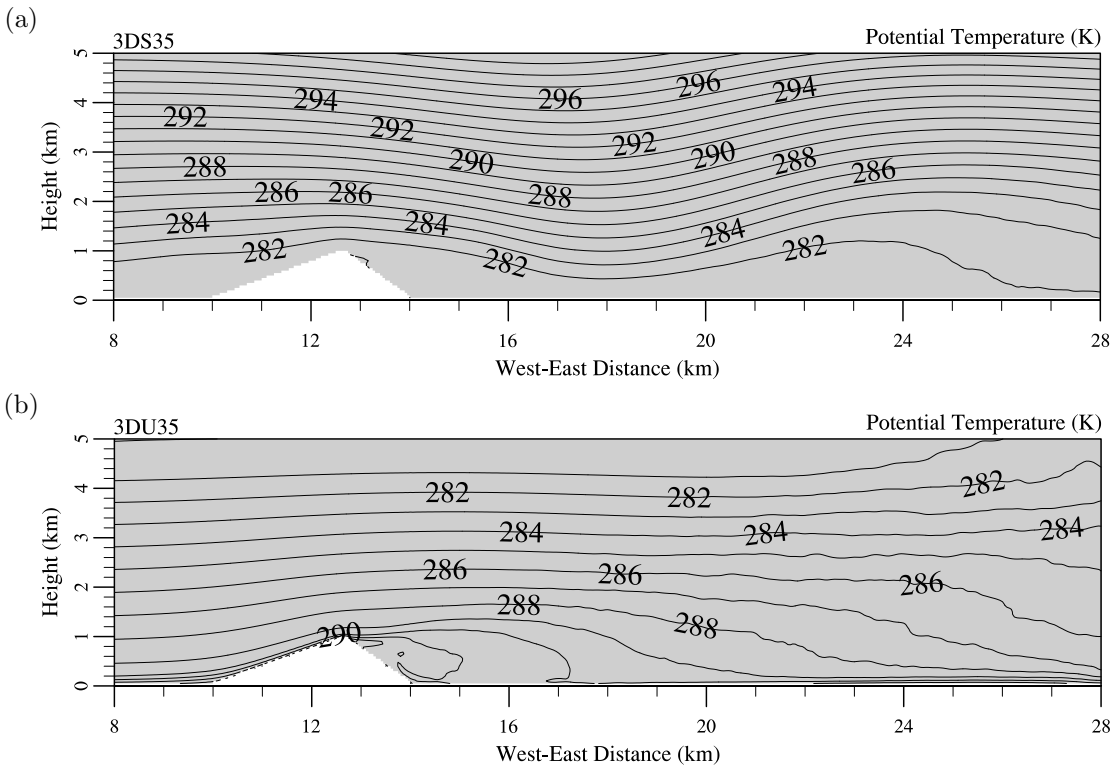

Figure 5.8: As in Figure 5.2, but for the (a) 3DS35 and (b) 3DU35 simulations. The vertical cross-section is taken through the middle of the y-axis.

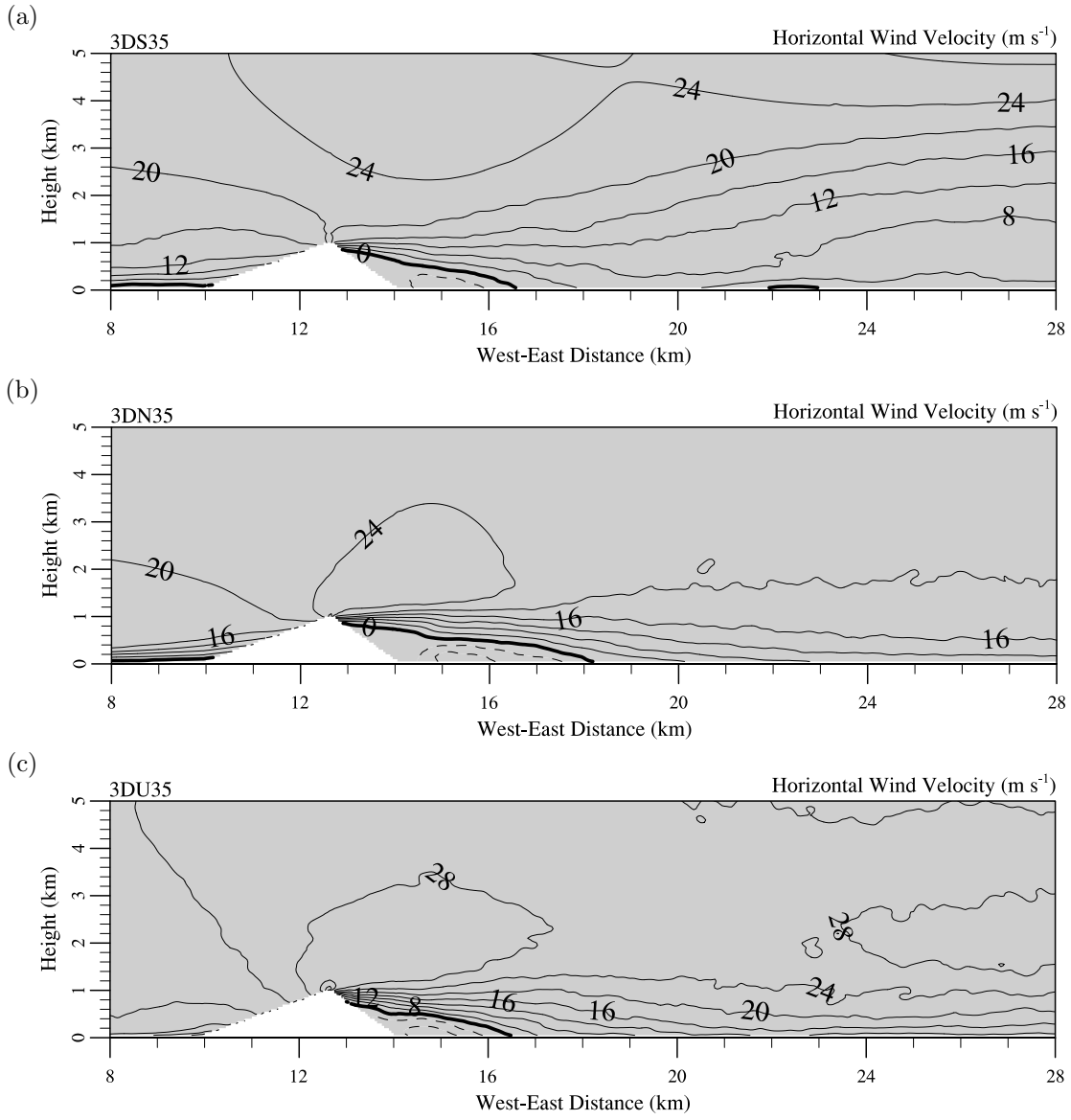

Figure 5.9: As in Figure 5.3, but for the (a) 3DS35 (b) 3DN35 and (c) 3DU35 simulations. The vertical cross-section is taken through the middle of the y-axis.

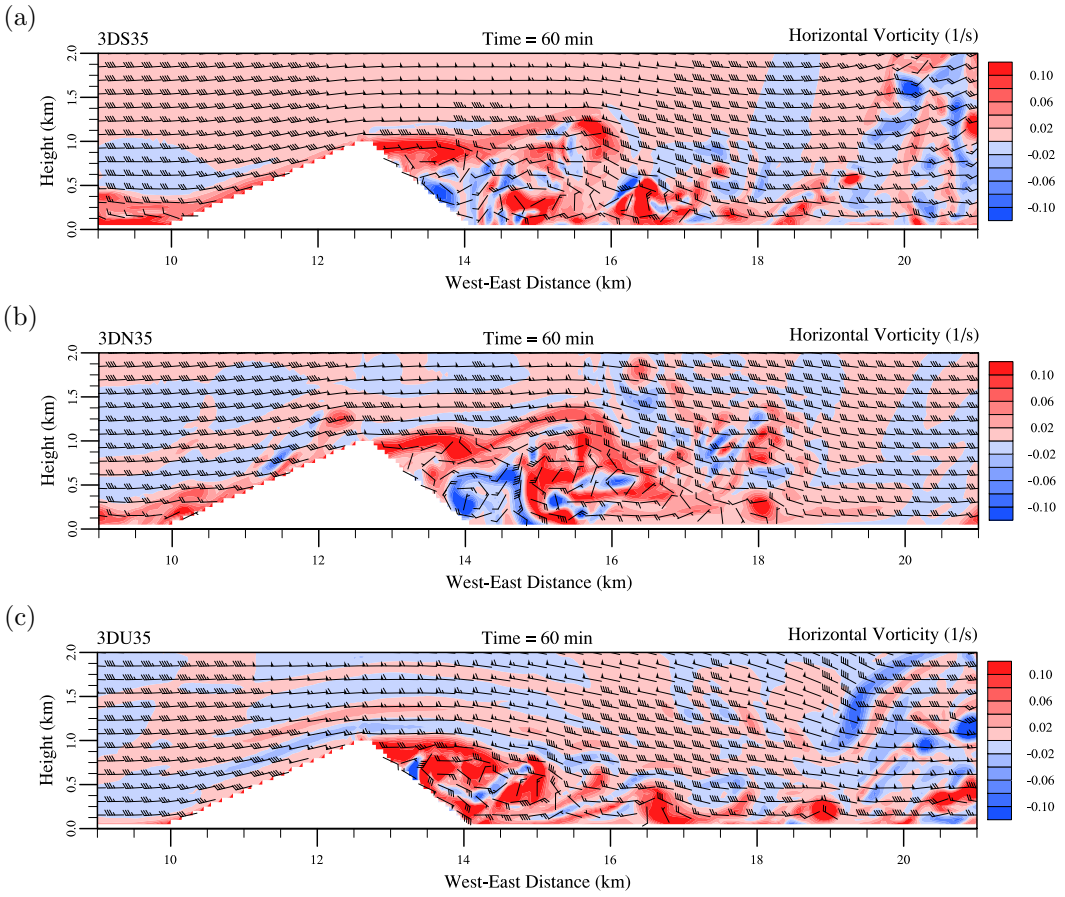

Figure 5.10: As in Figure 5.4, but for (a) 3DS35 (b) 3DN35 and (c) 3DU35 simulations. The vertical cross-section is taken through the middle of the y-axis.

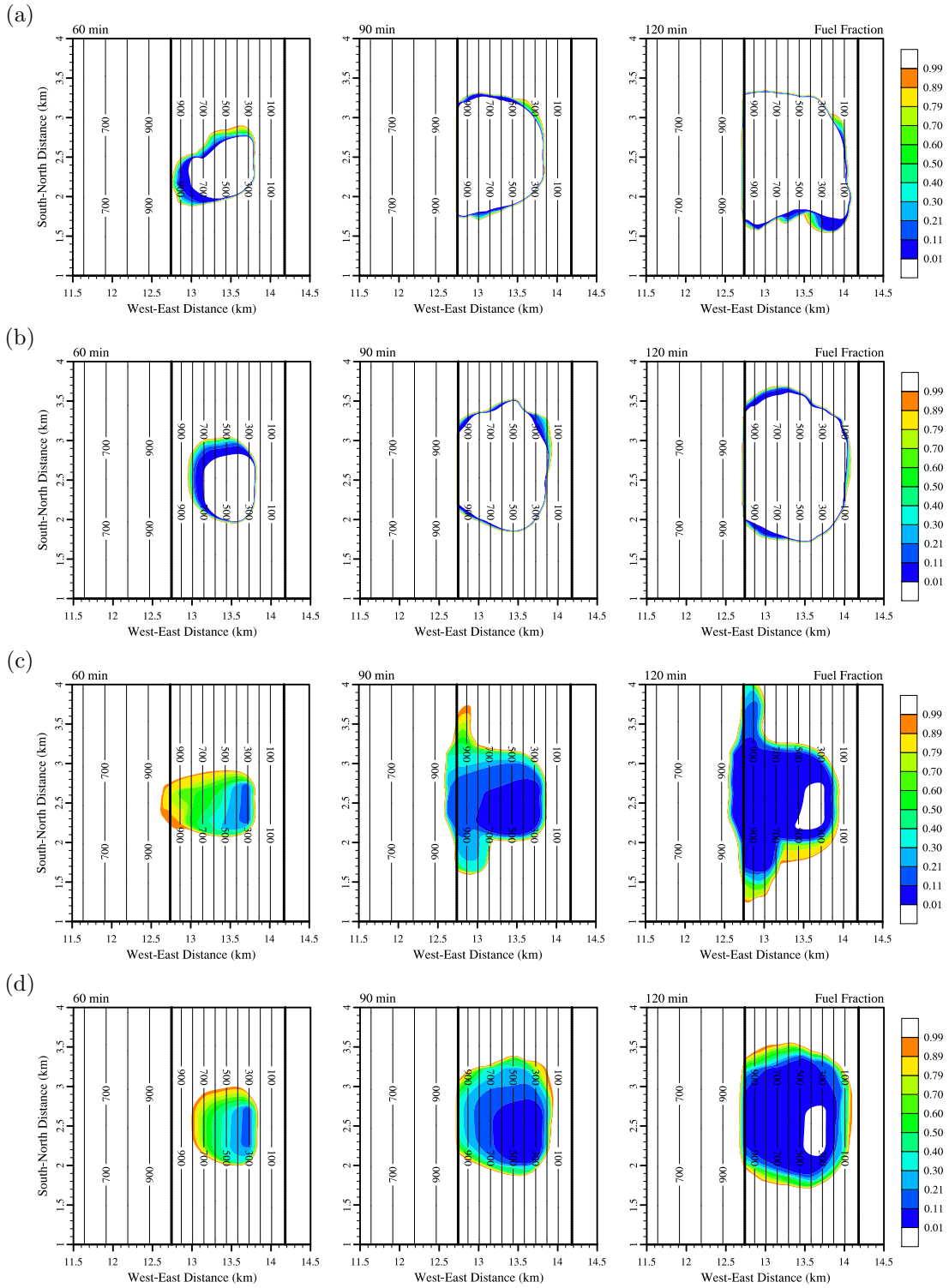

Figure 5.11: Contour plots of the instantaneous fuel fraction remaining at times of 60 (left), 90 (middle) and 120 min (right) for the (a) FCF05 (b) FNF05 (c) FCF13 and (d) FNF13 simulations. White shading is applied to regions where the fuel fraction remaining is over 99% or under 1%. Terrain contour lines are given at 100 m intervals and the solid black lines represent the mountain ridge line and the base of the leeward slope. The fire ignition region is indicated by the dash-filled region. A subset of the full SFIRE model domain is shown in each plot.

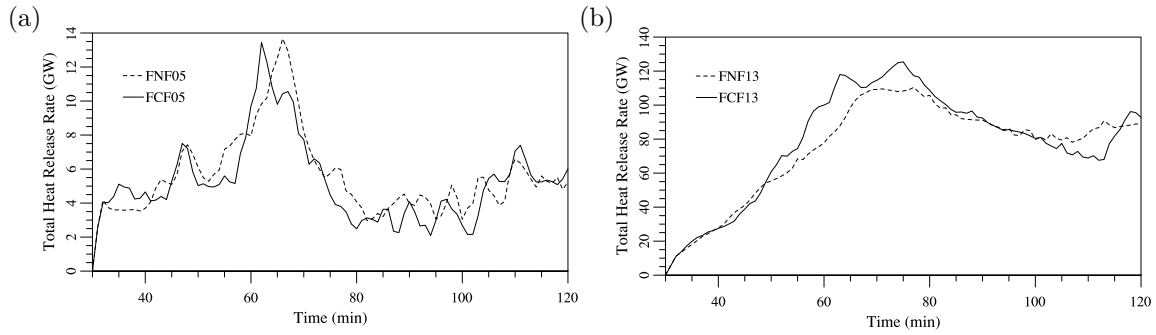

Figure 5.12: Timeseries of the total heat release rate for the (a) brush and (b) heavy logging slash fuel type simulations. In each simulation the fire is ignited at a time of 30 min, so the total heat release rate prior to this time is zero. The total heat release rate, which is determined across the full SFIRE model domain, is measured in gigawatts (GW) and the y-axis scales in (a) and (b) are an order of magnitude different. The solid and dashed black lines represent the total heat release rate for the coupled and uncoupled simulations, respectively.

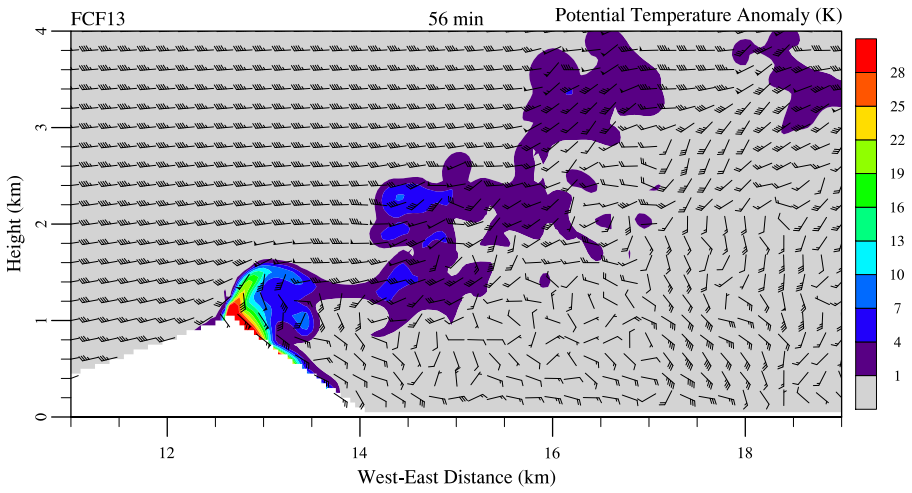

Figure 5.13: Potential temperature anomaly contours and wind barbs at a time of 56 min for the FCF13 simulation. The potential temperature anomaly has a contour interval of 3 K. The wind conditions are determined using the west-east and vertical wind components. Standard weather map wind barbs are used to indicate the wind speed (knots) and the direction, with each full feather indicating an additional 10 knots in wind speed. A subset of the full model domain is shown in each plot, with white shading used to represent the mountain. The vertical cross-section is taken at the mid-point of the y-axis.

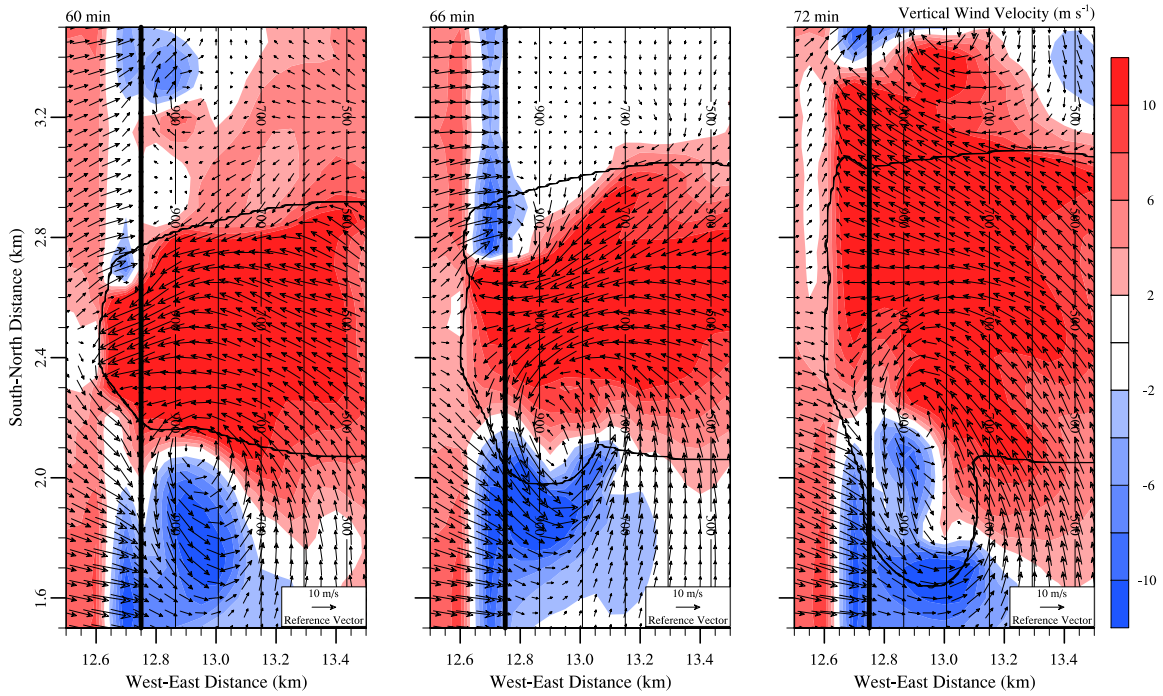

Figure 5.14: Vertical wind velocity contours and mid-flame height horizontal wind velocity vectors at times of 60, 66 and 72 min for the FCF13 simulation. The reference vector shown is a 10 m s^{-1} westerly wind. Terrain contour lines are given at 100-m intervals and the solid black lines represent the mountain ridge line. The fire perimeter is represented by a solid black line. The vertical wind velocity is taken at a height of ∼16 m and has a contour interval of 2 m s^{-1}. Vertical wind velocities between −2 and 2 m s^{-1} are shaded white to clearly show the updraft-downdraft interfaces. The horizontal wind vectors are taken at the mid-flame height and the reference vector shows a westerly wind velocity of 10 m s^{-1}. A subset of the full SFIRE model domain is shown.

Chapter 6

Summary and Conclusions

The primary aim of this thesis was to investigate atmospheric interactions with wildland fire through the application of the WRF NWP and WRF-Fire coupled atmosphere-fire models. This aim was achieved through a series of related studies that investigated fire weather and atmosphere-fire interactions across a range of atmospheric scales, from synoptic and mesoscale atmospheric processes over the complex terrain of New Zealand to microscale two-way coupled atmosphere-fire interaction processes over idealised terrain. Although the majority of the research was regionally focused on New Zealand, the research outcomes are internationally significant and will benefit both the scientific and fire management communities. The key research outcomes have been divided into three categories and are discussed below alongside their limitations and proposed further research.

6.1 Assessment of Fire Weather

NWP modelling is used extensively internationally in fire weather assessment to conduct wildland fire research and support operational fire management. However, there are only a limited number of international studies that have evaluated the suitability of NWP modelling of fire weather through comparison of NW model output with observational data. Chapter 2 investigated the suitability of WRF modelling of fire weather and concluded that although WRF is suitable for mesoscale modelling of seasonal fire weather across the non-mountainous terrain in New Zealand, there were systematic biases in the modelled fire weather variables, such as the air temperature and wind speed, and the FWI. However, the study was limited to consideration of only one fire season and further research is required to extend this analysis to a climatologically significant timescale.

The FWI is the primary tool used in fire weather assessment in New Zealand and is derived from atmospheric conditions at or below 10 m above ground level. The FWI does not account for vertical atmosphere-fire interactions, such as vertical circulations

associated with pyro-convective plume dynamics, that can directly influence fire behaviour. Future fire weather assessment in New Zealand should therefore include some representation of fire weather aloft, such as the vertical profiles of wind conditions, atmospheric stability and humidity. Chapter 3 studied the behaviour of the Haines Index (HI) and Continuous Haines Index (CHI), which measure the atmospheric stability and humidity aloft, during a fire season and concluded that they could provide an additional useful resource for fire weather assessment in New Zealand. However, the use of fixed atmospheric pressure levels prohibits their effective use in mountainous terrain in New Zealand. This study was limited to a highly averaged interpretation of the behaviour of the HI and CHI, and further research is needed to identify how the HI and CHI respond to specific atmospheric processes, such as sea and land breezes, in New Zealand.

Pearce (1996, 2003) and Pearce et al. (2011b) have developed a fire weather climatology for New Zealand based on weather station measurements of key weather variables and the derived fuel moisture and fire behaviour indices associated with the NZFDRS. Although this fire weather climatology is a valuable resource for wildland fire research and management in New Zealand, it has two important limitations. First, the interpolation of observational data throughout New Zealand does not account for spatial variations in weather and climate between observations. This could result in significant errors, particularly in data sparse regions or complex terrain, as the weather and climate of New Zealand can vary significantly over short distances. Second, the climatology is limited to consideration of near-surface weather variables and does not consider relevant atmospheric conditions aloft, such as the atmospheric stability. The development of a fire weather climatology for New Zealand, which considers both near-surface and aloft atmospheric properties, based on NWP modelling would provide an additional useful resource. The WRF model configuration described in Chapters 2 and 3 could be used as a starting point to develop this modelled fire weather climatology.

A full evaluation of the utility of fire weather indices in a fire management context in New Zealand was beyond the scope of this thesis. The investigation of the behaviour of the HI, CHI and FWI during the 2009/10 New Zealand wildland fire season in Chapter 3 represents an important first step towards such an evaluation. Chapter 3 concluded that the HI, CHI and FWI are not statistically related to wildland fire size, although they do provide useful theoretical insights into the fire weather conditions. However, this study was limited to a small sample size of 36 wildland fires and further research is required to identify if any statistical relationships exist between these indices and important aspects of fire behaviour, such as fire intensity and forward rate of spread, in New Zealand.

The current generation of fire weather indices used internationally in fire weather assessment are predominantly based on empirical relationships between weather variables and wildland fire behaviour (Potter, 2002). However, due to the complexity of

atmospheric interactions with fire behaviour, there is a need for the next generation of fire weather indices to have a more physically robust basis. In particular, there is a need to further incorporate vertical atmospheric interactions with fire behaviour into fire weather assessment, such as the vertical circulations associated with pyro-convective plume dynamics. Improved fire weather indices will subsequently benefit the fire danger rating systems that are used internationally in assessment of wildland fire risk and behaviour. However, the development of a new set of physically based fire weather indices was outside of the scope of this thesis and current international research continues to focus predominantly on empirically based indices.

6.2 Effects of Complex Terrain

New Zealand is known to experience highly variable weather due to its complex and high relief terrain, and extensive and complex coastline (Sturman et al., 1999). Given the widely acknowledged importance of mountain meteorological effects on wildland fire behaviour and risk (Sharples, 2009), it is therefore important to investigate the effects of complex terrain on fire weather across New Zealand. Chapters 2 and 3 showed that the 2009/10 seasonal fire weather was highly spatially and temporally variable across New Zealand, particularly in mountainous terrain. The spatial patterns in season-averaged near-surface fire weather conditions were largely consistent with the observed fire weather climatology of New Zealand (Pearce, 2003; Pearce et al., 2011b). Chapter 3 additionally considered the season-averaged behaviour of fire weather conditions aloft, which have not previously received much attention in New Zealand.

Foehn events are a relatively common meteorological feature worldwide and are widely acknowledged to influence fire weather through increased air temperatures and wind speeds, and decreased relative humidities. The "Canterbury Northwester" is a relatively common local foehn event in the South Island of New Zealand, although its influence on fire weather conditions in the lee of the Southern Alps has not been studied in detail. Chapter 4 presented a case study of a foehn event on 6 February 2011 and concluded that it resulted in widespread extreme fire weather across the eastern South Island. The interaction of the northwesterly synoptic flow and the mountainous terrain of the Southern Alps resulted in the development of mountain waves that had a direct and significant influence on fire weather conditions across the eastern South Island. A downslope windstorm was modelled along the foothills of the Canterbury Plains, whereas large amplitude trapped lee waves directly affected the near-surface wind speeds further south in Otago. The FWI and CHI were found to respond differently to the foehn winds and varying mountain wave characteristics. The FWI and CHI were both highest near the downslope windstorm, whereas the CHI was low in regions affected by large am-

plitude trapped lee waves. The high season-averaged HI, CHI and FWI values along the foothills of the Canterbury Plains seen in Chapter 3 could be related to the effect of foehn events and mountain waves on the CHI and FWI discussed in Chapter 4. However, Chapter 4 was limited to consideration of just one foehn event and further research is required to examine variations in foehn event characteristics and their influence on fire weather conditions across the South Island.

International research has typically found that varying the horizontal resolution of an NWP model does not significantly affect the modelled fire weather (Hoadley et al., 2004). However, these studies have typically focused on regions that have relatively less complex terrain than New Zealand. As the horizontal resolution affects the representation of topography, varying the horizontal resolution could therefore play a more important role in modelling fire weather in New Zealand than in other countries. For example, Chapter 2 concluded that the wind conditions were least accurately modelled near the Southern Alps, which is consistent with the widely understood difficulty in accurately modelling wind-terrain interactions in or downwind of complex terrain (Jiménez et al., 2010). However, this thesis has not specifically considered the effect of varying horizontal resolution on modelled fire weather across New Zealand and a study focused on this topic would be useful.

Fire channelling occurs in complex terrain and represents a serious risk to fire fighter and civilian safety, due to the associated atypical wildland fire spread, extensive spotting and downwind extension of the active flaming zone (Sharples et al., 2012). Although fire channelling was known to result from an interaction between the atmosphere, terrain and fire, the precise physical mechanism driving the lateral fire spread was not previously known. Chapter 5 presented a new physical explanation of the interaction processes responsible for driving the lateral fire spread, based on coupled atmosphere-fire modelling with WRF-Fire. Although the study was limited to consideration of a highly idealised fire environment, the results imply that fire channelling could be a relatively common method of fire spread in high relief terrain. In addition, the study was limited to a semi-empirical representation of wildland fire behaviour that did not include spotting, which could be an important aspect of fire behaviour during fire channelling. Further research is therefore required to identify past fire channelling events, their prerequisite environmental conditions, and the role of spotting in such events. In the context of fire suppression strategies, careful consideration should be given to the possibility of fire channelling in complex terrain. This topic highlights the importance of further research on atmospheric interactions with wildland fire behaviour in complex terrain, which are not well understood.

6.3 Applications of Numerical Modelling

A number of specialised variants of the WRF model have recently been developed that couple the WRF NWP model with models of other aspects of the physical environment, including chemisty (WRF-Chem) (Grell et al., 2005) and wildland fire (WRF-Fire) (Mandel et al., 2011; Coen et al., 2013). The WRF-Fire model, which couples the large eddy simulation variant of WRF with a wildland fire spread model, was used in Chapter 5. It is one of the few existing numerical models that is capable of directly modelling, albeit in a simplistic manner, the interaction processes between a wildland fire and the surrounding fire environment. This study demonstrated that WRF-Fire is capable of simulating the atypical fire spread during fire channelling, and the atmosphere-fire interaction processes associated with it. WRF-Fire has also previously been utilised to model wildland fire behaviour in a real case study (Jordanov et al., 2012). This research has collectively demonstrated the usefulness of WRF-Fire in investigating atmosphere-fire interaction processes in both an idealised and real environment. WRF-Fire could be used in future research to investigate wildland fire behaviour and atmosphere-fire interaction processes in complex topographical layouts that are known to be dangerous to fire fighters, such as canyons and valleys (Viegas and Pita, 2004).

Fire management agencies currently predominantly utilise empirically based wildland fire behaviour models in developing fire suppression strategies. However, these models are incapable of representing the full complexity of wildland fire behaviour, particularly in fire environments that do not have a high degree of uniformity. This can lead to inaccurate predictions of wildland fire behaviour that could negatively affect wildland fire suppression operations. Further research is needed to develop wildland fire behaviour modelling tools that are based on physical interactions between the fire environment and fire behaviour. For example, atmosphere-fire interactions over high relief terrain are particularly complex and can best be predicted by coupled atmosphere-fire modelling. An additional advantage of physically based wildland fire behaviour models is that they can be used to derive simpler tools that can be more readily utilised by fire management.

The WRF NWP model was utilised throughout this thesis to simulate atmospheric processes across a wide range of scales, from synoptic and mesoscale processes over New Zealand for a period of days to months, to microscale processes over idealised terrain for a period of hours. Outside of this thesis, WRF has been applied to a number of topics, including regional climate modelling (Leung and Qian, 2009) and large eddy simulation of the turbulent planetary boundary layer (Moeng et al., 2007). This thesis and other studies collectively demonstrate the versatility of the WRF and WRF-Fire numerical models and their usefulness in investigating fire weather and atmospheric interactions with wildland fire. NWP and coupled atmosphere-fire models are valuable tools in

modern wildland fire research, although due to their complexity of use they are still not widely utilised by fire management agencies. However, fire management agencies would certainly benefit from a more pragmatic approach towards utilising these models operationally.

Acknowledgements

I first want to thank Andrew Sturman and Peyman Zawar-Reza for their academic supervision throughout my research. I acknowledge the Department of Geography at the University of Canterbury for supporting my research through the provision of travel funding to attend a number of domestic and international conferences and workshops. I also want to thank all the staff and students at the Department of Geography for their valuable support and assistance.

The research was supported through a doctoral scholarship provided by the Bushfire Cooperative Research Centre (Bushfire CRC), Melbourne, Australia. The Bushfire CRC further provided funding to attend three annual Bushfire CRC conferences in Australia and to conduct a two month research trip to the USA in 2011. During this research trip, I visited a number of researchers throughout the USA who I wish to thank for their constructive comments and assistance.

I want to thank Jason Sharples, Jason Evans and Matthew McCabe of the University of New South Wales and Rick McRae of the Australian Capital Territory Emergency Services Agency for providing me with an opportunity to conduct research with them at Canberra, Australia, for three months in 2011. I acknowledge the valuable assistance of researchers at the Rural Fire Research Group of Scion in Christchurch, New Zealand. I also acknowledge David Hunt of the Department of Conservation and Murray Dudfield of the National Rural Fire Authority for their support of my doctoral scholarship application to the Bushfire CRC.

I acknowledge the organisations and individuals responsible for developing and maintaining the numerous computer systems, software and datasets used throughout my research. I want to thank Tony Dale and his colleagues for operating the BlueFern supercomputing system at the University of Canterbury. I also want to thank the individuals and organisations responsible for developing and maintaining the WRF and WRF-Fire models, and the NCAR NCL data processing and visualisation software. Finally, I want to thank the National Institute of Water and Atmospheric Research (NIWA), who are responsible for maintaining the National Climate Database in New Zealand, and Gary Lockyer of the National Rural Fire Authority for providing information on wildland fire events in New Zealand.

Deputy Vice-Chancellor's Office
Postgraduate Office

UNIVERSITY OF CANTERBURY
Te Whare Wānanga o Waitaha
CHRISTCHURCH NEW ZEALAND

Co-Authorship Form

This form is to accompany the submission of any PhD thesis that contains research reported in co-authored work that has been published, accepted for publication, or submitted for publication. A copy of this form should be included for each co-authored work that is included in the PhD thesis. Completed forms should be included at the front (after the thesis abstract) of each copy of the thesis submitted for examination and library deposit (including electronic copy).

Please indicate the chapter/section/pages of this thesis that are extracted from co-authored work and provide details of the publication or submission from the extract comes:

Chapter 2 in the thesis is entitled "Verification of WRF Modelled Fire Weather for the 2009/10 New Zealand Wildland Fire Season" and is based on a paper accepted with minor revisions by the International Journal of Wildland Fire.

Please detail the nature and extent (%) of contribution by the PhD candidate:

The PhD candidate was responsible for the computer modelling, data analysis and write-up of this paper (90%). The co-authors provided regular advice and feedback on the paper as it was developed (10%).

Certification by Co-authors:

If there is more than one co-author then a single co-author can sign on behalf of all

The undersigned certifys that:

- The above statement correctly reflects the nature and extent of the PhD candidate's contribution to this co-authored work
- In cases where the PhD candidate was the lead author of the co-authored work he or she wrote the text

Name: *Andrew Sturman* Signature:  Date: *14 May 2013*

Deputy Vice-Chancellor's Office
Postgraduate Office

UNIVERSITY OF CANTERBURY
Te Whare Wānanga o Waitaha
CHRISTCHURCH NEW ZEALAND

Co-Authorship Form

This form is to accompany the submission of any PhD thesis that contains research reported in co-authored work that has been published, accepted for publication, or submitted for publication. A copy of this form should be included for each co-authored work that is included in the PhD thesis. Completed forms should be included at the front (after the thesis abstract) of each copy of the thesis submitted for examination and library deposit (including electronic copy).

Please indicate the chapter/section/pages of this thesis that are extracted from co-authored work and provide details of the publication or submission from the extract comes:

Chapter 3 of the thesis is entitled "Behaviour of WRF Modelled Fire Weather Indices for the 2009/10 New Zealand Wildland Fire Season" and is based on a paper accepted with major revisions by the International Journal of Wildland Fire.

Please detail the nature and extent (%) of contribution by the PhD candidate:

The PhD candidate was responsible for the computer modelling, data analysis and write-up of this paper (90%). The co-authors provided regular advice and feedback on the paper as it was developed (10%).

Certification by Co-authors:

If there is more than one co-author then a single co-author can sign on behalf of all

The undersigned certifys that:

- The above statement correctly reflects the nature and extent of the PhD candidate's contribution to this co-authored work
- In cases where the PhD candidate was the lead author of the co-authored work he or she wrote the text

Name: *Andrew Sturman* Signature:  Date: *14 May 2013*

Deputy Vice-Chancellor's Office
Postgraduate Office

UNIVERSITY OF CANTERBURY
Te Whare Wānanga o Waitaha
CHRISTCHURCH NEW ZEALAND

Co-Authorship Form

This form is to accompany the submission of any PhD thesis that contains research reported in co-authored work that has been published, accepted for publication, or submitted for publication. A copy of this form should be included for each co-authored work that is included in the PhD thesis. Completed forms should be included at the front (after the thesis abstract) of each copy of the thesis submitted for examination and library deposit (including electronic copy).

Please indicate the chapter/section/pages of this thesis that are extracted from co-authored work and provide details of the publication or submission from the extract comes:

Chapter 4 in the thesis is entitled "Fire Weather of an Extreme Foehn Event in South Island, New Zealand" and is based on a paper submitted to Monthly Weather Review.

Please detail the nature and extent (%) of contribution by the PhD candidate:

The PhD candidate was responsible for the computer modelling, data analysis and write-up of this paper (90%). The co-authors provided regular advice and feedback on the paper as it was developed (10%).

Certification by Co-authors:

If there is more than one co-author then a single co-author can sign on behalf of all

The undersigned certifys that:

- The above statement correctly reflects the nature and extent of the PhD candidate's contribution to this co-authored work
- In cases where the PhD candidate was the lead author of the co-authored work he or she wrote the text

Name: *Andrew Sturman* Signature:  Date: *14 May 2013*

Deputy Vice-Chancellor's Office
Postgraduate Office

UNIVERSITY OF CANTERBURY
Te Whare Wānanga o Waitaha
CHRISTCHURCH NEW ZEALAND

Co-Authorship Form

This form is to accompany the submission of any PhD thesis that contains research reported in co-authored work that has been published, accepted for publication, or submitted for publication. A copy of this form should be included for each co-authored work that is included in the PhD thesis. Completed forms should be included at the front (after the thesis abstract) of each copy of the thesis submitted for examination and library deposit (including electronic copy).

Please indicate the chapter/section/pages of this thesis that are extracted from co-authored work and provide details of the publication or submission from the extract comes:

Chapter 5 in the thesis is entitled "Large Eddy Simulation of Atypical Wildland Fire Spread on Leeward Slopes" and is based on a paper accepted for publication in the International Journal of Wildland Fire.

Please detail the nature and extent (%) of contribution by the PhD candidate:

The PhD candidate was responsible for the computer modelling, data analysis and write-up of this paper (90%). The co-authors provided regular advice and feedback on the paper during its development (10%).

Certification by Co-authors:
If there is more than one co-author then a single co-author can sign on behalf of all
The undersigned certifys that:

- The above statement correctly reflects the nature and extent of the PhD candidate's contribution to this co-authored work
- In cases where the PhD candidate was the lead author of the co-authored work he or she wrote the text

Name: *Jason Sharples* Signature:  Date: *16/1/2013*

Bibliography

Achtemeier GL (2008). Effects of moisture released during forest burning on fog formation and implications for visibility. *Journal of Applied Meteorology and Climatology* **47**(5), 1287–1296.

Albini FA (1976). *Estimating wildfire behavior and effects.* Intermountain Forest and Range Experiment Station, Forest Service, US Department of Agriculture.

Albini FA (1983a). *Potential spotting distance from wind-driven surface fires.* Intermountain Forest and Range Experiment Station, Forest Service, US Department of Agriculture.

Albini FA (1983b). Transport of firebrands by line thermals. *Combustion science and technology* **32**(5/6), 277–288.

Alexander ME (1992). Standard specifications for Fire Weather Index System calculations. Paper prepared for discussion at the 3rd meeting of the Advisory Committee on Forest and Rural Fire Research. 21 October 1992. NZ Fire Service National Headquarters, Wellington, New Zealand.

Alexander ME (1994). Proposed revision of fire danger class criteria for forest and rural fire areas in new zealand. National Rural Fire Authority, Wellington, in association with the New Zealand Forest Research Institute, Rotorua. 73 pp.

Alexander ME (2008). Proposed revision of fire danger class criteria for forest and rural fire areas in new zealand. 2nd Edition. National Rural Fire Authority, Wellington, in association with Scion, Rural Fire Research Group, Christchurch. 62 pp. [Reprint with corrections].

Allen T, Brown AR (2002). Large-eddy simulation of turbulent separated flow over rough hills. *Boundary-Layer Meteorology* **102**, 177–198.

Anderson HE (1982). Aids to determining fuel models for estimating fire behaviour. *USDA Forest Service, Intermountain Forest and Range Experiment Station* **INT-122**.

Anderson S (2005). Forest and rural fire danger rating in New Zealand. In: Colley, M. (Ed.). Forestry Handbook. New Zealand Institute of Forestry, Christchurch. pp241-244.

Ayotte KW (2008). Computational modelling for wind energy assessment. *Journal of Wind Engineering and Industrial Aerodynamics* **96**, 1571–1590.

Banta RM, Olivier LD, Holloway ET, Kropfli RA, Bartram BW, Cupp RE, Post MJ (1992). Smoke-column observations from two forest fires using doppler lidar and doppler radar. *Journal of Applied Meteorology* **31**, 1328–1349.

Barry R (1992). *Mountain weather and climate.* Routledge.

Beer T (1991). The interaction of wind and fire. *Boundary-Layer Meteorology* **54**(3), 287–308.

Beer T (1993). The speed of a fire front and its dependence on wind-speed. *International Journal of Wildland Fire* **3**(4), 193–202.

Blier W (1998). The sundowner winds of Santa Barbara, California. *Weather and Forecasting* **13**(3), 702–716.

Brinkmann W (1970). The chinook at Calgary (Canada). *Theoretical and Applied Climatology* **18**(3), 269–278.

Brinkmann W (1971). What is a foehn? *Weather* **26**, 230–239.

Brinkmann W (1974). Strong downslope winds at Boulder, Colorado. *Monthly Weather Review* **102**, 592–602.

Brown TJ, Hall BL, Westerling AL (2004). The impact of twenty-first century climate change on wildland fire danger in the western United States: An applications perspective. *Climatic Change* **62**(1), 365–388.

Butler B, Bartlette R, Bradshaw L, Cohen J, Andrews P, Putnam T, Mangan R, Brown H (2001). The South Canyon fire revisited: lessons in fire behavior. *Fire Management Today* **61**(1), 14–20.

Butler BW, Cohen J, Latham DJ, Schuette RD, Sopko P, Shannon KS, Jimenez D, Bradshaw LS (2004). Measurements of radiant emissive power and temperatures in crown fires. *Canadian Journal of Forest Research* **34**(8), 1577–1587.

Byram GM (1954). *Atmospheric conditions related to blowup fires.* US Department of Agriculture, Southeastern Forest Experiment Station.

Byram GM (1959). Combustion of forest fuels. *Forest Fire: Control and Use* **1**, 61–89.

Byram GM, Nelson RM (1951). The possible relation of air turbulence to erratic fire behavior in the Southeast. *Fire Control Notes* **12**(3), 1–8.

Chandler C, Cheney P, Thomas P, Trabaud L, Williams D, et al. (1983). *Fire in forestry. Volume 1. Forest fire behavior and effects. Volume 2. Forest fire management and organization.* John Wiley & Sons, Inc.

Chen F, Dudhia J (2001). Coupling an advanced land-surface/ hydrology model with the Penn State/ NCAR MM5 modeling system. Part I: Model description and implementation. *Monthly Weather Review* **129**, 569–585.

Cheney NP, Gould JS, Catchpole WR (1998). Prediction of fire spread in grasslands. *International Journal of Wildland Fire* **8**(1), 1–13.

Cheney PJ, Gould J, McCaw L (2001). The dead-man zone: A neglected area of fire fighter safety. *Australian Forestry* **64**, 45–50.

Clark TL, Coen J, Latham D (2004). Description of a coupled atmosphere-fire model. *International Journal of Wildland Fire* **13**, 49–63.

Clark TL, Jenkins MA, Coen J, Packham D (1996a). A coupled atmosphere-fire model: Convective feedback on fire-line dynamics. *Journal of Applied Meteorology* **35**, 875–901.

Clark TL, Jenkins MA, Coen JL, Packham DR (1996b). A coupled atmosphere-fire model: Role of the convective Froude number and dynamic fingering at the fireline. *International Journal of Wildland Fire* **6**(4), 177–190.

Clark TL, Radke L, Coen J, Middleton D (1999). Analysis of small-scale convective dynamics in a crown fire using infrared video camera imagery. *Journal of Applied Meteorology* **38**(10), 1401–1420.

Clements CB, Perna R, Jang M, Lee D, Patel M, Street S, Zhong S, Goodrick S, Li J, Potter BE, et al. (2007). Observing the dynamics of wildland grass fires: Fireflux-a field validation experiment. *Bulletin of the American Meteorological Society* **88**(9), 1369–1382.

Clements CB, Potter BE, Zhong S (2006). In situ measurements of water vapor, heat, and co2 fluxes within a prescribed grass fire. *International Journal of Wildland Fire* **15**(3), 299–306.

Clifford VR, Pearce HG (2009). Fire behaviour case study: Mt Cook Station fire, 16 January 2008. Scion Report No: 17031. Scion, Rural Fire Research Group, Christchurch, New Zealand. 49pp.

Coen J, Mahalingam S, Daily J (2004). Infrared imagery of crown-fire dynamics during FROSTFIRE. *Journal of Applied Meteorology* **43**(9), 1241–1259.

Coen JL (2005). Simulation of the Big Elk fire using coupled atmosphere-fire modeling. *International Journal of Wildland Fire* **14**, 49–59.

Coen JL, Cameron M, Michalakes J, Patton EG, Riggan PJ, Yedinak KM (2013). Wrf-Fire: Coupled weather-wildland fire modeling with the Weather Research and Forecasting model. *Journal of Applied Meteorology and Climatology* **52**, 16–38.

Countryman CM (1964). *Mass fires and fire behavior*. Pacific Southwest Forest and Range Experiment Station, Forest Service, US Department of Agriculture.

Countryman CM (1969). Project Flambeau: An investigation of mass fire (1964-1967), Vol. 1. *US Department of Agriculture, US Forest Service, Berkeley, California* .

Countryman CM (1971). Fire whirls: Why, when, and where. Technical report, USDA Forest Service, Pacific Southwest Forest and Range Experiment Station, Berkeley, California.

Countryman CM (1972). *The fire environment concept*. Pacific Southwest Forest and Range Experiment Station.

Cruz MG, Sullivan AL, Gould JS, Sims NC, Bannister AJ, Hollis JJ, Hurley RJ (2012). Anatomy of a catastrophic wildfire: The Black Saturday Kilmore East fire in Victoria, Australia. *Forest Ecology and Management* **284**, 269–285. doi:10.1016/j.foreco.2012.02.035.

Cunningham P, Goodrick SL, Yousuff Hussaini M, Linn RR (2005). Coherent vortical structures in numerical simulations of buoyant plumes from wildland fires. *International Journal of Wildland Fire* **14**, 61–75.

Cunningham P, Linn RR (2007). Numerical simulations of grass fires using a coupled atmosphere-fire model: Dynamics of fire spread. *Journal of Geophysical Research* **112**.

Davis C, Carr F (2000). Summary of the 1998 workshop on mesoscale model verification. *Bulletin of the American Meteorological Society* **81**, 809–819.

Deeming JE, Burgan RE, Cohen JD (1977). The national fire-danger rating system-1978. USDA Forest Service General Technical Report INT-39. Intermountain Forest and Range Experiment Station, Ogden, UT. 63pp.

Ding L, Calhoun RJ, Street RL (2003). Numerical simulation of strongly stratified flow over a three-dimensional hill. *Boundary-Layer Meteorology* **107**, 81–114.

Doyle JD, Durran DR (2002). The dynamics of mountain-wave-induced rotors. *Journal of the Atmospheric Sciences* **59**, 186–201.

Doyle JD, Durran DR (2007). Rotor and subrotor dynamics in the lee of three-dimensional terrain. *Journal of the Atmospheric Sciences* **64**, 4202–4221.

Drobinski P, Dabas AM, Haeberli C, Flamant PH (2001). On the small-scale dynamics of flow splitting in the Rhine valley during a shallow foehn event. *Boundary-Layer Meteorology* **99**(2), 277–296.

Dudhia J (1989). Numerical study of convection observed during the winter monsoon experiment using a mesoscale two-dimensional model. *Journal of the Atmospheric Sciences* **46**, 3077–3107.

Flannigan MD, Krawchuk MA, de Groot WJ, Wotton BM, Gowman LM (2009). Implications of changing climate for global wildland fire. *International Journal of Wildland Fire* **18**(5), 483–507.

Fogarty LG, , Pearce HG, Catchpole WR, Alexander ME (1998). Adoption vs Adaptation: Lessons from applying the Canadian Forest Fire Danger Rating System in New Zealand. In *Proceedings of the III International Conference on Forest Fire Research*. 14th Conference on Fire and Forest Meteorology. Luso, Portugal ADAI: Coimbra, Portugal.

Forthofer JM, Goodrick SL (2011). Review of vortices in wildland fire. *Journal of Combustion* 1–14. doi:10.1155/2011/984363.

Fox-Hughes P (2012). Springtime fire weather in Tasmania, Australia: Two case studies. *Weather and Forecasting* **27**(2), 379–395.

Fromm M, Lindsey DT, Servranckx R, Yue G, Trickl T, Sica R, Doucet P, Godin-Beekmann S, et al. (2010). The untold story of pyrocumulonimbus. *Bulletin of the American Meteorological Society* **91**(9), 1193.

Fromm MD, Servranckx R (2003). Transport of forest fire smoke above the tropopause by supercell convection. *Geophysical Research Letters* **30**(10), 1542.

Gatebe CK, Varnai T, Poudyal R, Ichoku C, King MD (2012). Taking the pulse of pyrocumulus clouds. *Atmospheric Environment* **52**, 121–130.

Gibbons P, van Bommel L, Gill AM, Cary GJ, Driscoll DA, Bradstock RA, Knight E, Moritz MA, Stephens SL, Lindenmayer DB (2012). Land management practices associated with house loss in wildfires. *PloS one* **7**(1), e29212.

Goens DW, Andrews PL (1998). *Weather and fire behavior factors related to the 1990 Dude Fire near Payson, AZ.* NWCG Wildland Fire Leadership Development Program.

Gorski C, Farnsworth A (2000). Fire weather and smoke management. in "mountain meteorology fundamentals and applications" .

Gosai A, Griffiths G (2004). An updated validation of seasonal fire weather climate outlooks. NZFSC Research Report No. 77. New Zealand Fire Service Commission, Wellington, New Zealand. 9pp.

Gosai A, Griffiths G, Salinger J (2004). Climate and severe fire seasons: Part IV - Daily weather sequences and high fire severity in Auckland, West/Waikato, North Canterbury, McKenzie Basin and Central Otago/Inland Southland. NZFSC Research Report No. 76. New Zealand Fire Service Commission, Wellington, New Zealand. 32pp.

Gosai A, Heydenrych C, Salinger J (2003). Climate and severe fire seasons: Part III - Climate patterns and high fire severity in Northland and Canterbury. NZFSC Research Report No. 75. New Zealand Fire Service Commission, Wellington, New Zealand. 19pp. + appendices.

Grell GA, Peckham SE, Schmitz R, McKeen SA, Frost G, Skamarock WC, Eder B (2005). Fully coupled online chemistry within the WRF model. *Atmospheric Environment* **39**(37), 6957–6975.

Griffiths G (2004). Climate and severe fire seasons: Part V - Daily weather sequence and high fire severity in Auckland East/Coromandel, Bay of Plenty, Gisborne/Hawke's Bay, Manawatu/Wairarapa, Wellington/Marlborough and coastal Otago. NIWA Client Report AKL2004-135. National Institute of Water and Atmospheric Research. 54 pp.

Guyette RP, Muzika RM, Dey DC (2002). Dynamics of an anthropogenic fire regime. *Ecosystems* **5**(5), 472–486.

Haines DA (1988). A lower atmosphere severity index for wildland fires. *National Weather Digest* **13 (2)**, 23–27.

Hamilton R (2007). Operational 10-day forecasts of fire weather indices. NZFSC Research Report No. 70. New Zealand Fire Service Commission, Wellington, New Zealand. 4pp.

Heilman WE (1992). Atmospheric simulations of extreme surface heating episodes on simple hills. *International Journal of Wildland Fire* **2**(3), 99–114.

Heilman WE, Fast JD (1992). Simulations of horizontal roll vortex development above lines of extreme surface heating. *International Journal of Wildland Fire* **2**(2), 55–68.

Heimann D (1997). Mesoscale surface-wind characteristics and potential gravity-wave formation during cross-Alpine airflow. *Meteorology and Atmospheric Physics* **62**(1), 49–70.

Hennigan CJ, Westervelt DM, Riipinen I, Engelhart GJ, Lee T, Collett Jr JL, Pandis SN, Adams PJ, Robinson AL (2012). New particle formation and growth in biomass burning plumes: An important source of cloud condensation nuclei. *Geophysical Research Letters* **39**(9), L09805.

Hertenstein RF, Kuettner JP (2005). Rotor types associated with steep lee topography: Influence of the wind profile. *Tellus* **57A**, 117–135.

Heydenrych C, Salinger J (2002). Climate and severe fire seasons: Part II - New Zealand fire regions. NZFSC Research Report No. 73. New Zealand Fire Service Commission, Wellington, New Zealand. 46pp.

Heydenrych C, Salinger J, Renwick J (2001). Climate and severe fire seasons: a report on climatic factors contributing to severe fire seasons in New Zealand. NZFSC Research Report No. 11. New Zealand Fire Service Commission, Wellington, New Zealand. 117pp.

Hoadley JL, Westrick K, Ferguson SA, Goodrick SL, Bradshaw L, Werth P (2004). The effect of model resolution in predicting meteorological parameters used in fire danger rating. *Journal of Applied Meteorology* **43**, 1333–1347.

Hoinka KP (1985). Observation of airflow over the Alps during a foehn event. *Quarterly Journal of the Royal Meteorological Society* **111**, 199–224.

Hong SY, Lim JOJ (2006). The WRF Single-Moment 6-Class Microphysics Scheme (WSM6). *Journal of the Korean Meteorological Society* **42**, 129–151.

Janjic ZI (1990). The step-mountain coordinate: physical package. *Monthly Weather Review* **118**, 1429–1443.

Janjic ZI (1996). The surface layer in the NCEP Eta model. In *Eleventh Conference on Numerical Weather Prediction*, 354–355. American Meteorological Society, Boston, MA, Norfolk, VA.

Janjic ZI (2002). Nonsingular implementation of the Mellor-Yamada Level 2.5 Scheme in the NCEP Meso model. NCEP Office Note, No. 437, 61pp.

Jiménez PA, González-Rouco JF, García-Bustamante E, Navarro J, Montávez JP, de Arellano JVG, Dudhia J, Muñoz-Roldan A (2010). Surface wind regionalization over complex terrain: evaluation and analysis of a high-resolution WRF simulation. *Journal of Applied Meteorology and Climatology* **49**(2), 268–287.

Johnson EA, Miyanishi K (2001). *Forest fires: behavior and ecological effects*. Academic Press.

Jolliffe IT, Stephenson DB (2003). *Forecast Verification: A Practitioner's Guide in Atmospheric Science*. Wiley.

Jordanov G, Beezley J, Dobrinkova N, Kochanski A, Mandel J, Sousedík B (2012). Simulation of the 2009 Harmanli fire (Bulgaria). *Large-Scale Scientific Computing* 291–298.

Kain JS (2004). The Kain-Fritsch convective parameterization: An update. *Journal of Applied Meteorology* **43**, 170–181.

Katurji M, Zhong S, Zawar-Reza P (2011). Long-range transport of terrain-induced turbulence from high-resolution numerical simulations. *Atmospheric Chemistry and Physics* **11**, 11793–11805.

Kidson E (1932). The Canterbury "Northwester". *New Zealand Journal of Science and Technology* **14**, 65–75.

Kiefer M, Lin Y, Charney J (2008). A study of two-dimensional dry convective plume modes with variable critical level height. *Journal of the Atmospheric Sciences* **65**(2), 448–469.

Kiefer MT, Parker MD, Charney JJ (2009). Regimes of dry convection above wildfires: Idealized numerical simulations and dimensional analysis. *Journal of the Atmospheric Sciences* **66**(4), 806–836.

Kirkil G, Mirocha J, Bou-Zeid E, Chow FK, Kosovic B (2012). Implementation and evaluation of dynamic subfilter-scale stress models for large-eddy simulation using WRF. *Monthly Weather Review* **140**, 266–284.

Klemp J, Lilly D (1975). The dynamics of wave-induced downslope winds. *Journal of Atmospheric Sciences* **32**, 320–339.

Klemp JB, Dudhia J, Hassiotis AD (2008). An upper gravity-wave absorbing layer for NWP applications. *Monthly Weather Review* **136**, 3987–4004.

Lamb PC (1975). The Nor'wester's advance across the Canterbury Plains, New Zealand. *NZ Journal of Science and Technology* **17**, 65–75.

Lawson BD, Armitage OB (2008). Weather guide for the Canadian Forest Fire Danger Rating System. Natural Resources Canada, Canadian Forest Service, Northern Forestry Centre, Edmonton, Alberta, Canada.

Lentile LB, Holden ZA, Smith AMS, Falkowski MJ, Hudak AT, Morgan P, Lewis SA, Gessler PE, N C B (2006). Remote sensing techniques to assess active fire characteristics and post-fire effects. *International Journal of Wildland Fire* **15**(3), 319–345.

Leung LR, Qian Y (2009). Atmospheric rivers induced heavy precipitation and flooding in the western US simulated by the WRF regional climate model. *Geophysical Research Letters* **36**(3), L03820.

Lilly DK (1978). A severe downslope windstorm and aircraft turbulence event induced by a mountain wave. *Journal of the Atmospheric Sciences* **35**(1), 59–77.

Linn R, Reisner J, Colman JJ, Winterkamp J (2002). Studying wildfire behaviour using FIRETEC. *International Journal of Wildland Fire* **11**, 233–246.

Linn R, Winterkamp J, Edminster C, Colman JJ, Smith WS (2007). Coupled influences of topography and wind on wildland fire behaviour. *International Journal of Wildland Fire* **16**(2), 183–195. doi: 10.1071/WF06078.

Luderer G, Trentmann J, Andreae MO (2009). A new look at the role of fire-released moisture on the dynamics of atmospheric pyro-convection. *International Journal of Wildland Fire* **18**(5), 554–562.

Luderer G, Trentmann J, Winterrath T, Textor C, Herzog M, Graf HF, Andreae MO, et al. (2006). Modeling of biomass smoke injection into the lower stratosphere by a large forest fire (Part II): sensitivity studies. *Atmospheric Chemistry and Physics Discussions* **6**(4), 6081–6124.

Mandel J, Beezley JD, Kochanski AK (2011). Coupled atmosphere-wildland fire modeling with WRF 3.3 and SFIRE 2011. *Geoscientific Model Development* **4**, 591–610.

Mass CF, Ovens D, Westrick KJ, Colle BA (2002). Does increasing horizontal resolution produce more skillful forecasts? *Bulletin of the American Meteorological Society* **83**, 407–430.

McArthur AG (1966). Weather and grassland fire behaviour Forestry and Timber Bureau Leaflet No. 100. Department of National Development, Canberra, Australia.

McArthur AG (1967). Fire behaviour in eucalypt forests. Forestry and Timber Bureau Leaflet No. 107. Department of National Development, Canberra, Australia. 36pp.

McCauley MP, Sturman AP (1999). A study of orographic blocking and barrier wind development upstream of the Southern Alps, New Zealand. *Meteorology and Atmospheric Physics* **70**(3), 121–131.

McCutchan MH, Fox DG (1986). Effect of elevation and aspect on wind, temperature and humidity. *Journal of climate and applied meteorology* **25**(12), 1996–2013.

McGowan HA (1997). Meteorological controls on wind erosion during foehn wind events in the eastern Southern Alps, New Zealand. *Canadian Journal of Earth Sciences* **34**(11), 1477–1485.

McGowan HA (2003). Observations of foehn interaction with lake breeze and valley wind circulations, Lake Tekapo, New Zealand. In *International Conference on Alpine Meteorology and MAP Meeting*, volume 13, 536–538. Meteo Swiss.

McGowan HA, Sturman AP (1996). Regional and local scale characteristics of foehn wind events over the South Island of New Zealand. *Meteorology and Atmospheric Physics* **58**(1), 151–164.

McGowan HA, Sturman AP, Kossmann M, Zawar-Reza P (2002). Observations of foehn onset in the Southern Alps, New Zealand. *Meteorology and Atmospheric Physics* **79**(3), 215–230.

McGowan HA, Sturman AP, Owens IF (1996). Aeolian dust transport and deposition by foehn winds in an alpine environment, Lake Tekapo, New Zealand. *Geomorphology* **15**(2), 135–146.

McKendry IG, Sturman AP, Owens IF (1985). A study of interacting multi-scale wind systems, Canterbury Plains, New Zealand. *Meteorology and atmospheric physics* **35**(4), 242–252.

McKendry IG, Sturman AP, Owens IF (1988). Numerical simulation of local thermal effects on the wind field of the Canterbury Plains, New Zealand. *New Zealand Journal of Geology and Geophysics* **31**(4), 511–524.

McRae R (2004). Breath of the dragon - observations of the January 2003 ACT bushfires. In *Proceedings of 2004 Australasian Bushfire Research Conference.*

McRae RH, Sharples JJ, Wilkes SR, Walker A (2013). An Australian pyro-tornadogenesis event. *Natural Hazards* 1–11.

Mell W, Jenkins MA, Gould J, Cheney P (2007). A physics-based approach to modelling grassland fires. *International Journal of Wildland Fire* **16**, 1–22.

Mell W, Maranghides A, McDermott R, Manzello S (2009). Numerical simulation and experiments of burning douglas fir trees. *Combustion and Flame* **156**(10), 2023–2041.

Mell WE, Manzello SL, Maranghides A, Butry D, Rehm RG (2010). The wildland–urban interface fire problem–current approaches and research needs. *International Journal of Wildland Fire* **19**(2), 238–251.

Miller NL, Schlegel NJ (2006). Climate change projected fire weather sensitivity: California Santa Ana wind occurrence. *Geophysical Research Letters* **33**(15), L15711.

Mills GA, McCaw WL (2010). Atmospheric stability environments and fire weather in Australia - extending the Haines Index. Centre for Australian Weather and Climate Research Technical Report No. 20. Melbourne, Australia.

Mirocha JD, Lundquist JK, Kosovic B (2010). Implementation of a nonlinear subfilter turbulence stress model for large-eddy simulation in the Advanced Research WRF model. *Monthly Weather Review* **138**, 4212–4228.

Mlawer EJ, Taubman SJ, Brown PD, Iacono MJ, Clough SA (1997). Radiative transfer for inhomogeneous atmosphere: RRTM, a validated correlated-k model for the long-wave. *Journal of Geophysical Research* **102 (D14)**, 16663–16682.

Moeng C, Dudhia J, Klemp J, Sullivan P (2007). Examining two-way grid nesting for large eddy simulation of the PBL using the WRF model. *Monthly weather review* **135**(6), 2295–2311.

Mölders N (2008). Suitability of the Weather Research and Forecasting (WRF) model to predict the June 2005 fire weather for interior Alaska. *Weather and Forecasting* **23**, 953–973.

Mutch RW (1970). Wildland fires and ecosystems–a hypothesis. *Ecology* 1046–1051.

NZMS (1983). Climatic Map Series (1:2,000,000) Part 2: Climate regions. *NZMS Miscellaneous Publication 175* .

Oreskes N, Shrader-Frechette K, Belitz K (1994). Verification, validation, and confirmation of numerical models in the earth sciences. *Science* **263**, 641–646.

Palmer TY (1981). Large fire winds, gases and smoke. *Atmospheric Environment* **15**(10), 2079–2090.

Pathirana A, Yamaguchi M, Yamada T (2003). Idealized simulation of airflow over a mountain ridge using a mesoscale atmospheric model. *Annual Journal of Hydraulic Engineering* **47**, 31–36.

Pearce G (1996). An initial assessment of fire danger in New Zealand's climatic regions. Fire Technology Transfer Note. Forest and Rural Fire Research Programme, New Zealand Forest Research Institute, Rotorua, New Zealand. 28pp.

Pearce HG (2003). A fire danger climatology for New Zealand. NZFSC Research Report No. 39. New Zealand Fire Service Commission, Wellington, New Zealand. 289pp.

Pearce HG, Clifford V (2008). Fire weather and climate of New Zealand. *New Zealand Journal of Forestry* **53 (3)**, 13–18.

Pearce HG, Kerr J, Clark A, Mullan B, Ackerley D, Carey-Smith T, Yang E (2011a). Improved estimates of the effect of climate change on NZ fire danger. Scion Client Report No. 18087. Scion, Rural Fire Research Group, Christchurch, New Zealand. National Institute of Water and Atmospheric Research, Wellington, New Zealand. 84pp.

Pearce HG, Kerr JL, Clifford VR, Wakelin HM (2011b). Fire climate severity across New Zealand. Scion Client Report No. 18264. Scion, Rural Fire Research Group, Christchurch, New Zealand. 78pp.

Pearce HG, Moore JR (2004). Use of long-term fire danger data sets to predict fire season severity. Forest Research Client Report No. 11512. Forest Research and Rural Fire Research Programme, Christchurch, New Zealand. 22 pp. + appendices.

Pearce HG, Mullan AB, Salinger MJ, Opperman TW, Woods D, Moore JR (2005). Impacts of climate change on long-term fire danger. NZFSC Research Report No. 50. New Zealand Fire Service Commission, Wellington, New Zealand. 70pp.

Pearce HG, Salinger J, Renwick J (2007). Impact of climate variability on fire danger. NZFSC Research Report No. 72. New Zealand Fire Service Commission, Wellington, New Zealand. 117pp.

Pearce HG, Whitmore MA (2009). Analysis of seasonal trends in the Drought Code in New Zealand. Scion Client Report No. 12788. Scion, Rural Fire Research Group, Christchurch, New Zealand. 59pp.

Penman TD, Christie FJ, Andersen AN, Bradstock RA, Cary GJ, Henderson MK, Price O, Tran C, Wardle GM, Williams RJ, York A (2011). Prescribed burning: how can it work to conserve the things we value? *International Journal of Wildland Fire* **20**, 721–733.

Pielke Sr RA (2002). *Mesoscale Meteorological Modelling.* Academic Press, second edition. ISBN 0 12 554766 8.

Potter BE (1996). Atmospheric properties associated with large wildfires. *International Journal of Wildland Fire* **6**(2), 71–76.

Potter BE (2002). A dynamics based view of atmosphere-fire interactions. *International Journal of Wildland Fire* **11**, 247–255.

Potter BE (2005). The role of released moisture in the atmospheric dynamics associated with wildland fires. *International Journal of Wildland Fire* **14**(1), 77–84.

Potter BE (2012a). Atmospheric interactions with wildland fire behaviour–I. Basic surface interactions, vertical profiles and synoptic structures. *International Journal of Wildland Fire* **21**, 779–801.

Potter BE (2012b). Atmospheric interactions with wildland fire behaviour–II. Plume and vortex dynamics. *International Journal of Wildland Fire* **21**, 802–817.

Potter BE, Goodrick S, Brown T (2003). Development of a statistical validation methodology of fire weather indices. In 2nd International Wildland Fire Ecology and Fire Management Congress, 5th Symposium on Fire and Forest Meteorology, 16-20 November, Orlando, FL. American Meteorological Society, Boston, MA. 5pp.

Pyne SJ, Andrews PL, Laven RD (1996). *Introduction to wildland fire.* Wiley.

Radeloff V, Hammer R, Stewart S, Fried J, Holcomb S, McKeefry J (2005). The wildland-urban interface in the United States. *Ecological Applications* **15**(3), 799–805.

Raphael MN (2003). The Santa Ana Winds of California. *Earth Interactions* **7**, 1–13.

Raupach MR (1995). Vegetation-atmosphere interaction and surface conductance at leaf, canopy and regional scales. *Agricultural and Forest Meteorology* **73**(3), 151–179.

Renwick J, Salinger J, Zheng X, Pearce G (2007). Prediction of fire weather and fire danger. NZFSC Research Report No. 83. New Zealand Fire Service Commission, Wellington, New Zealand. 38pp.

Renwick J, Salinger MJ (2004). Validation of seasonal fire climate outlooks. NIWA Client Report AKL2003-34. National Institute of Water and Atmospheric Research, Auckland, New Zealand. 6pp.

Renwick JA (2011). Kidsons synoptic weather types and surface climate variability over New Zealand. *Weather and Climate* **31**, 3–23.

Robin AG, Wilson GU (1958). The effect of meteorological conditions on major fires in the Riverina (New South Wales) district. *Australian Meteorological Magazine* **21**, 49–75.

Rorig ML, Ferguson SA (1999). Characteristics of lightning and wildland fire ignition in the Pacific Northwest. *Journal of Applied Meteorology* **38**(11), 1565–1575.

Rosenfeld D, Fromm M, Trentmann J, Luderer G, Andreae MO, Servranckx B (2007). The chisholm firestorm: observed microstructure, precipitation and lightning activity of a pyro-cumulonimbus. *Atmospheric Chemistry and Physics* **7**(3), 645–659.

Rothermel RC (1972). *A mathematical model for predicting fire spread in wildland fuels*, volume 115. Intermountain Forest & Range Experiment Station, Forest Service, US Department of Agriculture.

Rothermel RC (1991). Predicting behavior and size of crown fires in the Northern Rocky Mountains .

Schär C, Durran DR (1997). Vortex formation and vortex shedding in continuously stratified flows past isolated topography. *Journal of the Atmospheric Sciences* **54**, 534–554.

Scorer RS (1949). Theory of waves in the lee of mountains. *Quarterly Journal of the Royal Meteorological Society* **75**, 41–56.

Sharples JJ (2008). Review of formal methodologies for wind-slope correction of wildfire rate of spread. *International Journal of Wildland Fire* **17**(2), 179.

Sharples JJ (2009). An overview of mountain meteorological effects relevant to fire behaviour and bushfire risk. *International Journal of Wildland Fire* **18**, 737–754.

Sharples JJ, McRae RHD (2011). Atypical bushfire spread driven by the interaction of terrain and extreme fire weather. In RP Thornton, editor, *Proceedings of Bushfire CRC & AFAC 2011 Conference Science Day*. Bushfire CRC, Sydney, Australia.

Sharples JJ, McRae RHD, Weber RO (2010a). Wind characteristics over complex terrain with implications for bushfire risk management. *Environmental Modelling & Software* **25**, 1099–1120.

Sharples JJ, McRae RHD, Wilkes SR (2012). Wind-terrain effects on the propagation of wildfires in rugged terrain: Fire channelling. *International Journal of Wildland Fire* Published online 23 January 2012.

Sharples JJ, Mills GA, McRae RHD, Weber RO (2010b). Foehn-like winds and elevated fire danger conditions in southeastern Australia. *Journal of Applied Meteorology and Climatology* **49**(6), 1067–1095.

Sharples JJ, Viegas DX, McRae RHD, Raposo JRN, Farinha HAS (2011). Lateral bushfire propagation driven by the interaction of wind, terrain and fire. In F Chan, D Marinova, RS Anderssen, editors, *MODSIM2011, 19th International Congress on Modelling and Simulation*, 235–241. Modelling and Simulation Society of Australia and New Zealand, Sydney, Australia. ISBN: 978-0-9872143-1-7.

Sharples JJ, Viegas DX, Rossa CG, McRae RHD (2010c). Small-scale observations of atypical fire spread caused by the interaction of wind, terrain and fire. In DX Viegas, editor, *Proceedings of the VI International Conference on Forest Fire Research*. Coimbra, Portugal.

Sheridan PF, Vosper SB (2006). Numerical simulations of rotors, hydraulic jumps and eddy shedding in the Falkland Islands. *Atmospheric Science Letters* **6**, 211–218.

Siddaway JM, Petelina SV (2011). Transport and evolution of the 2009 Australian Black Saturday bushfire smoke in the lower stratosphere observed by OSIRIS on Odins. *Journal of Geophysical Research* **116**(D6), D06203.

Simmers T (2005). Medium range forecasts of fire weather indices: an assessment of canonical correlation based forecasts from an ensemble prediction system. NZFSC Research Report No. 64. New Zealand Fire Service Commission, Wellington, New Zealand. 49pp.

Simpson CC, Pearce HG, Sturman AP, Zawar-Reza P (2013a). Behaviour of WRF modelled fire weather indices in the 2009/10 New Zealand wildland fire season. Accepted with revisions by International Journal of Wildland Fire.

Simpson CC, Pearce HG, Sturman AP, Zawar-Reza P (2013b). Verification of WRF modelled fire weather in the 2009/10 New Zealand wildland fire season. Accepted with revisions by International Journal of Wildland Fire.

Simpson CC, Sharples JJ, Evans JP, McCabe MF (2013c). Large eddy simulation of atypical wildland fire spread on leeward slopes. Online early at International Journal of Wildland Fire.

Simpson CC, Sturman AP, Zawar-Reza P, Pearce HG (2013d). Fire weather of an extreme foehn event in South Island, New Zealand. In Review in Monthly Weather Review.

Skamarock WC, Klemp JB, Dudhia J, Gill DO, Barker DM, Duda MG, Huang XY, Wang W, Powers JG (2008). *A Description of the Advanced Research WRF Version 3*, NCAR technical note 475 edition. Available at: http://www.mmm.ucar.edu/wrf/users/docs/.

Smith RB (1985). On severe downslope winds. *Journal of the Atmospheric Sciences* **42**(23), 2597–2603.

Smith RB, Woods BK, Jensen J, Cooper WA, Doyle JD, Jiang Q, Grubišic V (2008). Mountain waves entering the stratosphere. *Journal of the Atmospheric Sciences* **65**(8), 2543–2562.

Smolarkiewicz PK, Rotunno R (1989). Low Froude number flow past three-dimensional obstacles. Part I: Baroclinically generated lee vortices. *Journal of the Atmospheric Sciences* **46**(8), 1154–1164.

Stocks BJ, Alexander ME, Van Wagner CE, McAlpine RS, Lynham TJ, Dubé DE (1989). The Canadian Forest Fire Danger Rating System: An overview. *The Forestry Chronicle* **65**, 450–457.

Stocks BJ, Fosberg MA, Lynham TJ, Mearns L, Wotton BM, Yang Q, Jin JZ, Lawrence K, Hartley GR, Mason JA, et al. (1998). Climate change and forest fire potential in Russian and Canadian boreal forests. *Climatic Change* **38**(1), 1–13.

Sturman AP, McGowan HA, Spronken-Smith RA (1999). Mesoscale and local climates in New Zealand. *Progress in Physical Geography* **23**(4), 611–635.

Sturman AP, Smith RK, Page MA, Ridley RN, Steiner JT (1990). Meso-scale surface wind changes associated with the passage of cold fronts along the eastern side of the Southern Alps, New Zealand. *Meteorology and Atmospheric Physics* **42**(2), 133–143.

Sullivan AL (2009a). Wildland surface fire spread modelling, 1990–2007. 1: Physical and quasi-physical models. *International Journal of Wildland Fire* **18**(4), 349–368.

Sullivan AL (2009b). Wildland surface fire spread modelling, 1990–2007. 2: Empirical and quasi-empirical models. *International Journal of Wildland Fire* **18**(4), 369–386.

Sullivan AL (2009c). Wildland surface fire spread modelling, 1990–2007. 3: Simulation and mathematical analogue models. *International Journal of Wildland Fire* **18**(4), 387–403.

Sun R, Krueger SK, Jenkins MA, Zulauf MA, Charney JJ (2009). The importance of fire-atmosphere coupling and boundary-layer turbulence to wildfire spread. *International Journal of Wildland Fire* **18**, 50–60.

Taylor RJ, Evans ST, King NK, Stephens ET, Packham DR, Vines RG (1973). Convective activity above a large-scale bushfire. *Journal of Applied Meteorology* **12**, 1144–1150.

Trentmann J, Luderer G, Winterrath T, Fromm MD, Servranckx R, Textor C, Herzog M, Graf HF, Andreae MO, et al. (2006). Modeling of biomass smoke injection into the lower stratosphere by a large forest fire (Part I): reference simulation. *Atmospheric Chemistry and Physics Discussions* **6**(4), 6041–6080.

Van Wagner CE (1977). A method of computing fine fuel moisture content throughout the diurnal cycle. Fish. Environ. Can., Canadian Forest Service, Petawawa For. Exp. Stn., Chalk River, Ontario, Canada. Inf. Report PS-X-69. 15pp.

Van Wagner CE (1979). A laboratory study of weather effects on the drying rate of jack pine litter. *Canadian Journal of Forest Research* **9**(2), 267–275.

Van Wagner CE (1987). Development and structure of the Canadian Forest Fire Weather Index System. Forestry Technical Report 35. Government of Canada, Canadian Forestry Service, Ottawa, Ontario. 37pp.

Van Wagner CE, Pickett TL (1985). Equations and FORTRAN program for the Canadian Forest Fire Weather Index System. Forestry Technical Report 33. Government of Canada, Canadian Forestry Service, Ottawa, Ontario. 18pp.

Viegas DX (2004). Slope and wind effects on fire propagation. *International Journal of Wildland Fire* **13**, 143–156.

Viegas DX, Pita LP (2004). Fire spread in canyons. *International Journal of Wildland Fire* **13**(3), 253–274.

Weise DR, Biging GS (1997). A qualitative comparison of fire spread models incorporating wind and slope effects. *Forest Science* **43**(2), 170–180.

Werth J, Werth P (1998). Haines Index climatology for the western United States. *Fire Management Notes* **58**.

Westerling AL, Cayan DR, Brown TJ, Hall BL, Riddle LG (2004). Climate, Santa Ana winds, and autumn wildfires in southern California. *Eos* **85**(31), 289–296.

White BG, Peagle J, Steenburgh WJ, Horel JD, Swanson RT, Cook LK, Onton DJ, Miles JG (1999). Short-term forecast validation of six models. *Weather Forecasting* **14**, 84–108.

Whiteman CD (2000). *Mountain meteorology fundamentals and applications*. Oxford University Press, New York.

Whiteman CD, Doran JC (1993). The relationship between overlying synoptic-scale flows and winds within a valley. *Journal of Applied Meteorology* **32**(11), 1669–1682.

Wicker LJ, Skamarock WC (2002). Time splitting methods for elastic models using forward time schemes. *Monthly Weather Review* **130**, 2088–2097.

Willmott CJ (1981). On the validation of models. *Physical Geography* **2**, 184–194.

Winkler JA, Potter BE, Wilhelm DF, Shadbolt RP, Piromsopa K, Bian X (2007). Climatological and statistical characteristics of the Haines Index for North America. *International Journal of Wildland Fire* **16**(2), 139–152.

Wratt DS, Ridley RN, Sinclair MR, Larsen H, Thompson SM, Henderson R, Austin GL, Bradley SG, Auer A, Sturman AP, et al. (1996). The New Zealand Southern Alps Experiment. *Bulletin of the American Meteorological Society* **77**, 683–692.

Zeng X, Beljaars A (2005). A prognostic scheme of sea surface skin temperature for modeling and data assimilation. *Geophysical Research Letters* **32**, L14605. Doi:10.1029/2005GL023030.